

# **CHARACTERIZATION OF SUSPENSIONS AND FILMS OF CELLULOSE NANOCRYSTALS**

by

Catherine D. Edgar

A Thesis submitted to the Faculty of Graduate Studies and Research in  
partial fulfillment of the requirements of the degree of Doctor of Philosophy

Department of Chemistry

McGill University

Montreal, Canada

May, 2002

© Catherine D. Edgar, 2002



National Library  
of Canada

Bibliothèque nationale  
du Canada

Acquisitions and  
Bibliographic Services

Acquisitions et  
services bibliographiques

395 Wellington Street  
Ottawa ON K1A 0N4  
Canada

395, rue Wellington  
Ottawa ON K1A 0N4  
Canada

*Your file* *Votre référence*

*ISBN: 0-612-85702-6*

*Our file* *Notre référence*

*ISBN: 0-612-85702-6*

The author has granted a non-exclusive licence allowing the National Library of Canada to reproduce, loan, distribute or sell copies of this thesis in microform, paper or electronic formats.

L'auteur a accordé une licence non exclusive permettant à la Bibliothèque nationale du Canada de reproduire, prêter, distribuer ou vendre des copies de cette thèse sous la forme de microfiche/film, de reproduction sur papier ou sur format électronique.

The author retains ownership of the copyright in this thesis. Neither the thesis nor substantial extracts from it may be printed or otherwise reproduced without the author's permission.

L'auteur conserve la propriété du droit d'auteur qui protège cette thèse. Ni la thèse ni des extraits substantiels de celle-ci ne doivent être imprimés ou autrement reproduits sans son autorisation.

**Canada**

## ABSTRACT

Suspensions of cellulose nanocrystals may be prepared by hydrolysing wood pulp or cotton filter paper with sulfuric acid. Due to the rod-like shape of the nanocrystals, these aqueous suspensions display liquid crystalline behaviour. This thesis examines these unique suspensions at three different concentration ranges. At low cellulose concentrations the suspensions are disordered, becoming ordered upon reaching a critical concentration, which depends on the aspect ratio of the rods. AFM and TEM were used to characterize particle size and polydispersity. Just beyond the critical concentration for anisotropic phase formation is an intermediate concentration range in which the isotropic and anisotropic phases co-exist. This biphasic region was examined for its potential to partition dextran molecules. At extremely high cellulose concentrations, solid cellulose films that maintain some chiral nematic order may be obtained. The degree of order in the films has been measured using induced circular dichroism and optimized by magnetic alignment. These suspensions can also be used to create model surfaces of cellulose I. The smooth cellulose surfaces have been characterized by XPS, X-ray diffraction, and AFM.

## RÉSUMÉ

Des suspensions des nanocristaux de cellulose peuvent être préparées par hydrolyse de pâte à papier ou de papiers filtre de coton avec de l'acide sulfurique. Du fait de la forme en bâtonnet des nanocristaux, ces suspensions aqueuses présentent un comportement typique d'un liquide cristallin. Cette thèse examine ces suspensions uniques à trois niveaux différents de concentration. À de basses concentrations en cellulose les suspensions sont désordonnées. Elles s'ordonnent au delà d'une concentration critique, dont la valeur dépend des dimensions des bâtonnets. La microscopie à force atomique (MFA) et la microscopie électronique en transmission (MET) ont été employées pour caractériser les dimensions et la polydispersité des particules. Juste au-dessus de la concentration critique pour la formation de la phase anisotrope se situe une gamme intermédiaire de concentration où les phases isotropes et anisotropes coexistent. Cette région biphasique a été examinée pour son potentiel de séparation du polymère dextran. À des concentrations extrêmement élevées en cellulose, des films solides de cellulose maintenant un certain ordre chiral nématique peuvent être obtenus. Le degré d'ordre dans les films a été mesuré en utilisant le dichroïsme circulaire induit (DCI) et optimisé par l'alignement magnétique. Ces suspensions peuvent également être employées pour créer des surfaces modèles de la cellulose I. Les surfaces lisses de cellulose ont été caractérisées par spectroscopie de photoélectron de rayon X (SPX), diffraction de rayon X, et MFA.

## PREFACE

This thesis is structured as a collection of manuscripts, according to the Guidelines for Thesis Preparation:

As an alternative to the traditional thesis format, the dissertation can consist of a collection of papers of which the student is an author or co-author. These papers must have a cohesive, unitary character making them a report of a single program of research.

Candidates have the option of including, as part of the thesis, the text of one or more papers submitted, or to be submitted, for publication, or the clearly-duplicated text (not the reprints) of one or more published papers. These texts must conform to the "Guidelines for Thesis Preparation" with respect to font size, line spacing and margin sizes and must be bound together as an integral part of the thesis.

The thesis must be more than a collection of manuscripts. All components must be integrated into a cohesive unit with a logical progression from one chapter to the next. In order to ensure that the thesis has continuity, connecting texts that provide logical bridges between the different papers are mandatory.

The thesis must conform to all other requirements of the "Guidelines for Thesis Preparation" in addition to the manuscripts. The thesis must include the following: a table of contents; an abstract in English and French; an introduction, which clearly states the rationale and objectives of the research; a comprehensive review of the literature (in addition to that covered in the introduction to each paper); a final conclusion and summary.

As manuscripts for publication are frequently very concise documents, where appropriate, additional material must be provided (e.g., in appendices) in sufficient detail to allow a clear and precise judgement to be made of the importance and originality of the research reported in the thesis.

In general, when co-authored papers are included in a thesis the candidate must have made a substantial contribution to all papers included in the thesis. In addition, the

candidate is required to make an explicit statement in the thesis as to who contributed to such work and to what extent. This statement should appear in a single section entitled "Contributions of Authors" as a preface to the thesis. The supervisor must attest to the accuracy of this statement at the doctoral oral defence. Since the task of the examiners is made more difficult in these cases, it is in the candidate's interest to clearly specify the responsibilities of all the authors of the co-authored papers.

When previously published copyright material is presented in a thesis, the candidate must include signed waivers from the co-authors and publishers and submit these to the Thesis Office with the final deposition, if not submitted previously.

### **Contributions of Authors**

Chapter 3 has been submitted to a scientific journal. Dr. Derek Gray will be a co-author for this paper. Dr. Gray provided useful discussions regarding research ideas and analysis of results as well as editorial assistance in the writing of the paper.

Chapter 4 has been published in *Cellulose* 8(1), 5-12. Dr. Gray is a co-author for this paper. Dr. Gray provided guidance in developing the research ideas, interpreting the results, and in editing the manuscript.

Chapter 5 will be submitted to a scientific journal. Dr. Derek Gray, who provided assistance during the experimental and writing stages, will be a co-author for this paper. Experimental assistance was provided by the following people. The XPS analysis was carried out by Dr. Leena-Sisko Johansson at the Helsinki University of Technology. Dr. Robert Marchessault and his group (Dr. Jumpei Kawada and Emily Cranston) carried out the x-ray analysis and provided useful discussions for interpreting the results. Louis Godbout provided useful discussions on the casting of smooth films.

I hereby give copyright clearance for the inclusion of the following paper, of which I am a co-author, in the dissertation of Catherine Edgar:

“Induced circular dichroism of chiral nematic cellulose films.”

  
Dr. D. G. Gray  
Pulp and Paper Research Centre  
McGill University  
Montreal, Quebec  
H3A 2A7

Date: *May 14, 2002*

## ACKNOWLEDGEMENTS

I would like to start by thanking my research supervisor, Dr. Derek Gray, for his continued support over the years. He inspired me with his enthusiasm for research and gave me independence to explore new ideas on my own. He also encouraged and financed my attendance at several conferences. I am grateful for these opportunities and will always remember the Gordon Research Conferences on Liquid Crystals and the Chemistry of Polysaccharides.

Collaboration is an essential part of research. I would like to thank the following people for their contributions to my experimental results: Jean-François Revol (TEM); Leena-Sisko Johansson (XPS); Agnes Lejeune and Jean-Philippe Boisvert (XPS); Bob Marchessault, Jumpei Kawada, and Emily Cranston (X-ray). I would also like to thank the following people for their technical assistance and/or useful discussions: Andrew Rodenhiser, Fred Morin, Joanne Turnbull (Concordia), Louis Godbout, Michel Boulay, Rick Rossi, Seth Fraden (Brandeis), and Boris, the friendliest plumber to walk this campus.

I would also like to acknowledge the staff of both the Chemistry Department and the Pulp and Paper Research Centre, especially Colleen McNamee for bringing life into the building. I appreciate the support of the Chemistry Department, in particular the Departmental Chairs and Graduate Research Advisors: Drs. Lennox, Harpp, and Damha. I am grateful for financial support through the following scholarships: Pall Dissertation Scholarship, Eastman Summer Fellowship, Alexander McFee Memorial Fellowship, NSERC PGS B Scholarship, and the Max Stern Recruitment Scholarship.

As everyone knows, there is more to life than chemistry. I would like to thank the members of the CGSS who worked with me to expand the activities of the chemistry department beyond the lab bench. I will miss the cross-country and downhill ski trips organized by PAPRICAN each year, but will cherish the friendships made. I appreciate the Montreal-area orienteering clubs for giving me the opportunity to escape from the city and run fervently through the woods -- I'm sure my supervisor is thankful for John Charlow, orienteering authority, who taught me everything I needed to know to find my way back to the lab bench in Montreal.

Moving to Montreal to pursue a Ph. D. was not an easy decision, but now I am thankful to Brian Thorndyke for encouraging this choice and pushing me into grad school in the first place. I appreciate his supportive e-mails during the times when I was not as certain about life in grad school. I would also like to thank my friends and colleagues in Chemistry and Pulp and Paper for making Montreal eventually feel like home, especially those who coincidentally hail from my hometown. Special thanks to Jason, Maggie, Maren, Patrick, Ron, and Susan for helping me prepare for my defence.

The fun, the adventure, and the joie de vivre that is Quebec would not have been experienced without my enthusiastic companion, Sylvia, whom I met orienteering. Many thanks for dragging me out of the lab for excursions from dog sledding to canoeing to consuming trop de sirop d'érable. At times it was necessary to stay in the lab and work late -- these times were made easier because I knew others were thinking of me. Bob, an inspirational chemical educator, would frequently call the lab on Sundays from his lakeside cottage in beautiful British Columbia to offer encouraging words of support. And I would like to thank Dave who helped me make it through the final stretch by bringing me dinner in the lab.

Finally, I should mention something about my parents here because I know this is the only part of my thesis they will read. I would like to thank them for helping me establish strong roots, for giving me freedom when I needed to fly, and especially for the long distance calling card. I enjoyed the many phone conversations we shared and I appreciate their patience during my extensive academic career. Many thanks also to my brother, Mike, and sister-in-law, Colleen, for their friendship and support and their patience when I try to discuss chiral nematic liquid crystals made out of trees. In closing, I would like to thank my mom for supporting the pulp and paper industry by writing me weekly letters, which now make up a discourse longer than this thesis.

## TABLE OF CONTENTS

Abstract.....	ii
Résumé.....	iii
Preface.....	iv
Acknowledgements.....	vii
Table of Contents.....	ix
List of Figures.....	xii
List of Tables.....	xv
List of Symbols and Abbreviations.....	xvi

### **Chapter 1 General Introduction and Literature Review**

1.1 Introduction.....	2
1.2 Cellulose.....	2
1.3 Liquid Crystals.....	7
1.4 Colloidal Liquid Crystals.....	12
1.4.1 Colloidal Particles.....	12
1.4.2 Spherical Colloids.....	14
1.4.3 Rod-like Colloids.....	18
1.5 Cellulosic Liquid Crystals.....	20
1.5.1 Liquid Crystalline Phases of Cellulose and Cellulose Derivatives... 20	
1.5.2 Liquid Crystalline Phases of Colloidal Cellulose Nanocrystals..... 22	
1.6 Outline of Thesis Research.....	24
1.7 References.....	26

### **Chapter 2 Characterization of Cellulose Nanocrystals by Atomic Force Microscopy**

2.1 Introduction.....	30
2.2 Experimental.....	31
2.2.1 Sample Preparation.....	31
2.2.2 Atomic Force Microscopy.....	32

2.2.3	Transmission Electron Microscopy.....	33
2.3	Results and Discussion .....	33
2.4	Conclusions.....	44
2.5	References.....	45

### **Chapter 3 The Influence of Dextran on the Phase Behaviour of Suspensions of Cellulose Nanocrystals**

3.1	Introduction.....	47
3.2	Experimental.....	48
3.2.1	Materials and Stock Solutions.....	48
3.2.2	Preparation of Cellulose-Dextran Suspensions.....	48
3.2.3	Sample Analysis.....	49
3.3	Results and Discussion .....	50
3.3.1	Isotropic Samples.....	50
3.3.2	Biphasic Samples.....	51
3.3.3	Anisotropic Samples.....	58
3.4	Conclusions.....	65
3.5	References.....	66

### **Chapter 4 Induced Circular Dichroism of Chiral Nematic Cellulose Films**

4.1	Introduction.....	69
4.2	Experimental.....	71
4.2.1	Sample Preparation .....	71
4.2.2	Instrument Measurements.....	72
4.3	Results and Discussion .....	73
4.3.1	Films with reflection band in the infrared region .....	73
4.3.2	Films with reflection band in the visible region .....	75
4.3.3	Films with reflection band in the ultraviolet region .....	76
4.3.4	Magnetic Alignment.....	79
4.4	Conclusions.....	82
4.5	References.....	82

## **Chapter 5 Characterization of Model Cellulose I Surfaces Created from Nanocrystal Suspensions**

5.1	Introduction.....	85
5.2	Experimental.....	86
5.2.1	Sample Preparation .....	86
5.2.2	X-ray Photoelectron Spectroscopy.....	86
5.2.3	X-ray Analysis.....	87
5.2.4	Atomic Force Microscopy.....	87
5.3	Results and Discussion .....	88
5.3.1	X-ray Photoelectron Spectroscopy of Cellulose Films.....	88
5.3.2	X-ray Diffraction Analysis of Cellulose Films .....	90
5.3.3	Creating Smooth Cellulose I Surfaces .....	98
5.3.4	Creating Oriented Cellulose I Surfaces ..	101
5.3.5	Assessing the Stability of Cellulose Films.....	104
5.4	Conclusions.....	105
5.5	References.....	105

## **Chapter 6 General Conclusions**

6.1	Conclusions.....	108
6.2	Original Contributions to Knowledge.....	109
6.3	Suggestions for Future Research.....	110

APPENDIX.....	A1
Theories on the Phase Behaviour of Rod-like Particles and Rod-Coil Systems	

## LIST OF FIGURES

Figure 1.1	Schematic drawing of the anhydrocellobiosyl repeat unit that makes up the backbone of the cellulose chain.	4
Figure 1.2	Schematic drawing of a cotton fibre and a wood fibre. The lines within the primary and secondary walls depict the microfibril orientation.	5
Figure 1.3	Schematic drawings of isotropic, nematic, and smectic phases of rod-like particles.	10
Figure 1.4	Schematic drawing of a chiral nematic liquid crystal, shown over the distance $P/2$ , or half of the chiral nematic pitch.	11
Figure 1.5	Schematic drawing of the forces in DLVO theory.	15
Figure 1.6	Qualitative representation of the free energy versus the dispersion density for colloidal spheres in both the fluid and solid phases, showing that at low densities the fluid phase is more stable and at high densities the solid phase is more stable.	17
Figure 2.1	Schematic diagram of tip-sample convolution.	34
Figure 2.2	Contour profile (upper) and AFM image (lower) of cellulose nanocrystals illustrating particle length measurement.	35
Figure 2.3	AFM image of cellulose nanocrystals derived from Whatman filter paper illustrating the aggregation of longer particles. Image is 10 $\mu\text{m}$ by 10 $\mu\text{m}$ , shown in deflection mode.	37
Figure 2.4	AFM image of cellulose nanocrystals derived from wood pulp showing some clumping of particles. Image is 10 $\mu\text{m}$ by 10 $\mu\text{m}$ , shown in deflection mode.	38
Figure 2.5	AFM image of cellulose nanocrystals derived from Whatman filter paper showing a more even distribution of particles. Image is 4 $\mu\text{m}$ by 4 $\mu\text{m}$ , shown in deflection mode.	39
Figure 2.6	TEM image of cellulose nanocrystals derived from Whatman filter paper.	40
Figure 2.7	Histograms of particle lengths of cellulose nanocrystals derived from Whatman filter paper and measured by TEM (upper), derived from Whatman filter paper and measured by AFM (middle), and derived from wood pulp and measured by AFM (lower).	41
Figure 2.8	Histograms of particle widths of cellulose nanocrystals derived from Whatman filter paper and measured by TEM (upper), derived from Whatman filter paper and measured by	43

	AFM (middle), and derived from wood pulp and measured by AFM (lower).	
Figure 3.1	Digital photograph of samples with the same blue dextran concentration in each vial and increasing cellulose concentration from Vial A to E (see Table 3.1), showing the preferential partitioning of blue dextran into the upper isotropic phase.	53
Figure 3.2	Partition coefficients for dextran between isotropic and anisotropic phases versus cellulose concentration for samples B to E. Upper trend line (squares) shows experimental values and lower trend line (triangles) shows theoretical values calculated using Equation III.3.	54
Figure 3.3	Partial phase diagram of cellulose suspension with blue dextran added, using data from samples 1 to 5 (Table 3.2). The number densities of the rods and coils are multiplied by $R_g^3$ , where $R_g$ is the radius of gyration of the dextran coil, in order to make the values dimensionless. The isotropic region, I, is on the left hand side and the chiral nematic region, N, is in the lower right hand corner. The downward sloping tie lines in the biphasic region indicate that the isotropic phase is rich in coils and the anisotropic phase is rich in rods.	57
Figure 3.4	Volume fraction of upper isotropic phase versus time for phase separation of an initially anisotropic sample (13.0 wt% nanocrystals) induced by adding increasing amounts of blue dextran to Vials I to IV.	59
Figure 3.5	Partition coefficient versus dextran concentration for biphasic samples 2 to 5 and anisotropic samples III and IV. Upper trend line (squares) shows experimental values and lower trend line (triangles) shows theoretical values, calculated using Equation III.3.	61
Figure 3.6	Photomicrograph between crossed polarizers of the upper dextran-rich phase (scale bar 100 $\mu\text{m}$ ).	62
Figure 3.7	Photomicrograph between crossed polarizers of a completely anisotropic sample before the addition of blue dextran showing characteristic fingerprint texture and only a few disclinations (scale bar 100 $\mu\text{m}$ ).	63
Figure 3.8	Photomicrograph between crossed polarizers of a lower dextran-poor phase showing distorted fingerprint texture and numerous disclinations (scale bar 100 $\mu\text{m}$ ).	64

Figure 4.1	ICD spectra of cellulose films with reflection band in the IR region. The films were doped with Trypan blue ( $1.9 \times 10^{-5}$ , $4.8 \times 10^{-5}$ , $9.6 \times 10^{-5}$ g).	74
Figure 4.2	Photomicrograph between crossed polars of the grainy polydomain texture of a cellulose film that reflects light in the IR region (scale bar 1mm).	78
Figure 4.3	Photomicrographs between crossed polars of cellulose films (reflection band in IR region) aligned in a 2.1 T magnetic field (upper) and a 7.1 T magnetic field (lower). The magnetic field was oriented normal to the plane of the images (scale bar 1mm).	80
Figure 4.4	ICD spectra of cellulose films (reflection band in IR region) doped with Trypan blue ( $9.6 \times 10^{-5}$ g) and dried (a) with no aligning field; (b) in a 2.1 T magnetic field; (c) in a 7.1 T magnetic field. The magnetic field was applied normal to the plane of the film.	81
Figure 5.1	High-resolution carbon spectra for cellulose films derived from Whatman (upper) and wood pulp (lower) suspensions. The right-most peak at 285 eV is the C1 peak, the middle peak is the C2 peak, and the left-hand peak is the C3 peak. The area under the tail of C3 peak has been added to the C3 peak.	91
Figure 5.2	The valence band spectrum for a cellulose film derived from the Whatman suspension shows the pattern expected for a cellulose sample.	93
Figure 5.3	Schematic diagram showing the 002, $10\bar{1}$ , and 101 planes for both cellulose I and cellulose II.	95
Figure 5.4	An X-ray powder diffraction diagram for a cellulose film derived from the Whatman suspension, showing the major diffraction rings $10\bar{1}$ , 101, 021, and 002.	96
Figure 5.5	AFM images of a film cast from the Whatman suspension (upper) and a film cast from the wood pulp suspension (lower). A contour profile from a line across the middle of the image is shown next to each sample. Images are $1 \mu\text{m}$ by $1 \mu\text{m}$ , shown in height mode.	102
Figure 5.6	A digital image between crossed polarizers of a cellulose suspension spin-coated onto a glass surface, showing the radial orientation of the cellulose nanocrystals. The polarizers are oriented vertically and horizontally and the scale bar is 5 mm.	103

## LIST OF TABLES

Table 3.1	Composition of biphasic samples with fixed total dextran concentration and increasing concentration of cellulose nanocrystals.	52
Table 3.2	Composition of biphasic samples with increasing total dextran concentration and fixed concentration of cellulose nanocrystals.	56
Table 5.1	Elemental surface concentrations for cellulose films derived from wood pulp and Whatman suspensions.	89
Table 5.2	Surface concentrations of carbon for cellulose films derived from wood pulp and Whatman suspensions compared to theoretical values.	92
Table 5.3	X-ray band intensity and d-spacing of our model cellulose film compared to literature values.	97
Table 5.4	$2\theta$ angles for samples of cotton in both cellulose I and cellulose II forms compared to our model cellulose film.	99
Table 5.5	Roughness values determined from AFM images for cellulose films prepared by a variety of methods compared to mica.	100

## LIST OF SYMBOLS AND ABBREVIATIONS

$A_L$	Absorption of left-handed CPL
$A_R$	Absorption of right-handed CPL
$B_{rc}$	Second virial coefficient of the rod-coil interactions
$c_r^n$	Number density of rods in the nematic phase
$c_r^i$	Number density of rods in the isotropic phase
$d$	Interplanar spacings
$D$	Diameter of rods
$D_{eff}$	Effective diameter of rods
$d_a$	Concentration of blue dextran in the anisotropic phase
$d_i$	Concentration of blue dextran in the isotropic phase
$h$	Distance between the surface of spheres
$I$	Isotropic region
$K$	Partition coefficient
$k_B T$	Thermal energy
$L$	Length of rods
$\lambda$	Wavelength of maximum reflection
$\lambda_0$	Wavelength of the chiral nematic reflection band
$\lambda_{ab}$	Wavelength of dye absorption
$n$	Average refractive index
$N$	Chiral nematic region
$P$	Chiral nematic pitch
$R$	Radius of spheres
$R_g$	Radius of gyration of coils
$R_{max}$	Maximum z-range
$R_q$	Root-mean-square roughness
$\varphi$	Angle of incidence
$\varphi_a$	Volume fraction of rods in the anisotropic phase
$\varphi_i$	Volume fraction of rods in the isotropic phase

$\phi_r$	Volume fraction of rods
AFM	Atomic force microscopy
APC	Acetoxypropyl cellulose
CD	Circular dichroism
CPL	Circularly polarized light
DLVO Theory	Derjaguin, Landau, Verwey, and Overbeek Theory
DP	Degree of polymerization
HPC	Hydroxypropyl cellulose
ICD	Induced circular dichroism
IR	Infrared
ORD	Optical rotatory dispersion
PTFE	Poly(tetrafluoroethylene)
TEM	Transmission electron microscopy
TMV	Tobacco mosaic virus
UV	Ultraviolet
XPS	X-ray photoelectron spectroscopy

## **Chapter 1**

### **General Introduction and Literature Review**

## 1.1 INTRODUCTION

This research brings together the unique properties of both cellulose and liquid crystals. Cellulose and liquid crystals have been studied individually for many years, but research on cellulosic liquid crystals is relatively recent. By way of introduction, we will first explore some general properties of cellulose, including its chemical composition and macromolecular structure. Then we will examine some basic properties of the main types of liquid crystals, focusing on the chiral nematic phase formed by cellulose nanocrystals. Since the liquid crystals studied in this thesis consist of colloidal particles, we will discuss some background on colloidal particles and introduce examples of liquid crystals formed from both spherical and rod-like colloids. Finally, we will review the existing research on cellulosic liquid crystals.

## 1.2 CELLULOSE

Cellulose nanocrystals were prepared from two different sources: wood pulp and cotton. Wood has four main components: cellulose, hemicellulose, lignin, and extractives; however, the latter three components can be removed during the pulping process, resulting in a fairly pure cellulose. Since wood initially consists of 40-50% cellulose, extensive processing is required to isolate the desired material. On the other hand, cotton requires minimal initial processing as it contains a very high percentage of cellulose, ranging from 95-99%<sup>1</sup>. Highly purified wood pulp, which was used for this research, known as chemical cellulose or dissolving pulp, also contains 95-99% cellulose.

Cellulose fibres are hierarchical structures built up of several different levels of organization. At the atomic level, cellulose consists of carbon, oxygen, and hydrogen arranged to form anhydro-D-glucose residues. Two anhydroglucose residues rotated 180° about the chain direction and linked in a  $\beta$ -1,4 bond form anhydrocellobiosyl, the repeating unit of crystalline cellulose. The anhydroglucose residues adopt the stable chair conformation with the hydrogen atoms in the axial positions and the larger hydroxyl groups in the equatorial positions, allowing for close packing of cellulose chains<sup>2</sup>.

Cellulose is a relatively rigid, straight chain glucose polymer with  $\beta$ -1,4 linkages (Figure 1.1). In contrast, other D-glucose polymers are more flexible, such as amylose, which has  $\alpha$ -1,4 linkages, and dextran, which has  $\alpha$ -1,6 linkages with some  $\alpha$ -1,3 branching.

In the first level of the supermolecular structure of cellulose, several long cellulose chains are packed together at regular lateral intervals with hydrogen bonding between the chains. The basic repeat unit of this chain packing arrangement, which was determined using X-ray diffraction, is called the unit cell. Several unit cells are connected to form elementary fibrils, which in turn are combined to form microfibrils. The microfibrils come together to form sheets, or lamellae, which make up the layers in the cellulose fibre wall.

The fibre structures of wood and cotton are quite similar, as seen in Figure 1.2. Both fibres contain a primary wall in which the microfibrils wind in both directions. The secondary wall of both fibres is made up of three layers: a thin outer S1 layer, a thick S2 layer with a small microfibril angle, and a thin S3 layer. The dominant S2 layer determines most of the fibre properties. Although the fibre wall structures are similar, a more detailed examination reveals differences between cotton and wood, such as their composition, as stated previously, and their crystallinity.

When cellulose chains come together in elementary fibrils they form both highly ordered regions and disordered regions. According to the fringed micellar model, highly ordered crystalline areas lead into disordered amorphous areas without a distinctive boundary<sup>3</sup>. The crystalline regions, or crystallites, or nanocrystals, can be 100-250 nm long with average cross-sections of 3 nm x 10 nm<sup>4</sup>. The exact size of the crystallites will depend on the source of cellulose, the method of purification, and the technique used to determine the crystallite dimensions. Since the crystalline regions are much more resistant to acid degradation than the amorphous regions, the crystallite length can be determined by measuring the degree of polymerization (DP) after prolonged exposure to acid. This leveling-off DP shows that, in general, cotton crystallites are longer than wood crystallites, with average literature values ranging from 200-350 for cotton and 150-300 for wood cellulose<sup>5</sup>. Not only do the crystallites tend to be larger in cotton samples, but also the degree of crystallinity, which indicates the proportion of crystalline cellulose, is higher for cotton than for wood<sup>4,6,7</sup>.

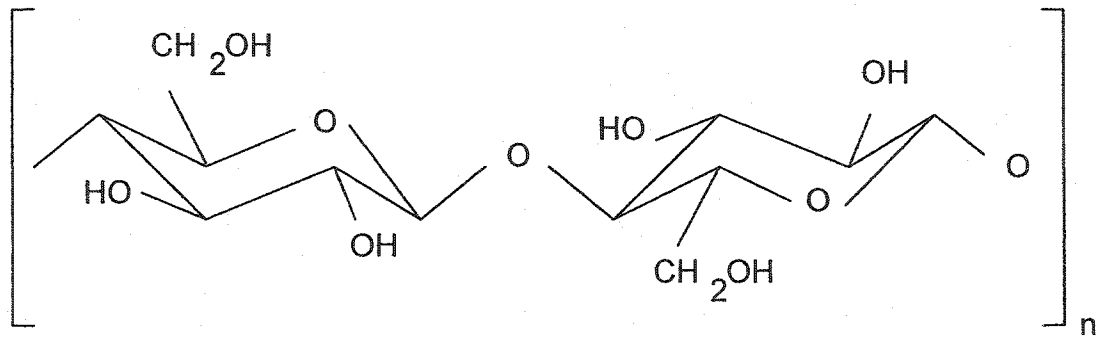


Figure 1.1 Schematic drawing of the anhydrocellobiosyl repeat unit that makes up the backbone of the cellulose chain.

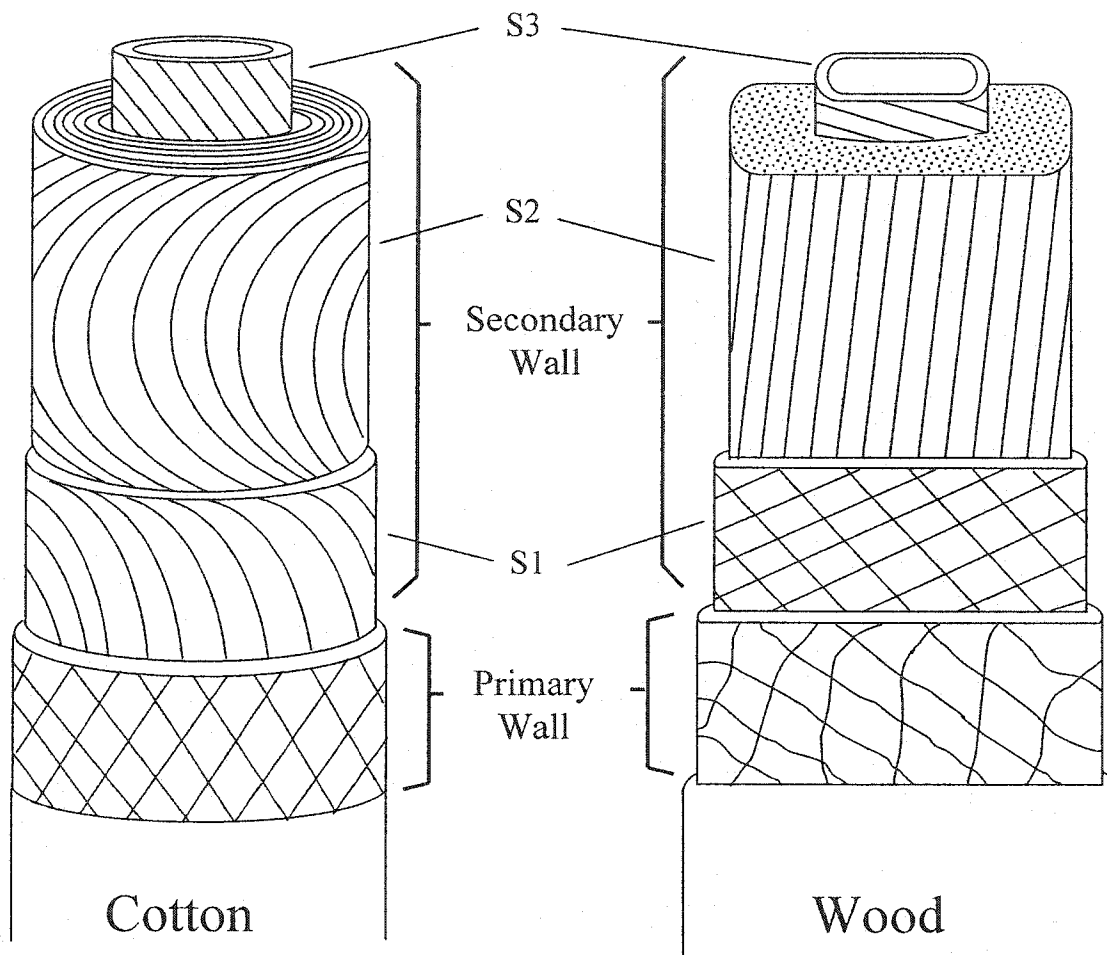


Figure 1.2 Schematic drawing of a cotton fibre and a wood fibre. The lines within the primary and secondary walls depict the microfibril orientation.

Examination of the crystalline regions of cellulose by X-ray diffraction indicates the existence of multiple crystalline forms, or polymorphs<sup>8</sup>. From the X-ray diffraction data, one can determine the dimensions of the unit cell. It was found that some chemical treatments changed the arrangement of cellulose chains within the unit cell. Native cellulose, termed cellulose I, has a distinct diffraction pattern from those of the “man-made” crystalline forms, known as cellulose II, III, and IV. Although there is still some controversy as to the exact structure of the unit cell, early work in this area by Meyer and Misch determined the unit cell dimensions for cellulose I to be  $a=0.835$  nm,  $b=0.79$  nm,  $c=1.03$  nm (fibre axis), and  $\gamma=96^\circ$ <sup>9</sup>. These researchers suggested that the two chains in the monoclinic unit cell were antiparallel, but more recent research supports a parallel arrangement of chains<sup>10</sup>.

The controversy surrounding the precise structure of cellulose I is partly because it is actually composed of two distinct crystalline forms, cellulose  $I_\alpha$  and cellulose  $I_\beta$ <sup>11</sup>. Cellulose  $I_\alpha$ , which is present in greater proportions in algal and bacterial cellulose, has a triclinic unit cell; cellulose  $I_\beta$ , which is predominant in higher plants, has a monoclinic unit cell<sup>12,13</sup>. A recent study using synchrotron X-ray and neutron fiber diffraction has determined the cellulose  $I_\beta$  dimensions to be  $a=0.7784$  nm,  $b=0.8201$  nm,  $c=1.038$  nm (fibre axis), and  $\gamma=96.5^\circ$ <sup>14</sup>. The two distinct forms of cellulose I co-exist within microfibrils. Research has shown that for algal cellulose,  $I_\alpha$  is predominant on the surface<sup>15</sup>. More research is required to determine the locations of  $I_\alpha$  and  $I_\beta$  cellulose in higher plants, such as wood and cotton.

Both crystalline forms of cellulose I can be distinguished from regenerated cellulose. In the regenerated forms of cellulose, the cellulose chains are shifted and turned with respect to the native form and they sometimes switch from a parallel to an antiparallel arrangement. Cellulose II is a common form of regenerated cellulose because its antiparallel packing structure makes it thermodynamically stable<sup>16</sup>. As a result, the transformation from cellulose I to cellulose II is irreversible. Since the arrangement of chains, and thus the intra- and inter-chain hydrogen bonding, is different in native cellulose its reactivity will be different than that of the regenerated forms<sup>17</sup>.

Cellulose fibres consist of a unique hierarchical structure built up from glucose molecules, to cellobiose, to cellulose chains packed in a unit cell, to elementary fibrils, to

microfibrils joined in lamellae to form the fibre walls. Since D-glucose is optically active, and organized structures composed of chiral materials are also chiral, cellulose is a chiral biopolymer. Cellulose is one of the most accessible chiral materials, but little use has been made of this property. The chiral properties of cellulose are exhibited differently at different levels of structure, from individual cellulose chains, to microfibrils within wood fibres, to macroscopic materials. In this work, the liquid crystalline behaviour of the cellulose nanocrystals is greatly influenced by the chiral nature of cellulose. The rod-like shape of the cellulose nanocrystals allows the formation of a nematic liquid crystal, but the chirality of the material adds an extra twist, forming a chiral nematic liquid crystal.

### 1.3 LIQUID CRYSTALS

The three common states of matter are familiar and tangible, but liquid crystals seem mysterious and paradoxical; even the name seems contradictory. Liquid crystals are actually fluids, but they possess characteristics both of liquids, having some degree of fluidity, and of solids, displaying some long-range order and anisotropy. There are several classes of liquid crystals, including nematic, smectic, and cholesteric phases, which have different organizational patterns. Just as cellulose varies in its degree of order from crystalline to amorphous regions, liquid crystals may vary in their degree of order, undergoing phase transitions between ordered states, similar to solid-liquid-gas transitions.

The transition to a liquid crystal phase was first observed by Friedrich Reintzer, an Austrian botanist studying the role of cholesterol in plants, who noticed that some cholesterol derivatives seemed to have two melting points, first melting to a cloudy fluid and subsequently to a clear fluid<sup>18</sup>. Otto Lehmann, a German physicist, characterized the fluid and crystalline behaviour of these samples using a polarized light microscope and a heating stage, and called the new substances liquid crystals<sup>18</sup>.

Although ordered structures can be formed with spherical particles, liquid crystals are typically formed by anisotropic particles, such as a rod, sheet, or disc<sup>19</sup>. This

anisotropic shape allows the liquid crystal to have both positional and orientational order, whereas spherical particles can only adopt positional ordering. Most liquid crystals possess orientational order, meaning that the particles align with their long axes oriented in a particular direction, and some liquid crystals possess positional order, meaning that the particles occupy a specific place relative to the other particles<sup>20</sup>. The positional order may be one, two, or three dimensional, but it is not as rigid as a true crystal where molecules are locked into specific lattice sites. The particles themselves are usually small molecules, but they can also be polymers, colloidal particles, or even micelles.

The transition to the liquid crystalline state may be induced by changing the temperature, thermotropic mesomorphism, or by changing the concentration, lyotropic mesomorphism<sup>21</sup>. Since the liquid crystalline state lies between the solid and liquid states, slow heating of a thermotropic solid will cause it to pass through the liquid crystal phase, which will appear cloudy, before progressing into the clear liquid phase. Sometimes the material may pass through more than one liquid crystal phase, such as from a highly ordered smectic phase to a less ordered nematic phase, as it melts into a liquid. As the material is heated, the rigid crystal structure of the solid is lost, but the particles maintain some order by generally orienting with their long axes along a given direction.

Increasing the concentration of rod-like particles suspended in a solvent will bring about the phase transition for a lyotropic liquid crystal. At dilute concentrations, the rods are all tumbling randomly, but as the concentration increases the rods tend to align parallel to neighbouring rods. It is important to note that this is not a rigid, static alignment, but more a preferred direction as the rods continue to move over time. This preferred direction, often designated by an arrow in schematic drawings, is called the director of the liquid crystal. An order parameter can be determined by averaging the directions of the rods with respect to the director using the formula

$$\frac{1}{2}(3 \cos^2 \theta - 1) \tag{I.1}$$

where  $\theta$  is the angle between the rod and the director<sup>22</sup>. An order parameter of 1 indicates perfect alignment, and 0 indicates complete randomness, as found in a normal liquid. For thermotropic liquid crystals, the order parameter decreases as the temperature increases.

The simplest type of liquid crystal is the nematic phase, where the rods are aligned in one preferred direction, with a random distribution of their centres of gravity (Figure 1.3). In a polarized microscope the nematic phase has many thread-like defects and so the phase was named for the Greek word for thread<sup>23</sup>. Nematic liquid crystals have a high degree of orientational order, but no positional order<sup>21</sup>. At lower temperatures many materials pass from nematic mesophases to smectic phases, from the Greek word for soap as many soaps form such phases<sup>18</sup>. Smectic phases have a higher degree of order than nematic phases because they not only possess the orientational order of a preferred rod direction, but also they have positional order as the rods align their centres of gravity to form layers (Figure 1.3). Numerous smectic phases, named with letters in order of discovery, have been identified by their unique appearance in a polarized microscope, all with a distinct positioning of rods. In the smectic A phase the rods are aligned perpendicular to the plane of the layers, while in the smectic C phase the rods do not stand straight up – they are slanted within each layer<sup>23</sup>.

Biopolymers, such as cellulose and chitin, have been shown to form liquid crystal phases. The inherent chirality of these materials influences the structure of the resultant liquid crystals. In the first layer, the rods are oriented in a preferred direction, like the nematic phase described above. In subsequent layers, however, the director is twisted with respect to the layer below, generating a helical superstructure in the direction perpendicular to the directors (Figure 1.4). Since cholesterol esters take on this helical structure, this phase has been named the cholesteric phase. Cholesteric, or chiral nematic, liquid crystals are interesting because they can have Bragg reflections in the visible spectrum, giving the material a characteristic colour.

The most common way to identify and characterize liquid crystal phases is with a polarizing light microscope<sup>24</sup>. The sample is placed on the microscope stage between two crossed polarizers. Normally, two linear polarizers oriented 90° to each other would extinguish all of the light; however, the ordered nature of liquid crystals allows light to pass through in a characteristic pattern. The observed pattern, or texture, is used to determine the order within the liquid crystal. The defects in an ordered phase add to the texture of the sample and aid in identification, since certain defects are common to particular types of liquid crystals.

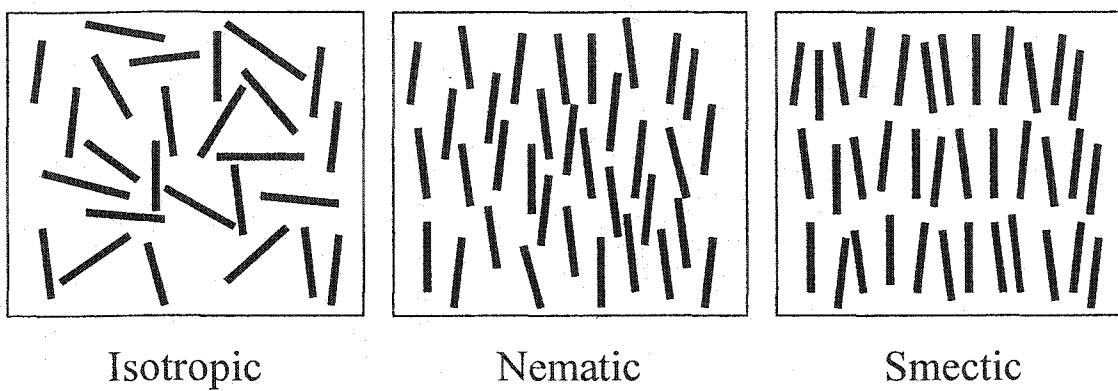


Figure 1.3 Schematic drawings of isotropic, nematic, and smectic phases of rod-like particles.

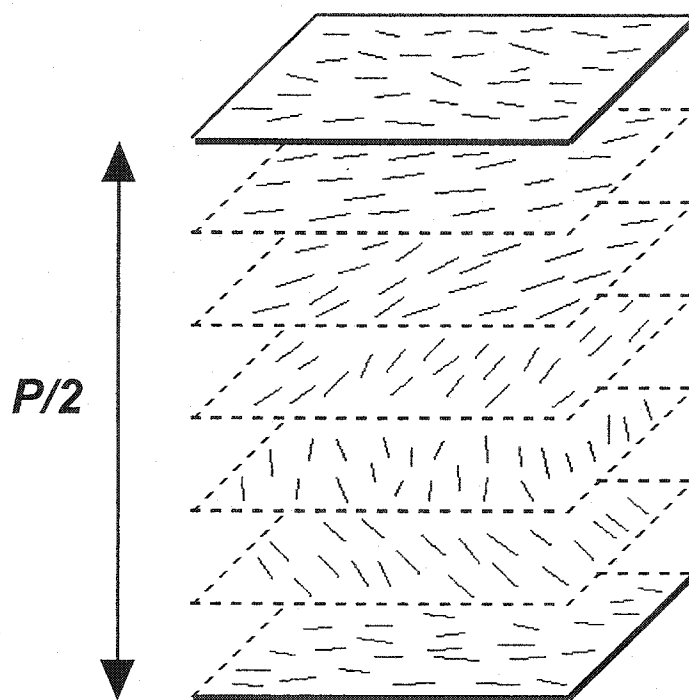


Figure 1.4 Schematic drawing of a chiral nematic liquid crystal, shown over the distance  $P/2$ , or half of the chiral nematic pitch.

Since cellulose nanocrystals form chiral nematic phases, we will examine these textures in more detail. The dominant textures formed by chiral nematic liquid crystals are Grandjean and fingerprint. The Grandjean, or planar texture, is seen when the helix axis is parallel to the viewing direction<sup>25</sup>. This texture has a coloured background broken up by dark lines running through it randomly like shattered glass. The background represents ordered domains and the dark lines are disclination lines, or areas where the liquid crystalline order is interrupted by imperfections. Fingerprint texture can be seen when the helical axis is perpendicular to the viewing direction. The texture appears as a series of light and dark lines, winding into a pattern much like a fingerprint. In a chiral nematic liquid crystal, the pitch of the helical superstructure is defined as the distance required for the rods, or the director, to complete one full rotation<sup>23</sup>. The lines in the fingerprint texture appear every time the rods point back to the same direction, which occurs every half-pitch<sup>25</sup>. When the parallel fingerprint lines come together at a point this indicates a defect, or disclination.

## **1.4 COLLOIDAL LIQUID CRYSTALS**

The first liquid crystal observed was composed of rigid molecules, and still today typical liquid crystals are molecular in nature. More recently, there has been an interest in the liquid crystalline properties of colloidal particles. Ordered phases of colloidal particles were first investigated with spherical particles. Subsequently, rod-like colloids were examined. In this section we will first discuss the unique properties of colloidal particles that distinguish them from other larger particles. Then we will review some of the research on ordered phases of spherical and rod-like colloids.

### **1.4.1 Colloidal Particles**

Colloidal particles are unique because of their small size. Size is the defining characteristic of colloid particles, which range from about 1 nm to 1  $\mu\text{m}$ <sup>26</sup>. Because of their small size, colloid particles have many unique characteristics. Colloids come in many different forms depending on whether solid, liquid, or gas particles are dispersed in

a solid, liquid or gas phase<sup>27</sup>. Solid particles dispersed in a liquid will be the main focus of this work. Such colloids are referred to as suspensions, dispersions, or sometimes sols.

The solid particles within the suspension are in constant motion, called Brownian motion, after its discoverer Robert Brown in 1827<sup>28</sup>. Brownian motion is caused by the random movement of molecules in the liquid part of the suspension. These molecules are constantly colliding with the solid particles in the suspension, causing a random motion. For particles within the colloidal range smaller particles vibrate more than larger particles, which are more difficult to move in collisions. Colloidal cellulose nanocrystals experience Brownian motion, whereas larger pulp fibres do not.

The term suspension is appropriate for describing this colloidal system because the small colloidal particles are suspended in the liquid. What keeps suspensions stable? What prevents the particles from all settling on the bottom, as would sand or pepper? As the particles begin to settle a concentration gradient is formed. Consider an imaginary horizontal line through a beaker of a colloidal suspension. Due to the concentration gradient there are more particles below the line than above the line. Still, all the particles are in Brownian motion moving in random directions. At the imaginary line there will be a net flux of particles in the upward direction simply because there are more particles below the line. This effect counteracts the settling of the particles under gravity. Thus, the diffusion effect of particles moving into less concentrated areas is actually due to Brownian motion.

The overall stability of colloidal suspensions can be determined by examining all of the forces acting on the colloid particles. The random forces involved in Brownian motion and van der Waals forces are both universal forces that act on colloidal particles. Electrostatic forces will also play a role if the particles are charged. External forces such as gravity and magnetic and electrical fields may also be present and have an influence on colloidal stability. The different forces present in a system often have opposing effects; therefore, it is important to determine which force is dominant for a particular system. Derjaguin, Landau, Verwey, and Overbeek devised a theory (DLVO theory) that combines the effects of van der Waals attractions and electrostatic repulsions, determining the dominant force as a function of particle separation<sup>28</sup>.

Electrostatic forces start at a finite value and the repulsion decreases as particle separation increases. Van der Waals forces are attractive and become larger as particles get closer until strong hard-core repulsion occurs at extremely small separations. The forces felt by the colloid particles will be the sum of van der Waals forces and electrostatic forces. The total potential energy of interaction is shown in Figure 1.5, as a sum of the repulsion energy and the attraction energy. The solid line in Figure 1.5 depicts a deep well, which is called the primary minimum, and a smaller well to the right, which is the secondary minimum -- the hill between the two is called the energy barrier.

The main factor in determining colloid stability is the energy barrier between the secondary and primary minimums, which prevents particles from coming into contact. If there is a large energy barrier the suspension will be stable. For a small energy barrier, the particles may reach the primary minimum and coagulate. Particles may come into contact in the secondary minimum as well, but if it is not very deep Brownian motion can break up the flocs. The magnitude of the energy barrier depends on the surface potential of the particles and on the ionic strength of the solution. Higher surface potentials lead to higher energy barriers. In contrast, an increase in electrolyte concentration leads to a decrease in energy barrier. Thus, adding salt to a suspension will cause coagulation at a critical concentration. In order to compare experimental results with theory, certain parameters of the experimental system must be measured. For example, for DLVO theory important parameters include surface potential and electrolyte concentration.

As the concentration of colloidal particles in a suspension increases, space becomes a premium. At a given concentration, the random behaviour of the particles changes in order to maximize the space available. In the next section we will discuss the spontaneous formation of ordered phases of spherical colloidal particles.

### **1.4.2 Spherical Colloids**

Researchers have been familiar with colloidal suspensions of spherical particles for many years. Since these colloidal spheres share some similarities with atomic and molecular systems, researchers have been able to draw on existing knowledge about the behaviour of simple liquids. Interest in these colloidal systems increased with technological advances enabling the production of uniform spherical particles, with a size

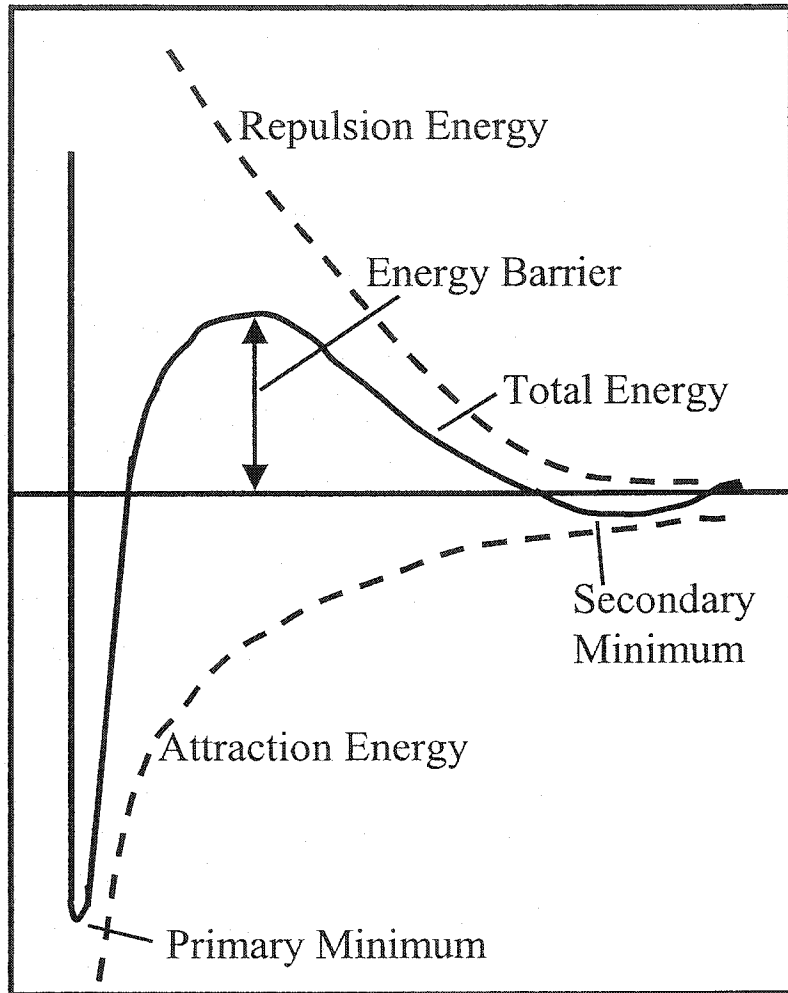


Figure 1.5 Schematic drawing of the forces in DLVO theory.

polydispersity of less than 5%<sup>29</sup>. The uniform particle size allows for more accurate comparisons of experimental results with theoretical predictions and computer simulations, to help gain a greater understanding of particle-particle interactions.

Due to their relatively large size (as compared with atoms), the phase behaviour of these colloidal spheres can often be studied by optical means. As the density of the spherical particles within a host liquid is increased, a disorder-order transition may be observed. At low densities the spheres are in a “fluid phase” with all the particles distributed randomly, while at high densities the spheres form a “solid phase” or “colloid crystal phase” with the spheres adopting regular positions in a structured lattice.

As mentioned in the previous section, many colloidal systems are stabilized by electrostatic repulsion. When dispersed in polar liquids, spherical dispersions can be stabilized by surface charges<sup>30</sup>. In addition, the surface of the spheres can be modified, for example by grafting a short polymer chain to the surface, in order to sterically stabilize the colloidal dispersion. When the polymer chain is much shorter than the diameter of the sphere, the colloids behave very much like hard-spheres, and their interactions can be modelled by two basic forces: an excluded volume repulsion and a van der Waals attraction.

It has been shown, using van der Waals theory, that the order-disorder transition in hard sphere colloidal particles is driven by entropy, based on the concept of free volume<sup>29</sup>. If only one particle is in a volume,  $V$ , then the total volume is available to that particle. However, if two particles are in a volume,  $V$ , then each particle excludes a certain volume from the other particle since the particles cannot penetrate each other. Thus, for  $N$  particles in a volume,  $V$ , the free volume available to the particles is only a fraction of the total volume. As the free volume decreases, the entropy decreases, and the free energy of the system increases. In order to minimize the free energy, the system will phase shift in order to maximize the free volume.

Baus *et al.* calculated the free energy for both the fluid phase and the solid phase of colloidal spheres and plotted each against the density of the dispersion. This plot, which has been reproduced qualitatively in Figure 1.6, shows that at low densities the fluid phase exists and at high densities the solid phase is more stable. Thus, as the density of the dispersion increases the spheres take on a close-packed arrangement in

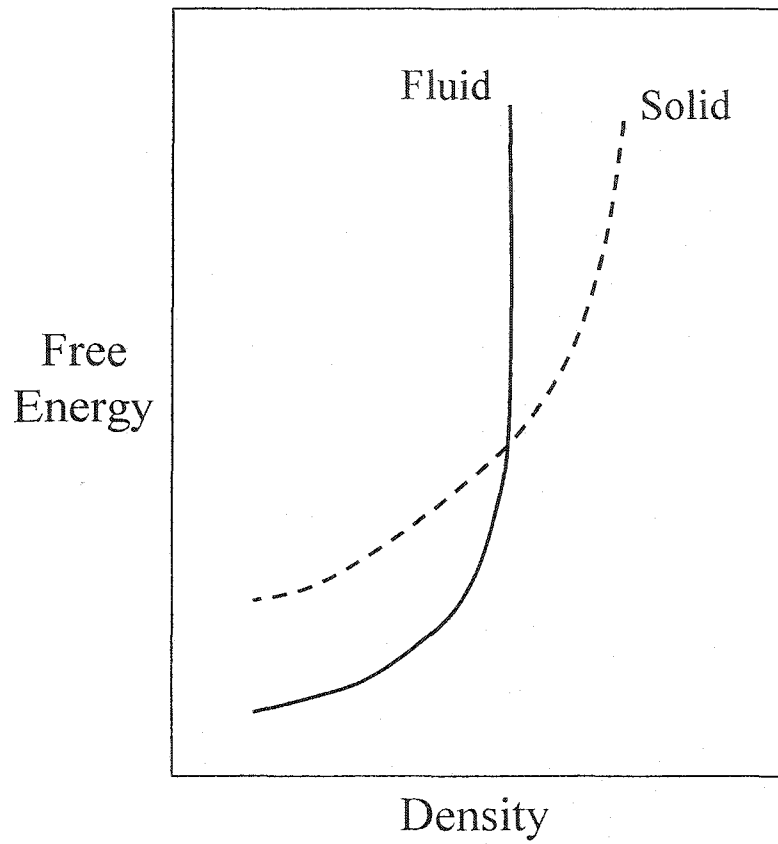


Figure 1.6 Qualitative representation of the free energy versus the dispersion density for colloidal spheres in both the fluid and solid phases, showing that at low densities the fluid phase is more stable and at high densities the solid phase is more stable.

order to maximize the free volume of the system. This disorder-order transition to a close-packed array of colloidal spheres has been observed in several experimental systems<sup>30-32</sup>.

### 1.4.3 Rod-like Colloids

As the concentration of rod-like colloids in a suspension increases, the particles adopt a close-packed arrangement in order to maximize the free space. This entropy-driven phase transition is similar to the behaviour of colloidal spheres. However, the anisotropic shape of the rod-like particles allows for the formation of more intricate phases. In addition to the positional order, observed in a spherical colloid crystal, the rod-like colloids can have orientational order. This extra degree of order enables the formation of several unique liquid crystalline phases, including nematic, smectic, and chiral nematic.

Phase separation of colloidal rods was first observed in 1936 with tobacco mosaic virus (TMV), a negatively charged rigid rod that undergoes an isotropic-nematic phase transition<sup>33</sup>. Below a certain rod density the particles tumble randomly in an isotropic suspension. Once the critical rod concentration is reached, the suspension separates into an upper isotropic layer and a lower nematic layer, with the rods oriented generally in one direction<sup>34</sup>. TMV is an ideal particle for the investigation of this phase transition because it is rigid, as shown by light scattering studies<sup>35</sup>, and it can be obtained in relatively monodisperse samples, with typical dimensions of 300 nm by 18 nm<sup>34,36</sup>.

The unique behaviour of the TMV rods attracted the attention of theoretical researchers. As the rods align into a nematic phase, they lose orientational entropy but this loss is compensated by a gain in free volume, or a decrease in excluded volume. Onsager considered this excluded volume effect, which is determined by the particle geometry, and devised a theory to determine the critical concentration at which the isotropic-nematic phase transition will occur<sup>37</sup>. The critical volume fraction for phase separation was deduced to be inversely proportional to the aspect ratio of the rods,  $L/D$ . Onsager theory is valid at low volume fractions of perfectly rigid, monodisperse rods with very high aspect ratios. A brief outline of Onsager's theory as well as SLO theory, which focuses on electrostatic interactions, is given in the appendix.

In contrast to the rigid TMV rods, somewhat flexible "whiskers" have been polymerized from tetrafluoroethylene, resulting in long rods with a uniform width of 20 nm and a length that varies from 1  $\mu\text{m}$  to over 20  $\mu\text{m}$ <sup>38</sup>. Upon standing for about four hours, the suspension of poly(tetrafluoroethylene) (PTFE) separates into an upper isotropic phase and a lower phase that is highly birefringent, characteristic of liquid crystalline nematic order. Although the longer PTFE particles (20  $\mu\text{m}$ ) fall outside the colloidal range, they still have enough mobility to form an ordered phase without flocculating. In addition to their great length, these PTFE whiskers are also flexible, showing that the isotropic-nematic phase transition is not restricted to rigid rods.

Colloidal boehmite,  $\gamma\text{-AlOOH}$ , can be prepared to form needles about 200 nm long and 10 nm wide<sup>39,40</sup>. These needles can be sterically stabilized by grafting a low molecular weight polymer to their surface<sup>41</sup>, similar to grafting of polymers on colloidal spheres. These grafted boehmite rods are presumed to act as model hard rods. The rods undergo an isotropic-nematic phase separation that qualitatively agrees with Onsager theory<sup>40</sup>.

Logically, inorganic akaganeite particles,  $\beta\text{-FeOOH}$ , in a colloidal suspension would behave much like inorganic  $\gamma\text{-AlOOH}$  particles. However,  $\beta\text{-FeOOH}$  particles actually form a smectic phase, a build up of schiller layers, meaning iridescent layers in German. After four to twelve months, dense sediment, with characteristic iridescent colours, deposits on the bottom of the reaction flask<sup>42</sup>. The thickness of the layers, which is determined by the particle length, must be comparable to the wavelength of light to see the iridescent colours. Since the height of each layer depends on the particle length, it is essential to have highly monodisperse particles in order to form a smectic phase. The phase behaviour of other mineral moieties is discussed in a recent review<sup>43</sup>.

The smectic phase has also been observed for some viruses, such as TMV, bacteriophage fd and the closely related M13 virus<sup>44,45</sup>. While many chemically synthesized systems are polydisperse, the dimensions of viruses are highly monodisperse, forming a system capable of adopting the highly ordered smectic phase. Molecular cloning techniques can be used to alter systematically characteristics of the resulting viruses, such as length and surface charge<sup>45</sup>.

Systems that exhibit smectic phases may also exhibit a nematic or chiral nematic phase. As the rod concentration increases, chiral fd virus goes from an isotropic phase to a chiral nematic phase, and subsequently to a smectic phase. Although it remains unclear as to how the chirality translates into the supermolecular helical structure, when viewed in a polarizing microscope the fd virus clearly shows the fingerprint texture characteristic of a chiral nematic liquid crystal<sup>44</sup>. Colloidal suspensions of the chiral biopolymers, cellulose and chitin, have also been shown to exhibit chiral nematic phases<sup>46,47</sup>. The phase behaviour of cellulose will be discussed in detail in the following section.

From the above descriptions of colloidal particles, it can be noted that the particles themselves are all rod-like, but they vary in origin, composition, and charge. Upon reaching a critical concentration rod-like particles form nematic phases, and if these rods are chiral a chiral nematic phase results. In order to form a smectic phase, a highly monodisperse sample of rods is required; consequently, there are fewer experimental examples of smectic phases. The fact that biological, synthetic and inorganic particles all form ordered phases indicates that it is more the particle geometry than the particle itself that influences phase separation.

## **1.5 CELLULOSIC LIQUID CRYSTALS**

Cellulose, the most abundant natural polymer, is used in a wide variety of applications. One of its unique and lesser-known properties is its ability to form liquid crystalline phases. The liquid crystalline behaviour of cellulose suspensions was first reported in 1959<sup>47</sup>, yet it was not until thirty years later that colloidal suspensions of cellulose were examined in detail. In the mean time, researchers discovered the liquid crystalline properties of cellulose derivatives, such as hydroxypropyl cellulose<sup>48</sup>. The following sections will recount the unique behaviour of macromolecular cellulose derivatives and suspensions of colloidal cellulose particles.

### **1.5.1 Liquid Crystalline Phases of Cellulose and Cellulose Derivatives**

Both lyotropic and thermotropic liquid crystals have been made from cellulose derivatives<sup>49</sup>. Evidence for these phases is obtained by optical analysis since chiral

nematic liquid crystals reflect light in the visible spectrum if their pitch is of the order of the wavelength of visible light. These characteristic reflections were first observed for cellulose in concentrated solutions of hydroxypropyl cellulose in water<sup>48</sup>. The reflected colour, which is determined by the pitch of the chiral nematic helix, varied inversely with cellulose concentration<sup>50</sup>. The colour was observed to change from a red-orange to green and finally to violet as the cellulose concentration increased. Other cellulose derivatives changed colour as the temperature changed. A thin layer of acetoxypropyl cellulose (APC) appeared violet at 85 °C. This thin layer was placed on a hot stage and as the temperature increased, the colour systematically progressed through the rainbow, becoming red at 125 °C, showing that the distance between nematic layers of APC increases with temperature<sup>49</sup>.

Evidence for the chiral nematic helix can also be obtained by measuring the optical rotatory dispersion (ORD) or circular dichroism (CD) of the sample. These measurements also determine whether the helix is right- or left-handed. The orientation of nematic-layers in a right-handed chiral nematic changes in a clockwise direction on moving away from the observer along the chiral nematic axis; the layers rotate counter-clockwise in a left-handed chiral nematic. It was believed that the handedness of various cellulose derivatives would be the same since they share a common cellulose backbone; however, both right- and left-handed helices have been observed. While hydroxypropyl cellulose in water, acetic acid, and methanol as well as ether and ester derivatives of HPC resulted in right-handed helices<sup>50</sup>, left-handed structures were observed for ethyl cellulose in acetic acid<sup>51</sup>. Further research has shown that chemical modifications to side-chain substituents can alter the handedness of cholesteric helices<sup>52</sup>. For example, the acetylation of ethyl cellulose changes its helical orientation<sup>53</sup>. As well, changes in solvent have an effect on the chiral nematic twist sense: in methylpropyl ketone cellulose tricarbonyl forms a right-handed twist, but in diethyleneglycol monoethyl ether the twist sense is left-handed<sup>54</sup>. Thus, some cellulose derivatives form right-handed helices and some left-handed, while still others can change from one form to the other. Interactions between the cellulose backbone, chain substituents, and the solvent all influence chiral forces and the resultant helical superstructure.

Although cellulose derivatives showed interesting phase behaviour and unique iridescent colours, there were some drawbacks. Cellulose derivatives are long flexible polymers that act less predictably than rigid colloidal particles. In addition, high concentrations were required to form ordered phases and therefore the suspensions were viscous and difficult to manipulate. Consequently, researchers began to investigate the liquid crystalline properties of colloidal cellulose particles.

### **1.5.2 Liquid Crystalline Phases of Colloidal Cellulose Nanocrystals**

Trying to produce novel cellulose products by degrading natural cellulose fibres may initially seem like a backwards approach. However, persistent research on the acid degradation of cellulose eventually led to the commercialization of microcrystalline cellulose in 1962. Microcrystalline cellulose particles are produced by hydrolysing cellulose with hydrochloric acid and then dispersing the freshly cleaved particles by a shearing action. The resulting colloidal crystals pile up like a heap of matchsticks, forming a cellulose gel with unique rheological properties<sup>55</sup>. Subsequent investigations using this 'backwards' approach of acid hydrolysis have produced charge-stabilized colloidal crystals that exhibit unique liquid crystalline properties.

Colloidal suspensions of cellulose nanocrystals with liquid crystalline properties were initially prepared by careful hydrolysis with sulfuric acid<sup>46,47</sup>. Subsequent work used hydrochloric acid instead in order to minimize the charge on the cellulose rods<sup>56</sup>. Suspensions have been prepared from a variety of cellulose sources including wood pulp<sup>46,57</sup>, cotton<sup>58</sup>, bacterial cellulose<sup>59</sup>, and microcrystalline cellulose<sup>56</sup>. Although particle size depends on both the starting material and the hydrolysis conditions, typical particle dimensions range from 100 nm to 300 nm long and 4 nm to 15 nm wide. Particle dimensions have been characterized by transmission electron microscopy<sup>57,58,60</sup> and photon correlation spectroscopy<sup>58</sup>, yet other methods such as atomic force microscopy may also prove to be useful.

At low concentrations these cellulose suspensions are isotropic with the rods tumbling randomly, while at high cellulose concentrations the rods tend to align parallel to neighbouring rods forming an anisotropic phase. As water evaporates from a dilute sample, tactoids, small domains of ordered particles, begin to form and as the

concentration continues to increase the tactoids coalesce to form the continuous fingerprint texture characteristic of a chiral nematic<sup>61</sup>. Upon reaching the critical concentration required for phase separation, most cellulose suspensions exhibit the classic fingerprint texture; however, a “birefringent glassy phase”<sup>62</sup> and a nematic phase<sup>59</sup> have also been observed. The observed chiral nematic order can be enhanced by placing the suspension in a magnetic field<sup>61</sup>, as cellulose has a negative diamagnetic susceptibility<sup>63</sup>, meaning that the rods tend to align perpendicular to the magnetic field.

The phase behaviour of cellulose rods has been found to agree qualitatively with Onsager’s theory, although the critical concentration for phase separation predicted theoretically always tends to be greater than experimental concentrations<sup>64</sup>. For suspensions prepared with sulfuric acid, and therefore charge stabilized by sulfate groups, the anisotropic phase typically forms around 5% by weight. Then a fairly large biphasic region exists, due to the polydispersity of the sample, and a pure anisotropic phase is obtained around 10 – 12% by weight. The precise values for phase separation are influenced by the ionic strength of the suspension<sup>64</sup> and the nature of the counterions<sup>65</sup>. As ionic strength increases, the effective diameter of the rods decreases and therefore a higher rod concentration is required for phase separation to occur. Similarly, for biphasic samples, the volume fraction of the anisotropic phase decreases as salt is added to the suspension<sup>64</sup>. This biphasic region is interesting because a sharp boundary between the isotropic and anisotropic phases can be seen, yet the interfacial tension is relatively small<sup>66</sup>, allowing the facile passage of particles from one phase to the other.

In addition to the ionic strength of the suspension, phase behaviour is also affected by the charge on the cellulose rods. Suspensions hydrolysed with hydrochloric acid have a minimal surface charge<sup>57</sup>, yet sulfate groups can be added by subsequent treatment with sulfuric acid<sup>56</sup>. Thus, through a slight modification of preparation conditions, the charge on the cellulose rods can be controlled. The cellulose rods prepared by this two-stage approach, however, show a “birefringent glassy phase” upon concentration, rather than the typical chiral nematic phase<sup>62</sup>.

Since the majority of the cellulose systems are electrostatically stabilized, they are typically restricted to polar solvents. A stable suspension of cellulose nanocrystals in a non-polar solvent was obtained by using surfactants as stabilizing agents<sup>60</sup>. The

surfactant-stabilized suspensions show typical fingerprint texture, but a significantly higher weight fraction (~36%) is required to obtain phase separation.

While electrostatically stabilized colloidal systems are modeled by DLVO theory, sterically stabilized systems exhibit a “hard repulsion.” Many systems of sterically stabilized spherical colloids exist, but there are fewer examples of sterically stabilized rods. Boehmite rods stabilized by poly (isobutene) grafts were shown to form stable nematic phases<sup>41</sup>. Cellulose rods grafted with poly (ethylene glycol) showed greatly enhanced stability, remaining stable after the addition of 2 *M* sodium chloride and having the ability to redisperse after freeze-drying<sup>67</sup>. The chiral nematic phase formed by the grafted cellulose rods was similar to the ungrafted samples.

While most of the work on the liquid crystalline behaviour of colloidal cellulose involves the fluid phase, these systems also show potential for use in composite materials and solid films. Most liquid crystals maintain an ordered arrangement solely in the fluid phase, but solid films with chiral nematic structure have been prepared from cellulose nanocrystals<sup>68</sup>. Due to the chiral nematic order, these films are iridescent and reflect one hand of circularly polarized light. The colour of the films may be controlled by changing the pitch of the chiral nematic helix.

## 1.6 OUTLINE OF THESIS RESEARCH

The liquid crystalline properties of cellulose derivatives have been studied extensively. In contrast, the investigation into the properties of colloidal cellulose nanocrystals is relatively new. This unique system of colloidal cellulose rods is the focus of my dissertation. The goal of my research is to further characterize these cellulose particles at several different concentration ranges.

At low cellulose concentrations the suspensions are disordered, becoming ordered upon reaching a critical concentration. Since this critical concentration depends on the aspect ratio of the cellulose rods it is important to devise an effective way of characterizing particle size. Chapter 2 describes the use of atomic force microscopy (AFM) to determine average particle length and width as well as the polydispersity of the

sample. It is important to determine particle dimensions in order to be able to compare experimental phase behaviour of the cellulose suspensions with that predicted theoretically.

Just beyond the critical concentration for anisotropic phase formation is an intermediate concentration range in which the isotropic and anisotropic phases co-exist. This biphasic region is the focus of Chapter 3. Dextran is added to suspensions of cellulose nanocrystals in order to determine the effect on the phase behaviour. Dextran, like cellulose, is a glucose polymer, but its  $\alpha$ -1,6 linkages result in a much more flexible polymer than cellulose. Thus, these two polymers are similar chemically but vary in shape. This conformational difference causes the dextran to be preferentially partitioned into the isotropic phase. Using the cellulose rod dimensions determined in Chapter 2, the phase behaviour of the cellulose-dextran system is compared to theoretical predictions.

As the name implies, liquid crystals are somewhat fluid, like a typical liquid. However, this system of cellulose rods is unique because as the suspension is slowly concentrated to form a solid film, some of the liquid crystalline order remains. Due to this chiral nematic structure, the films can display iridescent colours. In Chapter 4 circular dichroism spectroscopy is used as a tool to characterize the helical superstructure in the films. Changes to the chiral nematic pitch and degree of order can be monitored by measuring induced circular dichroism.

A major requirement to study surface interactions is a smooth, flat surface. Since Chapter 2 indicated that the cellulose nanocrystals are very narrow and Chapter 4 proved that solid films could be made, it seemed probable that a smooth, flat surface could be created from the cellulose suspensions. In Chapter 5 we devise a technique to create model surfaces of cellulose I. These model surfaces are characterized by X-ray photoelectron spectroscopy (XPS), X-ray diffraction, and AFM.

These colloidal suspensions provide a unique environment for the study of cellulose. This system allows us to investigate fundamental aspects of cellulose nanocrystals, colloidal suspensions, liquid crystals, phase separation, and thin films, using a variety of experimental techniques. The analysis of key concentration ranges provides a greater overall understanding of the cellulose suspensions and chiral nematic films.

## 1.7 REFERENCES

- (1) Young, R. A. In *Cellulose: Structure, Modification and Hydrolysis*; Young, R. A., Rowell, R. M., Eds.; John Wiley & Sons: New York, 1986.
- (2) Hon, D. N.-S. *Cellulose* **1994**, *1*, 1-25.
- (3) Mark, H. *Journal of Physical Chemistry* **1940**, *44*, 764-787.
- (4) Sjöström, E. *Wood Chemistry Fundamentals and Applications*; Academic Press: New York, 1981.
- (5) Fengel, D.; Wegener, G. *Wood Chemistry, Ultrastructure, Reactions*; Walter de Gruyter: Berlin, 1984.
- (6) Rowland, S. P.; Bertoniere, N. R. In *Cellulose Chemistry and its Applications*; Nevell, T. P., Zeronian, S. H., Eds.; John Wiley & Sons: New York, 1985.
- (7) Krässig, H. A. *Cellulose: Structure, Accessibility, and Reactivity*; Gordon and Breach Science Publishers: Yverdon, 1993.
- (8) Marchessault, R. H.; Sarko, A. *Advances in Carbohydrate Chemistry* **1967**, *22*, 421-482.
- (9) Meyer, K. H.; Misch, L. *Helvetica Chimica Acta* **1937**, *20*, 232-244.
- (10) Gardner, K. H.; Blackwell, J. *Biopolymers* **1974**, *13*, 1975-2001.
- (11) Atalla, R. H.; VanderHart, D. L. *Science (Washington, D. C., 1883-)* **1984**, *223*, 283-285.
- (12) Horii, F.; Hirai, A.; Kitamaru, R. *Macromolecules* **1987**, *20*, 2117-2120.
- (13) Sugiyama, J.; Vuong, R.; Chanzy, H. *Macromolecules* **1991**, *24*, 4168-4175.
- (14) Nishiyama, Y.; Langan, P.; Chanzy, H. *Journal of the American Chemical Society* **2002**, *124*, 9074-9082.
- (15) Wada, M.; Okano, T. *Cellulose (Dordrecht, Netherlands)* **2001**, *8*, 183-188.
- (16) Stipanovic, A. J.; Sarko, A. *Macromolecules* **1976**, *9*, 851-857.
- (17) Sarko, A. *Tappi* **1978**, *61*, 59-61.
- (18) Collings, P. J. *Liquid Crystals: Nature's Delicate Phase of Matter*; Princeton University Press: Princeton, 1990.
- (19) DuPré, D. B. In *Encyclopedia of Chemical Technology*; Kirk-Othmer, Ed.; Wiley-Interscience: New York, 1981; Vol. 14.
- (20) Collings, P. J.; Hird, M. *Introduction to Liquid Crystals*; Taylor & Francis Ltd.: London, 1998.
- (21) Chandrasekhar, S. *Liquid Crystals*; Cambridge University Press: Cambridge, 1977.
- (22) Haller, I. *Progress in Solid-State Chemistry* **1975**, *10*, 103-118.

- (23) Demus, D. In *Liquid Crystals*; Stegemeyer, H., Ed.; Springer: New York, 1994.
- (24) Hartshorne, N. H.; Stuart, A. *Crystals and the Polarising Microscope*; 3rd ed.; Edward Arnold Ltd.: London, 1960.
- (25) Chilaya, G. S.; Lisetski, L. N. *Molecular Crystals and Liquid Crystals* **1986**, *140*, 243-286.
- (26) Hiemenz, P. C. *Principles of Colloid and Surface Chemistry*; Marcel Dekker Inc.: New York, 1977.
- (27) Hunter, R. J. *Introduction to Modern Colloid Science*; Oxford University Press: Oxford, 1993.
- (28) Ross, S.; Morrison, I. D. *Colloidal Systems and Interfaces*; John Wiley & Sons: New York, 1988.
- (29) Baus, M.; Coussaert, T.; Achrayah, R. *Physica A (Amsterdam)* **1996**, *232*, 575-584.
- (30) Russel, W. B.; Saville, D. A.; Schowalter, W. R. *Colloidal Dispersions*; Cambridge University Press: New York, 1989.
- (31) Dinsmore, A. D.; Crocker, J. C.; Yodh, A. G. *Current Opinion in Colloid & Interface Science* **1998**, *3*, 5-11.
- (32) Pileni, M. P. *Langmuir* **1997**, *13*, 3266-3276.
- (33) Bawden, F. C.; Pirie, N. W.; Bernal, J. D.; Fankuchen, I. *Nature* **1936**, *138*, 1051-1052.
- (34) Fraden, S.; Maret, G.; Caspar, D. L. D.; Meyer, R. B. *Physical Review Letters* **1989**, *63*, 2068-2071.
- (35) Boedtker, H.; Simmons, N. S. *Journal of the American Chemical Society* **1958**, *80*, 2550-2556.
- (36) Hall, C. E. *Journal of the American Chemical Society* **1958**, *80*, 2556-2557.
- (37) Onsager, L. *Annals New York Academy of Sciences* **1949**, *51*, 627-659.
- (38) Folda, T.; Hoffman, H.; Chanzy, H.; Smith, P. *Nature* **1988**, *333*, 55-56.
- (39) Buining, P. A.; Pathmamanoharan, C.; Jansen, J. B. H.; Lekkerkerker, H. N. W. *Journal of the American Ceramic Society* **1991**, *74*, 1303-1307.
- (40) Buining, P. A.; Lekkerkerker, H. N. W. *Journal of Physical Chemistry* **1993**, *97*, 11510-11516.
- (41) Buining, P. A.; Veldhuizen, Y. S. J.; Pathmamanoharan, C.; Lekkerkerker, H. N. W. *Colloids and Surfaces* **1992**, *64*, 47-55.
- (42) Maeda, Y.; Hachisu, S. *Colloids and Surfaces* **1983**, *6*, 1-16.
- (43) Gabriel, J.-C. P.; Davidson, P. *Advanced Materials* **2000**, *12*, 9-20.
- (44) Dogic, Z.; Fraden, S. *Langmuir* **2000**, *16*, 7820-7824.

- (45) Dogic, Z.; Fraden, S. *Philosophical Transactions of the Royal Society of London, Series A* **2001**, *359*, 997-1015.
- (46) Revol, J.-F.; Bradford, H.; Giasson, J.; Marchessault, R. H.; Gray, D. G. *International Journal of Biological Macromolecules* **1992**, *14*, 170-172.
- (47) Marchessault, R. H.; Morehead, F. F.; Walter, N. M. *Nature* **1959**, *184*, 632-633.
- (48) Werbowyj, R. S.; Gray, D. G. *Molecular Crystals and Liquid Crystals (Letters)* **1976**, *34*, 97-103.
- (49) Tseng, S.-L.; Valente, A.; Gray, D. G. *Macromolecules* **1981**, *14*, 715-719.
- (50) Werbowyj, R. S.; Gray, D. G. *Macromolecules* **1984**, *17*, 1512-1520.
- (51) Vogt, U.; Zugenmaier, P. *Berichte der Bunsengesellschaft für Physikalische Chemie* **1985**, *89*, 1217-1224.
- (52) Gray, D. G. *Polymer Preprints* **1996**, *37*, 485-486.
- (53) Guo, J.-X.; Gray, D. G. *Macromolecules* **1989**, *22*, 2086-2090.
- (54) Siekmeyer, M.; Zugenmaier, P. *Die Makromolekulare Chemie, Rapid Communications* **1987**, *8*, 511-517.
- (55) Battista, O. A. *Microcrystal Polymer Science*; McGraw-Hill Book Company: New York, 1975.
- (56) Araki, J.; Wada, M.; Kuga, S.; Okano, T. *Journal of Wood Science* **1999**, *45*, 258-261.
- (57) Araki, J.; Wada, M.; Kuga, S.; Okano, T. *Colloids and Surfaces A* **1998**, *142*, 75-82.
- (58) Dong, X. M.; Revol, J.-F.; Gray, D. G. *Cellulose* **1998**, *5*, 19-32.
- (59) Araki, J.; Kuga, S. *Langmuir* **2001**, *17*, 4493-4496.
- (60) Heux, L.; Chauve, G.; Bonini, C. *Langmuir* **2000**, *16*, 8210-8212.
- (61) Revol, J.-F.; Godbout, L.; Dong, X.-M.; Gray, D. G.; Chanzy, H.; Maret, G. *Liquid Crystals* **1994**, *16*, 127-134.
- (62) Araki, J.; Wada, M.; Kuga, S.; Okano, T. *Langmuir* **2000**, *16*, 2413-2415.
- (63) Sugiyama, J.; Chanzy, H.; Maret, G. *Macromolecules* **1992**, *25*, 4232-4234.
- (64) Dong, X. M.; Kimura, T.; Revol, J.-F.; Gray, D. G. *Langmuir* **1996**, *12*, 2076-2082.
- (65) Dong, X. M.; Gray, D. G. *Langmuir* **1997**, *13*, 2404-2409.
- (66) Chen, W.; Gray, D. G. *Langmuir* **2002**, *18*, 633-637.
- (67) Araki, J.; Wada, M.; Kuga, S. *Langmuir* **2001**, *17*, 21-27.
- (68) Revol, J.-F.; Godbout, L.; Gray, D. G. *Journal of Pulp and Paper Science* **1998**, *24*, 146-149.

## **Chapter 2**

### **Characterization of Cellulose Nanocrystals by Atomic Force Microscopy**

## 2.1 INTRODUCTION

An anisotropic shape, such as a rod, sheet, or disc, is one requirement for the formation of a liquid crystal. Many synthetic and naturally occurring molecules form liquid crystal phases, with rod-shaped molecules being the most common<sup>1</sup>. Rod-like species such as tobacco mosaic virus<sup>2</sup>, poly(tetrafluoroethylene)<sup>3</sup>, and boehmite<sup>4</sup> all form nematic liquid crystals. Crystallites from the biopolymer cellulose have been shown to form chiral nematic liquid crystals upon reaching a critical concentration<sup>5</sup>. At low concentrations the cellulose particles are arranged randomly in an isotropic suspension. As the concentration increases, the rod-like cellulose particles spontaneously organize into the helicoidal superstructure of a chiral nematic liquid crystal.

This phase separation from an isotropic to an anisotropic suspension may occur at very low cellulose concentrations. Onsager predicted that the phase separation of rod-like species would depend primarily on particle geometry<sup>6</sup>. By considering both electrostatic repulsions and excluded volume between two cylindrical particles based on their geometry, Onsager determined that the critical concentration for phase separation was inversely proportional to the aspect ratio of the particles,  $L/D$ . Thus, an important and unique phase separation can be determined purely from the length,  $L$ , and diameter,  $D$ , of the rod-like particles.

Onsager's theory has been compared to experimental values using the following equations

$$\varphi_i = 3.3 D/L \quad \varphi_a = 4.5 D/L \quad (\text{II.1})$$

where  $\varphi_i$  is the volume fraction of the isotropic phase and  $\varphi_a$ , of the anisotropic phase. For suspensions of cellulose nanocrystals, the values predicted by theory were significantly larger than experimental values<sup>7</sup>. The charge on the rods is further accounted for using the following formula

$$\varphi_i = 4.7 D^2/L D_{eff} \quad (\text{II.2})$$

where  $D_{eff}$  is the effective diameter, augmented due to the charge on the rods<sup>8</sup>. Still, it was found that the critical volume fraction predicted by theory exceeded the experimental value. One reason for these discrepancies may be the polydispersity of the rods. One effect of polydispersity is to lower the volume fraction required for phase separation for a

given mean rod length. The longer particles within a disperse sample tend to preferentially form an anisotropic phase, leaving a greater proportion of the shorter particles suspended in the isotropic phase<sup>9</sup>. Hence, it is important to know not only the mean length and diameter of the particles, but also the polydispersity of the sample.

Onsager's theory has subsequently been expanded to focus on the effects of electrostatic repulsion. Stroobants, Lekkerkerker, and Odijk characterize electrostatic interactions using two parameters: one accounting for the increased effective diameter and another incorporating a twisting effect<sup>10</sup>. These parameters are affected by charge density and salt concentration. For cellulose nanocrystals, the charge on the rods can be measured by conductometric titration or by elemental analysis<sup>11</sup>. The particle dimensions must then be measured in order to determine charge density.

Since particle size has such a strong influence on the behaviour of suspensions of cellulose nanocrystals, it is important to have an efficient method of characterization. Atomic force microscopy (AFM) is a relatively inexpensive technique that does not require elaborate sample preparation and it produces a three-dimensional image. However, as with any microscopy technique it is important to ensure that a representative sample is being measured and to avoid artifacts. We have tried to avoid these potential pitfalls by developing a sample preparation technique to yield a uniform distribution of particles and by careful image analysis. In this chapter, the characterization by AFM of cellulose nanocrystals originating from both cotton and wood pulp will be described.

## **2.2 EXPERIMENTAL**

### **2.2.1 Sample Preparation**

Colloidal suspensions of cellulose nanocrystals were prepared from two different sources of cellulose: pulp fibres, from a high-cellulose-content dissolving grade softwood pulp (Aliceta HD, Western Pulp Partnership, Port Alice, British Columbia), and cotton fibres, from Whatman No. 1 filter paper. Both cellulose sources were first ground in a Wiley mill (Thomas-Wiley Laboratory Mill Model 4, Thomas Scientific, USA) to pass through a 1-mm mesh. The cellulose was hydrolyzed with 64-wt.% sulfuric acid at 45 °C for 45 minutes. Typically, 40 g of pulp or cotton was treated with 700 mL of acid.

Immediately following hydrolysis, the suspension was diluted tenfold to stop the reaction. The suspension was then washed repeatedly by diluting with water and centrifuging until the pH of the supernatant was greater than 1. Next, the sample was dialyzed against water for several days. The final step to achieve a colloidal suspension was repeated sonification (Branson Sonifier, Model 350) for 7-minute intervals for a total of 35 minutes, cooling in an ice bath between steps. The suspension was then allowed to stand over a mixed bed resin (Sigma) for 48 hours and then filtered through hardened ashless filter paper (Whatman, 541). The final aqueous suspension originating from the wood pulp was 2.0% concentration by weight with a pH of 2.7 and the suspension derived from the Whatman filter paper was 2.4% concentration by weight with a pH of 2.0.

### **2.2.2 Atomic Force Microscopy**

The original cellulose suspension was diluted to about  $1 \times 10^{-4}$  % concentration by weight and then filtered through a 0.45- $\mu\text{m}$  membrane. A piece of freshly cleaved mica ( $\sim 1 \text{ cm}^2$ ) was treated with a 1-mg/mL solution of poly-L-lysine (Sigma), washed with water, and then dried. One drop of filtered suspension was placed on the mica, allowed to sit, and then washed with water and dried by blotting on hardened ashless filter paper. The mica was then attached to an AFM specimen disc, ready for immediate analysis. The nanocrystals were imaged with a NanoScope IIIa Atomic Force Microscope (Digital Instruments), using an NP tip (Digital Instruments) with the 100- $\mu\text{m}$  long cantilever with a spring constant of approximately 0.58 N/m. Samples were scanned in contact mode under ambient conditions at 1-2 Hz with scan sizes ranging from 3 to 20  $\mu\text{m}$  using the J piezoelectric scanner (Digital Instruments). Particle sizes were determined using the section analysis tool provided with the AFM software (Digital Instruments, Version 4.32r1). Length and width dimensions were taken from the top, rather than the base, of the contour profile to compensate for widening due to the convolution of the tip and particle. By comparison with TEM, the uncertainty in AFM length measurements is estimated to be 10 nm, and the uncertainty in width measurements, 3 nm.

### 2.2.3 Transmission Electron Microscopy

Particle size was also determined by transmission electron microscopy (Philips EM 400T). A carbon coated microscope grid for TEM (J. B. EM Services Inc.) was treated with poly-L-lysine as above and then a drop of dilute cellulose suspension was added. Images were obtained at 10 000 x magnification. The TEM negatives were converted to JPEG file format and then the particles were counted manually using image analysis software (Image-Pro Plus) to measure particle dimensions.

## 2.3 RESULTS AND DISCUSSION

Atomic force microscopy is a versatile technique that can be used at many different length scales; however, problems arise when the dimensions of the particles being measured are roughly equal to or smaller than the dimensions of the tip. The most prevalent type of artifact in AFM arises from this tip-sample convolution<sup>12,13</sup>. As the tip scans over a particle, the particle size is augmented due to the thickness of the tip as shown in Figure 2.1. This sample widening has been vividly demonstrated by contrasting an AFM image of a *Valonia ventricosa* microfibril with the TEM image of the identical microfibril<sup>14</sup>.

One key advantage to AFM is that in addition to the x-y plane image the height along the z-axis is obtained. The height of a measured particle is much less affected by the width of the tip. Assuming that the cellulose nanocrystals are relatively square, the crystallite width will equal the height of the crystallite. We determined that it was most accurate to obtain the particle width from the height of the particle, measured using the contour profile. Previous research has shown that as scan rate increases (up to 78 Hz) the contour profile becomes flatter and wider<sup>14</sup>. In order to avoid this we used scan rates from 1 to 2 Hz, where no flattening was observed. The contour profile was also used to determine particle length, measuring the length across the top of the particle, as shown in Figure 2.2, rather than at the base, which has been broadened due to tip-sample convolution.

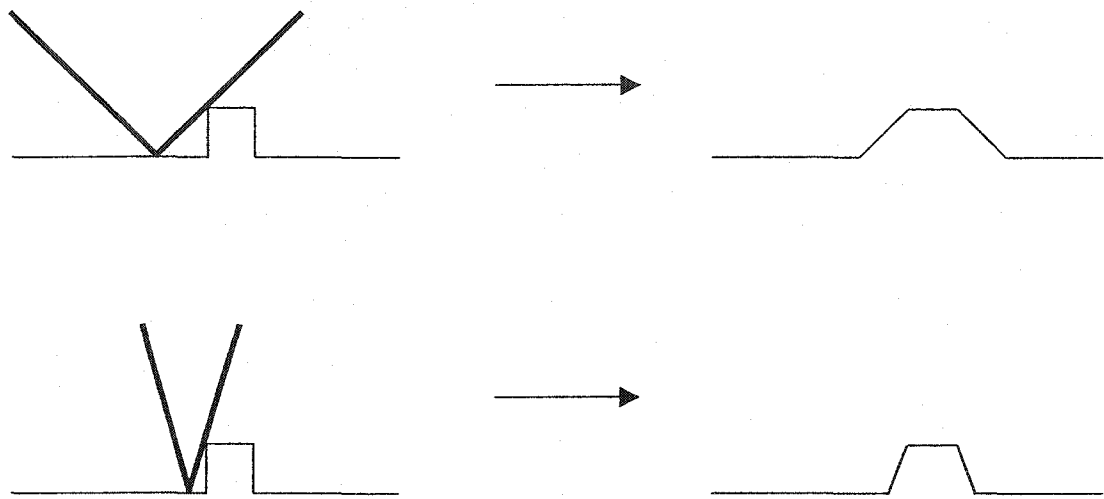


Figure 2.1 Schematic diagram of tip-sample convolution.

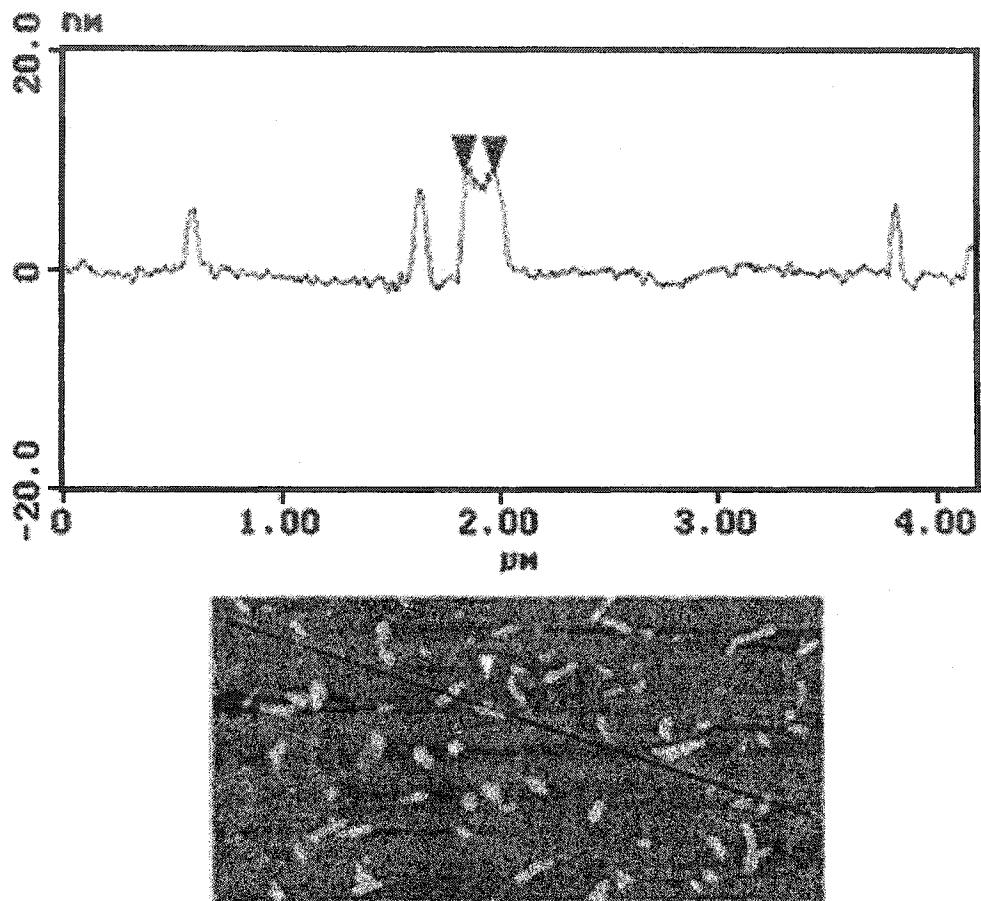


Figure 2.2 Contour profile (upper) and AFM image (lower) of cellulose nanocrystals illustrating particle length measurement.

To ensure that a representative sample was being measured, a 20  $\mu\text{m}$  x 20  $\mu\text{m}$  image of the cellulose suspension dried down on mica was scanned to see if the overall distribution of particles looked uniform. Subsequent scans covering an area of 4  $\mu\text{m}$  x 4  $\mu\text{m}$  were used to measure particle dimensions. An initial scan of cellulose nanocrystals derived from Whatman filter paper is shown in Figure 2.3. A non-uniform distribution of particles was obtained. The lower left-hand corner has very few particles. The particle density increases towards the upper right-hand corner of the image where many nanocrystals are clumped together. In addition, there is a non-uniform distribution of particle size. The longer particles tend to aggregate into high-density clumps, while the shorter particles are more evenly dispersed at the edge of this region. Thus, it is important to obtain an even particle distribution in order to avoid counting primarily short or long particles. A more even distribution of nanocrystals, derived from wood pulp, is shown in Figure 2.4; however, numerous large clumps are also present. Further investigation showed that the length of the clumps was about the same as the length of individual rods, indicating that the clumps may be aggregates of several rods.

The above samples were prepared by allowing a drop of aqueous suspension to dry overnight. As the liquid evaporated surface tension drew the particles together. The amount of particle aggregation was reduced by treating the mica with poly-L-lysine so the cellulose would be attracted to the surface, allowing the sample to be washed with water and blotted dry immediately. This technique also allowed samples to be prepared and analyzed on the same day, reducing delays while determining the optimum suspension concentration.

Figure 2.5 shows a relatively even distribution of Whatman nanocrystals for particles size determination. It is evident from this image that tip-sample convolution has occurred, making the particles appear wider than they actually are, especially when compared to the TEM micrograph of the same Whatman suspension (Figure 2.6). It is also apparent that the particles have a wide range of lengths. The average particle length was found to be  $113 \pm 46$  nm, with particle lengths ranging from 30 to 230 nm as shown in Figure 2.7. For the same Whatman suspension, TEM results gave an average length of

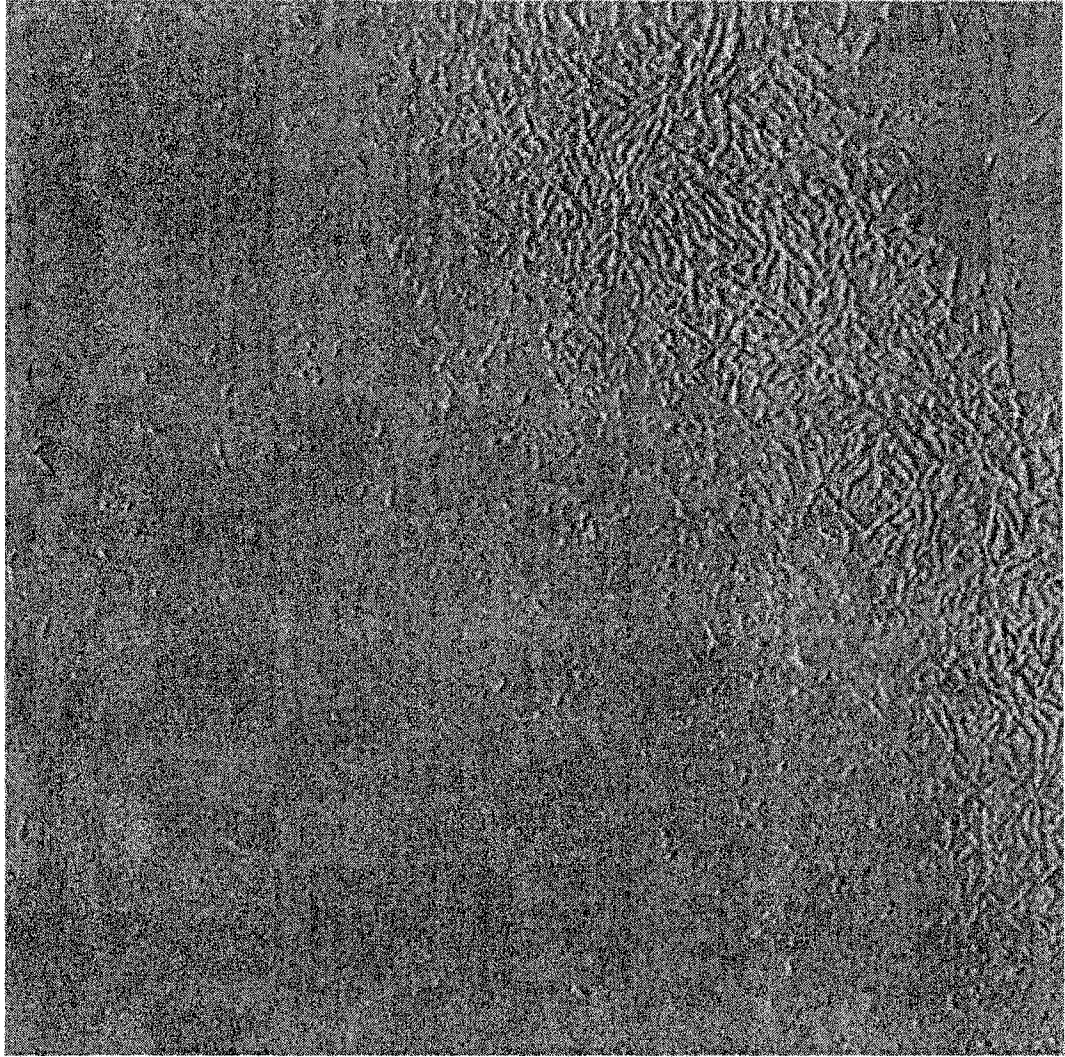


Figure 2.3 AFM image of cellulose nanocrystals derived from Whatman filter paper illustrating the aggregation of longer particles. Image is 10  $\mu\text{m}$  by 10  $\mu\text{m}$ , shown in deflection mode.

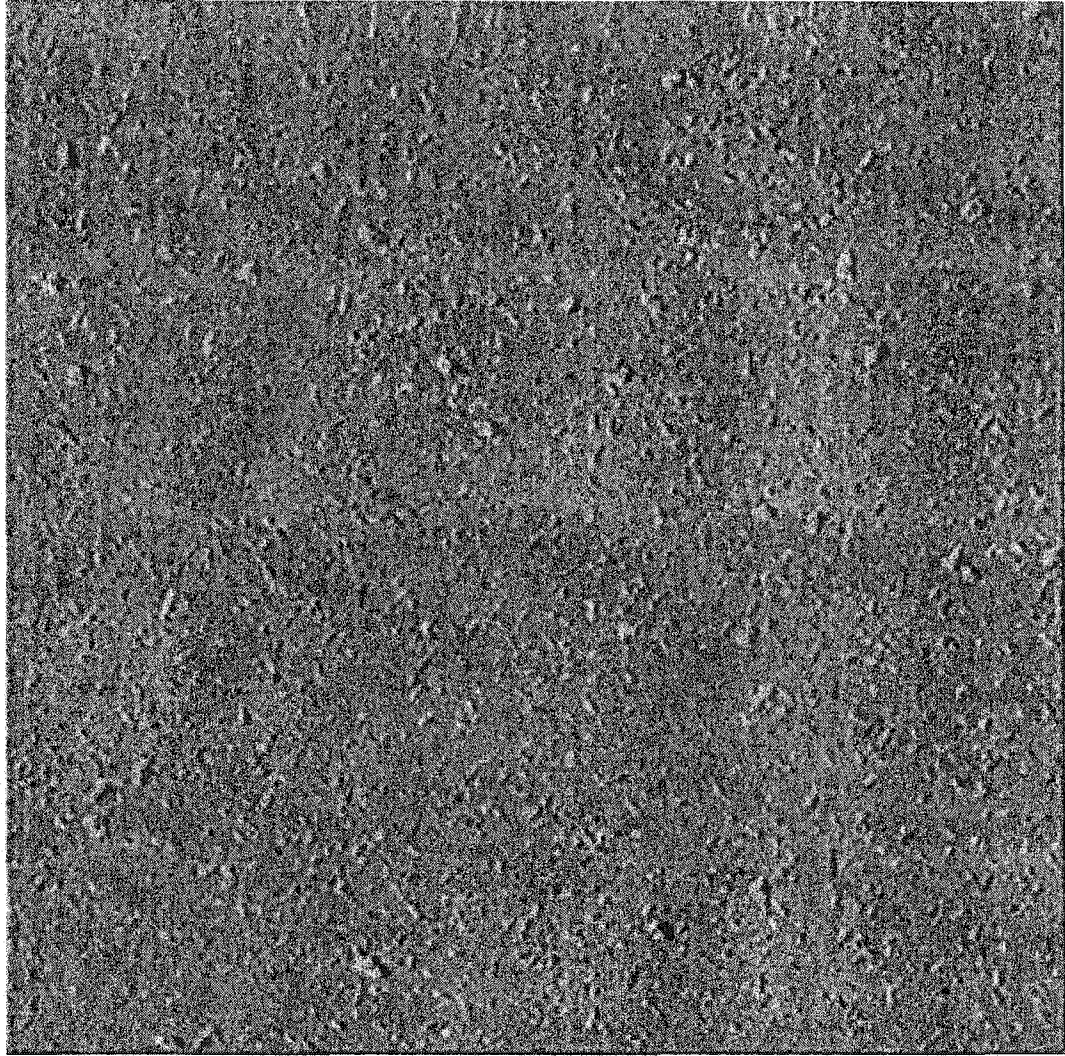


Figure 2.4 AFM image of cellulose nanocrystals derived from wood pulp showing some clumping of particles. Image is 10  $\mu\text{m}$  by 10  $\mu\text{m}$ , shown in deflection mode.

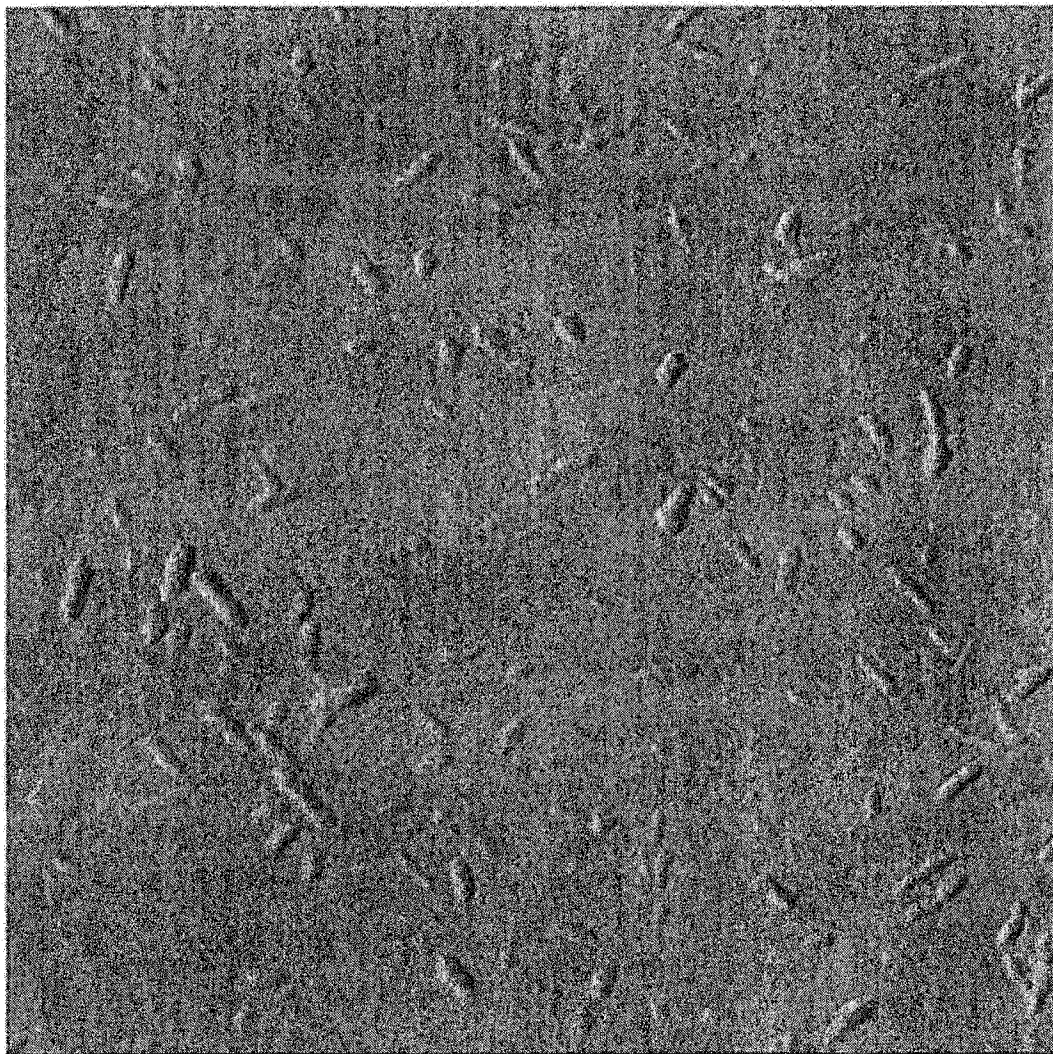


Figure 2.5 AFM image of cellulose nanocrystals derived from Whatman filter paper showing a more even distribution of particles. Image is 4  $\mu\text{m}$  by 4  $\mu\text{m}$ , shown in deflection mode.

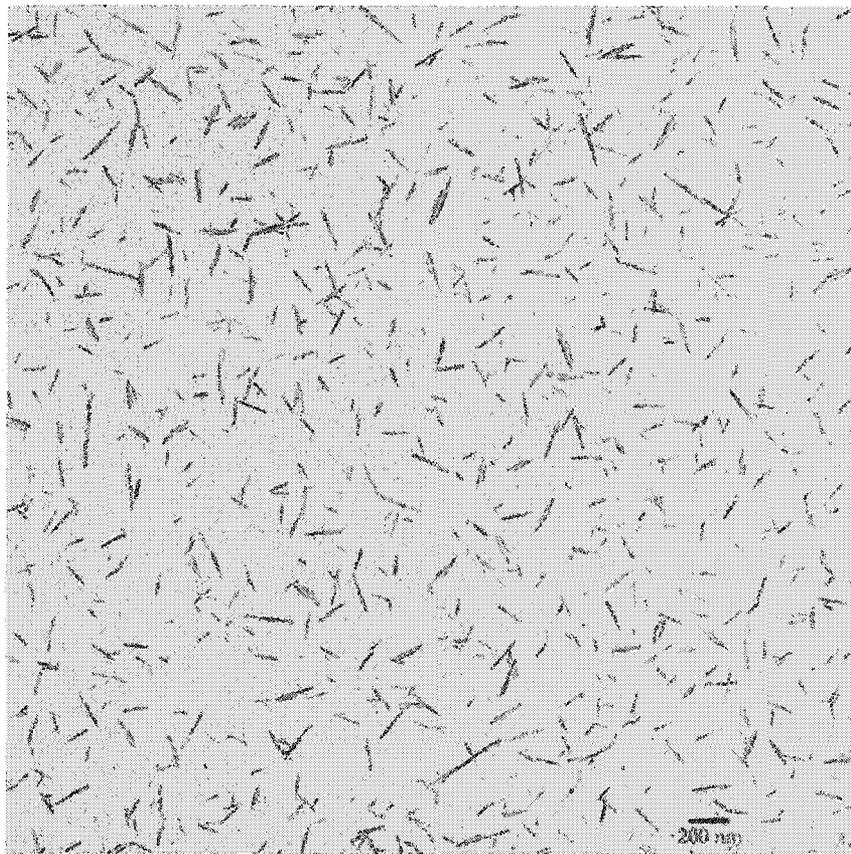


Figure 2.6 TEM image of cellulose nanocrystals derived from Whatman filter paper.

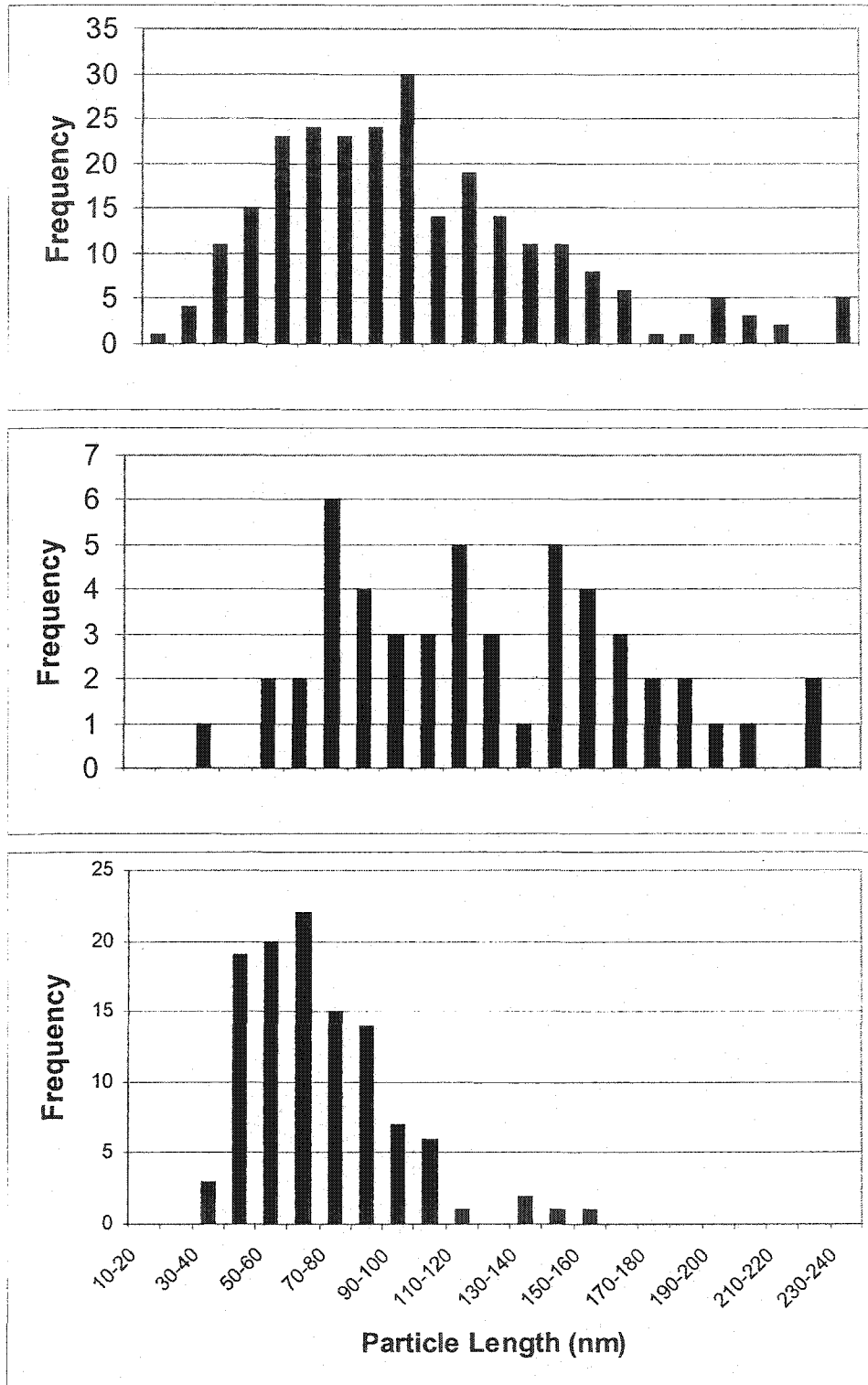


Figure 2.7 Histograms of particle lengths of cellulose nanocrystals derived from Whatman filter paper and measured by TEM (upper), derived from Whatman filter paper and measured by AFM (middle), and derived from wood pulp and measured by AFM (lower).

97 ± 45 nm. The large standard deviations obtained with both AFM and TEM indicate the polydisperse nature of the suspension of cellulose nanocrystals. Considering the large polydispersity in rod size, the values obtained by TEM and by AFM are in relatively good agreement, validating the AFM technique for measuring particle size.

The particle width was measured from both the AFM images, using the particle height obtained from the contour profile, and TEM images. The average width was found to be 9 ± 3 nm via AFM and 12 ± 3 using TEM. Although the values obtained are relatively close, we feel that the AFM results are more representative. Particle distributions are shown in Figure 2.8. The particle width in the TEM images was very small, making it difficult to measure precisely. The magnification used for analysis could only be increased marginally before the particle edge became too fuzzy to determine accurately. Due to the small number of pixels being measured several intermediate particle widths are never recorded. The image analysis using the AFM contour profile proved to be a more precise technique for determining particle width.

The dimensions of cellulose nanocrystals prepared by acid hydrolysis depend on both the hydrolysis conditions and the starting material<sup>11</sup>. The cellulose suspensions derived from cotton and from wood pulp were prepared under the same conditions – only the starting material varied. Particle size analysis by AFM indicated that the nanocrystals originating from the pulp sample were both shorter (Figure 2.7) and narrower (Figure 2.8) than those from the cotton sample. The average length was 70 ± 23 nm and the average width was 6 ± 2 nm.

What accounts for the large difference in particle size? The native fibre lengths of softwoods (4.0 mm) are much shorter than those of cotton (30 mm)<sup>15</sup>. However, in our procedure, most of the initial fibre length difference is reduced during grinding to pass a 1-mm mesh. More importantly, the cellulose nanocrystals exist at a lower level of structure than the cellulose fibres and will not be greatly influence by fibre dimensions. According to the fringed micellar model, fibrils of cellulose are composed of both amorphous and crystalline regions<sup>16</sup>. A single chain of cellulose may progress through more than one region and therefore chain ends may be found in both crystalline and amorphous regions, with those in crystalline regions being less susceptible to

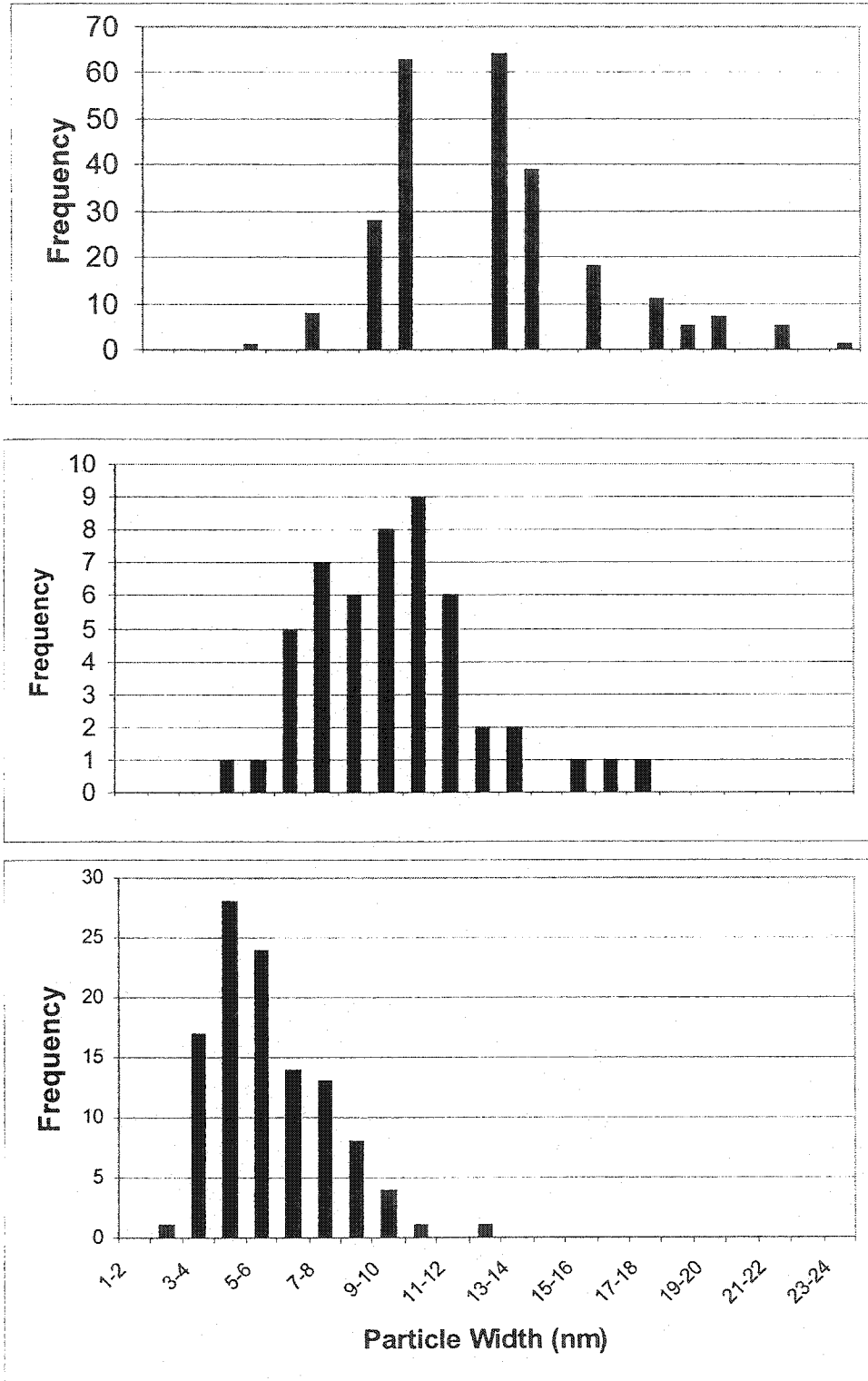


Figure 2.8 Histograms of particle widths of cellulose nanocrystals derived from Whatman filter paper and measured by TEM (upper), derived from Whatman filter paper and measured by AFM (middle), and derived from wood pulp and measured by AFM (lower).

degradation. The relative frequency and length of these crystalline regions, or crystallites, or nanocrystals, depend on the average cellulose chain length<sup>16</sup>. Since the average degree of polymerization (DP) of cellulose in cotton is greater than that in wood pulps, it is expected that cotton cellulose will have longer crystallites. Measurements of levelling-off DP show that, in general, cotton crystallites are longer than wood crystallites, with average literature values ranging from 200-350 for cotton and 150-300 for wood cellulose<sup>17</sup>. The resulting crystallite length as determined by this method will depend heavily on the specific hydrolysis conditions. Not only does cotton tend to have longer crystallites, but also cotton has a higher percentage of crystalline areas, making cotton fibres less accessible to acid hydrolysis. As determined by acid hydrolysis, the degree of crystallinity is 0.90 for cotton and 0.83 for wood pulps<sup>18</sup>. The lower yield obtained in our studies after hydrolysis of the wood pulp also indicates that the pulp is more susceptible to degradation than the more recalcitrant cotton. The fundamental structure of the cotton cellulose makes it more crystalline, with longer crystallites, than samples of pulp cellulose.

## 2.4 CONCLUSIONS

AFM has proven to be an effective method for characterizing cellulose nanocrystals. The contour profile provides a convenient way for measuring both particle length and width, while minimizing the effects of tip-sample convolution. Histograms of the resulting particle sizes give a good indication of the polydispersity of the sample. This characterization method is discriminating enough to show differences in particle size between nanocrystals prepared from pulp fibres and from cotton fibres. Particle size analysis by AFM will be useful to assess the effectiveness of fractionation methods or selective sample purification used to obtain a more monodisperse sample.

## 2.5 REFERENCES

- (1) Collings, P. J.; Hird, M. *Introduction to Liquid Crystals*; Taylor & Francis Ltd.: London, 1998.
- (2) Fraden, S.; Maret, G.; Caspar, D. L. D.; Meyer, R. B. *Physical Review Letters* **1989**, *63*, 2068-2071.
- (3) Folda, T.; Hoffman, H.; Chanzy, H.; Smith, P. *Nature* **1988**, *333*, 55-56.
- (4) Buining, P. A.; Lekkerkerker, H. N. W. *Journal of Physical Chemistry* **1993**, *97*, 11510-11516.
- (5) Revol, J.-F.; Bradford, H.; Giasson, J.; Marchessault, R. H.; Gray, D. G. *International Journal of Biological Macromolecules* **1992**, *14*, 170-172.
- (6) Onsager, L. *Annals New York Academy of Sciences* **1949**, *51*, 627-659.
- (7) Revol, J.-F.; Godbout, L.; Dong, X.-M.; Gray, D. G.; Chanzy, H.; Maret, G. *Liquid Crystals* **1994**, *16*, 127-134.
- (8) Buining, P. A. *Preparation and Properties of Dispersions of Colloidal Boehmite Rods*; Ph.D. Thesis, Universiteit te Utrecht, 1992.
- (9) Dong, X. M.; Kimura, T.; Revol, J.-F.; Gray, D. G. *Langmuir* **1996**, *12*, 2076-2082.
- (10) Stroobants, A.; Lekkerkerker, H. N. W.; Odijk, T. *Macromolecules* **1986**, *19*, 2232-2238.
- (11) Dong, X. M.; Revol, J.-F.; Gray, D. G. *Cellulose* **1998**, *5*, 19-32.
- (12) Grütter, P.; Zimmermann-Edling, W.; Brodbeck, D. *Applied Physics Letters* **1992**, *60*, 2741-2743.
- (13) Schwarz, U. D.; Haefke, H.; Reimann, P.; Güntherodt, H.-J. *Journal of Microscopy* **1994**, *173*, 183-197.
- (14) Hanley, S. J.; Giasson, J.; Revol, J.-F.; Gray, D. G. *Polymer* **1992**, *33*, 4639-4642.
- (15) Smook, G. A. *Handbook for Pulp & Paper Technologists*; Joint Textbook Committee of the Paper Industry: Atlanta, 1982.
- (16) Mark, H. *Journal of Physical Chemistry* **1940**, *44*, 764-787.
- (17) Fengel, D.; Wegener, G. *Wood Chemistry, Ultrastructure, Reactions*; Walter de Gruyter: Berlin, 1984.
- (18) Sjöström, E. *Wood Chemistry Fundamentals and Applications*; Academic Press: New York, 1981.

## **Chapter 3**

### **The Influence of Dextran on the Phase Behaviour of Suspensions of Cellulose Nanocrystals**

### 3.1 INTRODUCTION

Cellulose, derived from both softwood kraft pulp and cotton filter paper, can be hydrolysed with sulfuric acid to produce a suspension of colloidal cellulose nanocrystals<sup>1</sup>. Due to the rod-like shape of the nanocrystals, these suspensions display liquid crystalline behaviour above a critical concentration, in agreement with Onsager's theory for rigid rod-like particles<sup>2</sup>. At low cellulose concentrations the suspensions are isotropic, with a random arrangement of rods, while at high concentrations the suspensions are anisotropic, with the cellulose rods packed in a chiral nematic arrangement. Just beyond the critical concentration for anisotropic phase formation is a biphasic region in which the isotropic and anisotropic phases co-exist<sup>3</sup>.

This paper will examine the influence of dextran on the phase behaviour of cellulose nanocrystals. Cellulose is a  $\beta$ -1,4 linked polymer of glucose, with a relatively rigid structure<sup>4</sup>. In this work, the cellulose is in the form of rod-like nanocrystals, with dimensions on the order of 100 nm by 10 nm, in which the cellulose chains are in a cellulose I crystalline array. Dextran is also a glucose polymer, but the molecular chain is more flexible, forming a branched coil-like conformation that consists of  $\alpha$ -1,6 linkages with some  $\alpha$ -1,3 branching<sup>5</sup>. This combination provides an interesting system to study since the chemical constituents are very similar, with the major difference between the two components being their shape. It has been shown previously that if a physical property, such as shape or flexibility, of two components is different enough, a bulk demixing can occur<sup>6</sup>. In general, a random coil polymer or spherical particle will be excluded from an anisotropic phase made up of rod-like particles. This phenomenon has been shown to occur for several experimental systems<sup>6-13</sup>. The partitioning of the two different species has been explained by steric interactions between rods and coils<sup>14,15</sup> that cause a depletion attraction<sup>16</sup>.

In some experimental systems this drive to maximize entropy caused a complete exclusion of random coils from the ordered phase<sup>7</sup>, while in other systems detectable amounts of coiled polymers were found in the anisotropic phase<sup>8</sup>. In some cases, a more uniform distribution between the two phases was observed, the extent of which varied depending on the particular macromolecule added<sup>9</sup>. The various results reported in the

literature indicate that this phase separation is sensitive to several factors such as the chemical nature, the relative size, and the concentration of the two components.

Essentially, the anisotropic phase tends to reject the presence of spherical molecules in order to maintain its orientationally ordered structure. In cases where the spherical particles can be incorporated into the ordered structure, their exclusion in the anisotropic phase does not occur, as exhibited in the lamellar phase of bacteriophage fd virus rods and polystyrene latex spheres<sup>12</sup>. Investigations into systems of rods and coils have led to the discovery of several novel phases<sup>6,8,12</sup>. This paper is a preliminary investigation into the effect of blue dextran on the phase behaviour of suspensions of cellulose nanocrystals. Blue dextran was chosen because the glucose chain units are very similar to those of the cellulose nanocrystals, and small amounts of a blue chromophore is covalently bonded to the chain, rendering the concentration of dextran readily quantifiable.

## **3.2 EXPERIMENTAL**

### **3.2.1 Materials and Stock Solutions**

A colloidal suspension of cellulose nanocrystals was prepared by hydrolysing cotton filter paper (Whatman, 1) as described in Chapter 2. The final aqueous suspension was 2.4% concentration by weight. Previous experimental measurements on similarly prepared cellulose nanocrystals indicate that the surface charge density is about  $0.15\text{e}/\text{nm}^2$ <sup>17</sup>.

A 3-mg/mL solution of blue dextran (MW  $2 \times 10^6$ , Pharmacia Fine Chemicals) was prepared using purified water. The radius of gyration,  $R_g$ , for dextran of MW  $2 \times 10^6$  is 34 nm<sup>18</sup>. The blue colour of the dextran is due to 0.1 mmol Reactive Blue 2 dye per g. dextran that is bonded randomly to hydroxyl groups along the chain<sup>19</sup>. Each dye substituent contains three sulphonate groups, corresponding to about 600 charges per dextran coil.

### **3.2.2 Preparation of Cellulose-Dextran Suspensions**

Samples of increasing cellulose concentration were prepared by allowing aliquots of the original suspension to evaporate for several days in large petri dishes, forming both

biphasic and anisotropic samples. Vials A to E each contained 3 mL of cellulose suspension, increasing in concentration from Vial A to Vial E, and 70  $\mu$ L of blue dextran solution. Vials 1 to 5 were each filled with 2 mL of the same concentration of cellulose suspension and an increasing amount of blue dextran was added to each of these vials. The blue dextran was added in solid form rather than in solution in order to maintain the same concentration of cellulose suspension in each vial. Evidence of phase separation was already visible after one hour, but the vials were left to stand overnight. Samples were taken from the isotropic and anisotropic phases and diluted threefold prior to analysis. In a third set of samples, Vials I to IV, blue dextran was added, in increasing amounts, to completely anisotropic samples and the resulting phase separation was followed over a period of one month.

### 3.2.3 Sample Analysis

UV-visible absorption spectra were measured using a Perkin Elmer Lambda 14 UV/VIS Spectrometer, with the wavelength of maximum absorbance for blue dextran measured at 610 nm, using dextran-free suspensions of cellulose as the reference, giving a standard deviation of 0.02  $\mu$ mol/L. Partition coefficients were calculated prior to rounding off dextran concentrations, giving a standard deviation of 0.3. The concentration of cellulose in the samples was determined gravimetrically, weighing the samples before and after the evaporation of water. Repeated measurements showed that the standard deviation was about 0.3% by weight. For the samples containing blue dextran the weight of the dextran was calculated from the absorbance spectra and subtracted accordingly. The volume fraction of the two phases was determined by measuring the heights of the anisotropic and isotropic phases in each vial, with an uncertainty of 0.05 mL. The volume fraction of the anisotropic phase was calculated from these volumes, with an average uncertainty of 0.03. The size of the cellulose nanocrystals was determined by AFM in Chapter 2 and the mean values ( $L = 110$  nm and  $D = 10$  nm) were used for calculations. To convert cellulose concentrations in wt% to number density of nanocrystals, a cylindrical shape and a density of 1.6 g/mL were assumed for the nanocrystals. Photomicrographs were taken using a polarized light microscope (Nikon Microphot-FXA).

### 3.3 RESULTS AND DISCUSSION

The effects of blue dextran addition were observed on suspensions of cellulose nanocrystals at concentrations where isotropic, biphasic, and anisotropic phases were initially present.

#### 3.3.1 Isotropic Samples

Blue dextran was added to an isotropic suspension of cellulose rods, mixed by repeatedly inverting the vial, and allowed to stand. When no bulk demixing was observed, the concentration of blue dextran added was increased, up to the solubility limit of about 40 mg/mL. Still, no separation was evident after a period of several days. The depletion potential in systems of colloidal rods and spheres can be determined using the following equation<sup>13,20</sup>

$$W(h) = -\frac{2}{3}k_B T \phi_r \frac{L}{D} \frac{R}{D} \left(1 - \frac{h}{L}\right)^3 \quad (\text{III.1})$$

where  $k_B T$  is the thermal energy,  $\phi_r$  is the volume fraction of rods,  $L$  is the rod length,  $D$  is the rod diameter,  $R$  is the radius of the spheres, and  $h$  is the distance between the surface of spheres. This equation is valid in the limit of  $R \gg L$ . Our system, with  $R:L$  approximately 1:3 (where  $R$  is taken as  $R_g$  for the coil), clearly does not meet this criterion, but we may use it to get a rough idea of the volume fraction of rods at which demixing may be expected. Using  $3 k_B T$  as the minimum attraction energy required<sup>13,21</sup> we calculated the demixing transition to occur for a volume fraction of rods of about 12%. This volume fraction is above the volume fraction at which the isotropic-chiral nematic phase transition is expected to occur in our system, and so no demixing is expected for an isotropic suspension of cellulose rods in accordance with our observations. Depletion-induced phase separation has been observed at rod concentrations below the isotropic-nematic transition, but for mixing of rods having a much higher aspect ratio with large colloidal spheres<sup>13</sup>.

### 3.3.2 Biphasic Samples

The cellulose suspension was concentrated by evaporation to produce several biphasic samples, increasing in anisotropic volume fraction from Vial A to E (Table 3.1). When the blue dextran solution was added, the suspensions were mixed by repeatedly inverting the vials to obtain homogeneous suspensions. Immediately after mixing, the five vials looked identical; after a short period of time the blue colour began migrating upwards in the biphasic samples. Upon standing overnight the phase separation was complete, leaving a transparent blue upper phase and a cloudy lower ordered phase as shown in Figure 3.1. The intensity of the blue colour in the isotropic phase clearly increased from Vial A to Vial E.

The partitioning of blue dextran between the isotropic and anisotropic phases was quantified with an UV-visible spectrometer. The absorbance of blue dextran in the isotropic phase increased with increasing cellulose concentration. The absorbance in the anisotropic phase showed no distinct trend with cellulose concentration, and was taken to be the same within experimental error for the four vials. Although the absorbance in the anisotropic phase was significantly less than the absorbance in the isotropic regions, the absorbance was not zero, indicating that the blue dextran was not completely excluded from the ordered phase.

The relative amounts of blue dextran in each phase was quantified by calculating a partition coefficient,<sup>22</sup>  $K$ , the concentration of blue dextran in the isotropic phase,  $d_i$ , divided by the concentration of blue dextran in the anisotropic phase,  $d_a$ :

$$K = \frac{d_i}{d_a} \quad (\text{III.2})$$

The partition coefficient increased as the total cellulose concentration increased, as shown in Figure 3.2. However, increasing the overall cellulose concentration changes important system variables such as the relative volume fraction and the cellulose concentration of each phase. As the total cellulose concentration increases, the cellulose concentrations in both the isotropic phase and in the anisotropic phase increase, and also diverge slightly, as has been observed previously for this system of polyelectrolyte rods<sup>3</sup>. This is contrary to the predictions for hard-core monodisperse rods, where the

Table 3.1 Composition of biphasic samples with fixed total dextran concentration and increasing concentration of cellulose nanocrystals.

Sample	A	B	C	D	E
Total cellulose concentration (wt.%)	6.5	8.8	9.4	11.0	13.3
Cellulose in isotropic phase (wt.%)	6.5	7.2	8.1	10.5	10.8
Cellulose in anisotropic phase (wt.%)	-	9.6	10.5	12.0	14.0
Volume of isotropic phase (mL)	3.00	2.24	1.67	1.14	0.64
Volume of anisotropic phase (mL)	-	0.76	1.33	1.86	2.36
Anisotropic phase volume fraction	-	0.25	0.44	0.62	0.79
Concentration of dextran in isotropic phase, $\mu\text{mol/L}$	0.31	0.38	0.44	0.61	0.89
Concentration of dextran in anisotropic phase, $\mu\text{mol/L}$	-	0.25	0.22	0.25	0.28
Partition coefficient for dextran between phases	-	1.6	2.0	2.5	3.2

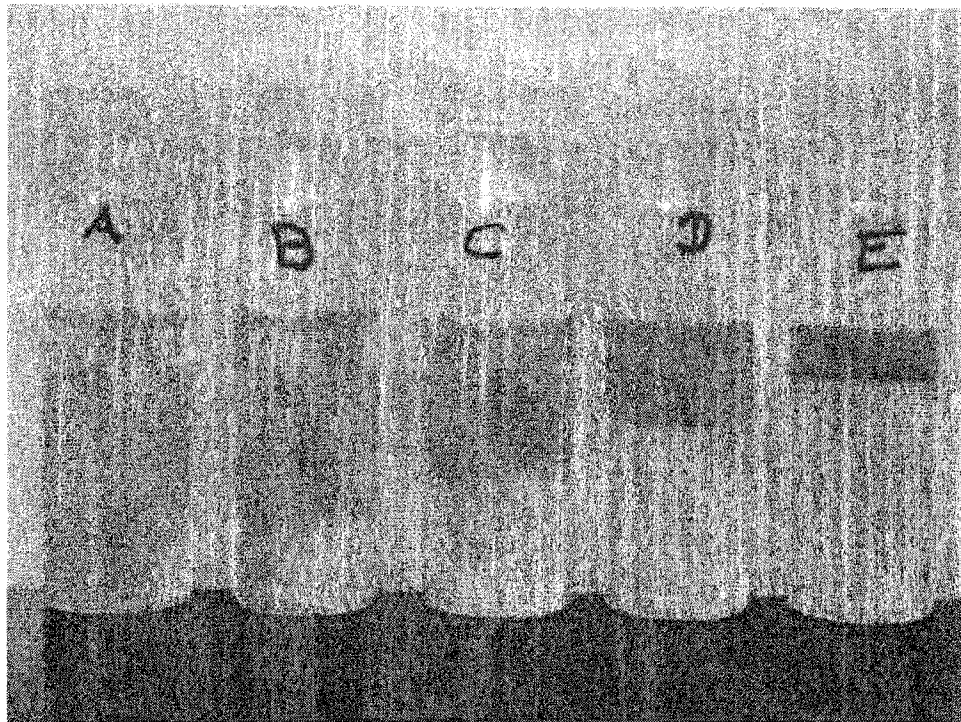


Figure 3.1 Digital photograph of samples with the same blue dextran concentration in each vial and increasing cellulose concentration from Vial A to E (see Table 3.1), showing the preferential partitioning of blue dextran into the upper isotropic phase.

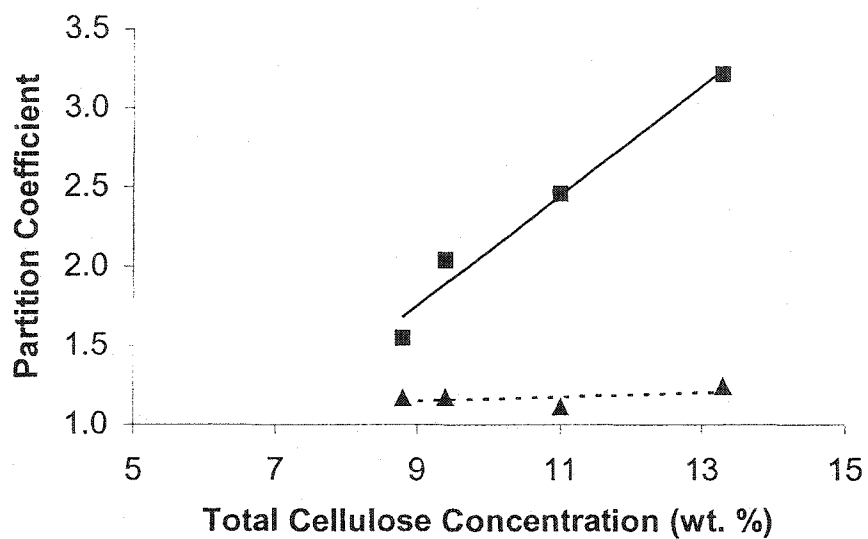


Figure 3.2 Partition coefficients for dextran between isotropic and anisotropic phases versus cellulose concentration for samples B to E. Upper trend line (squares) shows experimental values and lower trend line (triangles) shows theoretical values calculated using Equation III.3.

concentrations in the isotropic and anisotropic phases are predicted to remain constant across the biphasic region. As the concentration difference between the isotropic and anisotropic phases increases, more blue dextran partitions into the isotropic phase. This experimental observation has been predicted by the following equation<sup>23</sup>

$$K = \exp(B_{rc}(c_r^n - c_r^i)) \quad (\text{III.3})$$

where  $B_{rc}$  is the second virial coefficient of the rod-coil interactions, which depends on the relative sizes of rods and coils, and  $c_r^n$  and  $c_r^i$  are the number densities of rods in the nematic and isotropic phases, respectively. (More detail on equation III.3 is given in the appendix). The order of magnitude of the rod-coil second virial coefficient is given by  $B_{rc} \sim LD^{1/3}R_G^{5/3}$ . Our experimental partition coefficient is larger and increases more with nanocrystal concentration than is predicted by this theory (Figure 3.2). Since our observed concentrations in each phase are not constant across the biphasic region, and the theory gives an order of magnitude only, the discrepancy is not unexpected.

In order to try and minimize the effect of varying phase compositions across the biphasic region, another set of vials was prepared with the same concentration of cellulose suspension in each vial and a constant anisotropic volume fraction of 0.60. Vial 1 was left blank and increasing amounts of blue dextran were added to each subsequent vial. The compositions of the samples are given in Table 3.2. After phase separation it was readily visible that the blue dextran was enriched in the isotropic phase. As the concentration of blue dextran increased, the partition coefficient increased slightly. The experimental and theoretical partition coefficients are in closer agreement for the second set of vials. The experimental values for the partition coefficient were around 3 (Table 3.2) and values calculated from Equation III.3 were from 1.07 to 1.19, with both experimental and theoretical values increasing slightly as the dextran concentration increased.

All the vials were initially at the same cellulose concentration; however, after the dextran was added, the relative proportions of cellulose in each phase changed. This divergence in the isotropic and anisotropic cellulose concentrations on the addition of dextran is illustrated by a partial phase diagram (Figure 3.3). The number densities of

Table 3.2 Composition of biphasic samples with increasing total dextran concentration and fixed concentration of cellulose nanocrystals.

Sample	1	2	3	4	5
Total cellulose concentration (wt.%)	10.3	10.3	10.3	10.3	10.3
Cellulose in isotropic phase (wt.%)	9.9	9.8	9.7	9.4	9.0
Cellulose in anisotropic phase (wt.%)	10.9	10.8	11.3	11.3	11.7
Volume of isotropic phase (mL)	0.80				
Volume of anisotropic phase (mL)	1.20				
Anisotropic phase volume fraction	0.60				
Concentration of dextran in isotropic phase, $\mu\text{mol/L}$	-	0.14	0.37	0.64	0.92
Concentration of dextran in anisotropic phase, $\mu\text{mol/L}$	-	0.05	0.13	0.22	0.28
Partition coefficient for dextran between phases	-	2.7	2.9	2.9	3.3

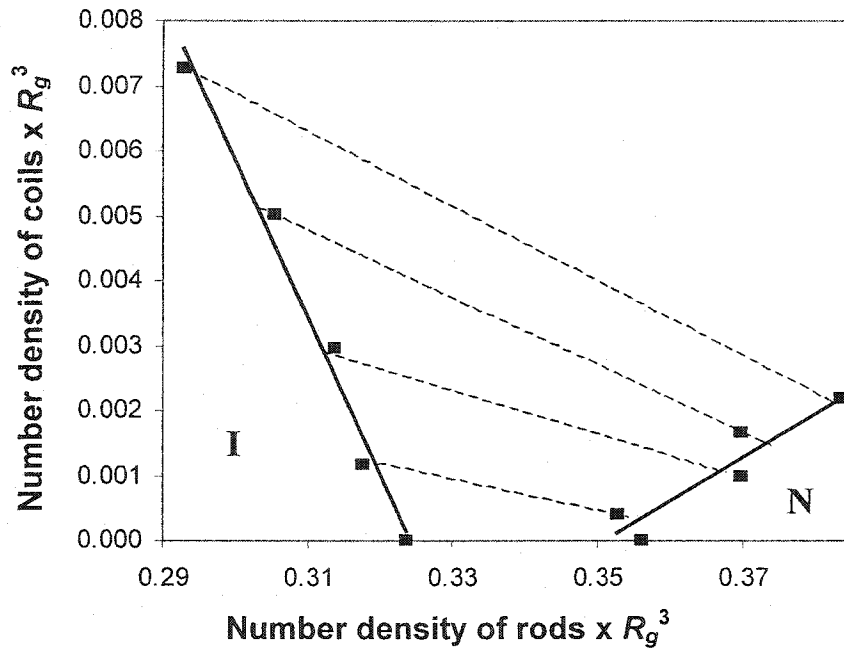


Figure 3.3 Partial phase diagram of cellulose suspension with blue dextran added, using data from samples 1 to 5 (Table 3.2). The number densities of the rods and coils are multiplied by  $R_g^3$ , where  $R_g$  is the radius of gyration of the dextran coil, in order to make the values dimensionless. The isotropic region, I, is on the left hand side and the chiral nematic region, N, is in the lower right hand corner. The downward sloping tie lines in the biphasic region indicate that the isotropic phase is rich in coils and the anisotropic phase is rich in rods.

cellulose rods and dextran coils were multiplied by  $R_g^3$  to make the values dimensionless, following Sear's theory<sup>23</sup>. The squares represent experimental values; the solid lines, which are best fit to the data, mark the phase boundaries, and the dotted lines are the tie lines. The left-hand portion of the diagram is the isotropic region, I, the lower right-hand corner is the chiral nematic region, N, and the middle represents the biphasic region. The downward slope of the tie lines shows that the density of dextran coils in the chiral nematic region is much less than in the isotropic region. The addition of dextran causes a widening of the biphasic region. This occurs for two reasons: the negative slope of the isotropic boundary line indicates that rod density decreases in the isotropic phase and the positive slope of the chiral nematic phase boundary indicates that rod density increases in the chiral nematic phase. There is a mutual exclusion between the cellulose rods and the dextran coils. As more dextran moves into the isotropic phase, the osmotic pressure increases. In order to balance the osmotic pressure, cellulose rods migrate from the isotropic phase to the chiral nematic phase, causing the observed widening of the biphasic region. The mutual exclusion of rods and coils was predicted theoretically by Flory who stated that the addition of coils replaces the rods in the isotropic phase and the rod concentration in the nematic phase consequently increases<sup>14</sup>. In our work, the chiral nematic region has a significant tolerance for dextran coils, indicating that the coils are somehow incorporated into the ordered structure. Thus, we next examined the effect of adding blue dextran to a completely ordered phase of cellulose rods.

### 3.3.3 Anisotropic Samples

Blue dextran was added in increasing amounts, from approximately 1  $\mu\text{mol/L}$  to 7  $\mu\text{mol/L}$ , to the completely anisotropic samples in Vials I to IV. The blue dextran initially spread evenly throughout the cellulose suspensions, but after a few days a phase separation occurred into a dark blue upper phase and a lighter blue lower phase. The volume fraction of the upper phase increased during the first week and slowly levelled off over the period of a month (Figure 3.4). The more blue dextran that was added to the vial, the larger the final volume of the upper phase. Thus, over time the addition of

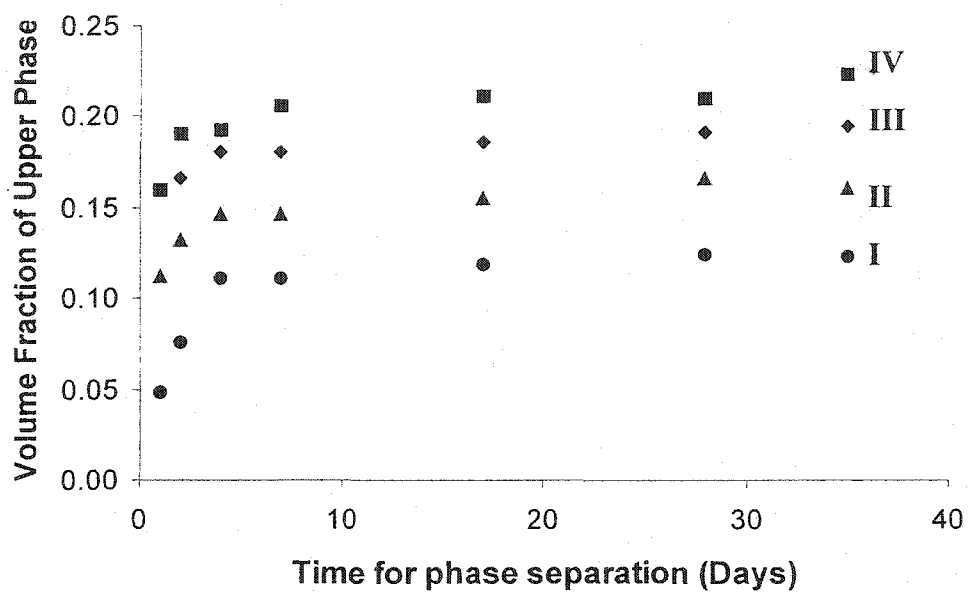


Figure 3.4 Volume fraction of upper isotropic phase versus time for phase separation of an initially anisotropic sample (13.0 wt% nanocrystals) induced by adding increasing amounts of blue dextran to Vials I to IV.

dextran forced the suspension into a two-phase system. (This behaviour contrasts with that of the more dilute biphasic samples, where the concentrations listed in Tables 3.1 and 3.2 remained constant for several months.)

The phase separation occurring in the anisotropic samples involves the upward migration of dextran and the downward migration of cellulose rods, similar to the mutual exclusion between these two particles in the biphasic samples. The initial concentration of the anisotropic phase was 13.0% cellulose by weight. After the induced phase separation, the upper phase was 5.3% and 6.6% and the lower phase was 13.2% and 15.5% in Vials III and IV, respectively. The blue dextran migrated preferentially into the phase with the lower density of cellulose rods, with partition coefficients of 6.2 and 7.6 for Vials III and IV, respectively. (The volume of the upper phase in Vials I and II was too small to separate for accurate measurements.)

Although there are still differences between experimental and theoretical partition coefficients, the results for the anisotropic samples correlate with those from the biphasic samples (Figure 3.5). The difference in rod concentration between the upper and lower phases plays a major role in the partitioning of dextran. With the biphasic samples, the initial concentration difference is augmented upon the addition of dextran; while for the anisotropic samples the addition of dextran instigates phase separation, creating a difference in rod concentration. There is a larger rod concentration difference for the initially anisotropic samples and therefore larger partition coefficients.

When the phases generated by adding dextran to an initially anisotropic sample were viewed between crossed polarizers, it was evident that the dextran-rich upper phase had become almost completely isotropic. The background was dark with a few bright tactoids, small volumes of suspension displaying short parallel white lines, indicating the initial stage of ordering of a chiral nematic liquid crystal (Figure 3.6). Before the addition of dextran, the anisotropic phase exhibited long continuous fingerprint lines with very few disclinations, characteristic of a well-ordered chiral nematic liquid crystalline phase (Figure 3.7). Adding dextran not only caused an isotropic phase to separate, but also caused changes in the texture of the anisotropic phase. The fingerprint lines decreased in pitch and followed a more tortuous path with many disclinations (Figure

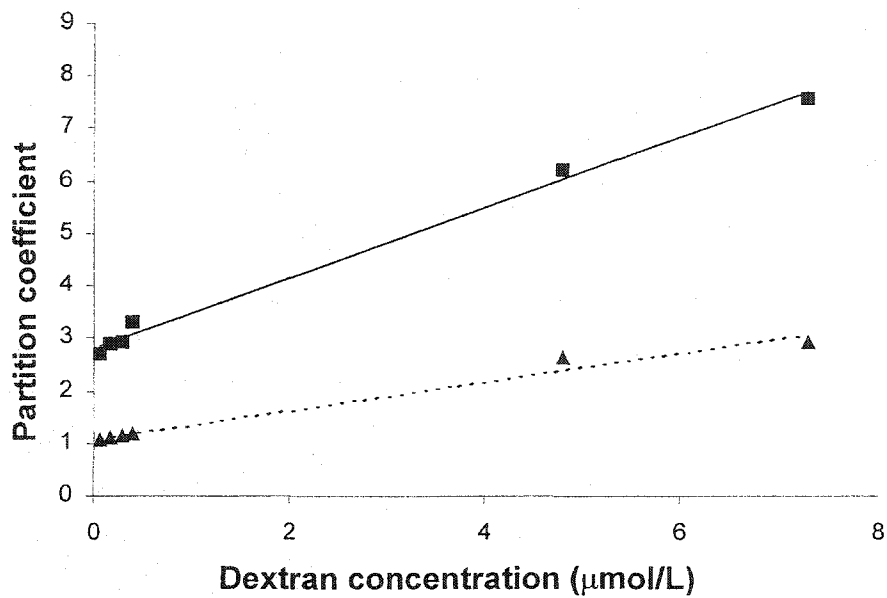


Figure 3.5 Partition coefficient versus dextran concentration for biphasic samples 2 to 5 and anisotropic samples III and IV. Upper trend line (squares) shows experimental values and lower trend line (triangles) shows theoretical values, calculated using Equation III.3.

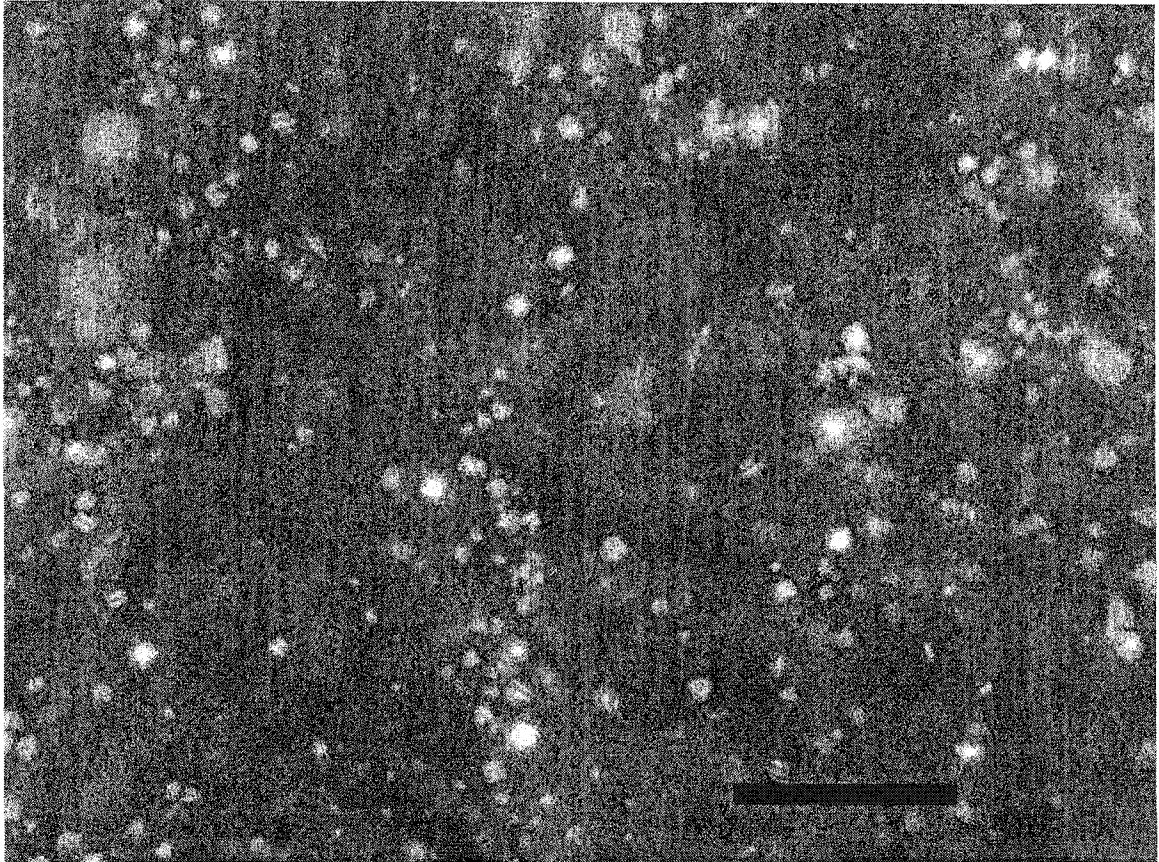


Figure 3.6 Photomicrograph between crossed polarizers of the upper dextran-rich phase (scale bar 100  $\mu\text{m}$ ).

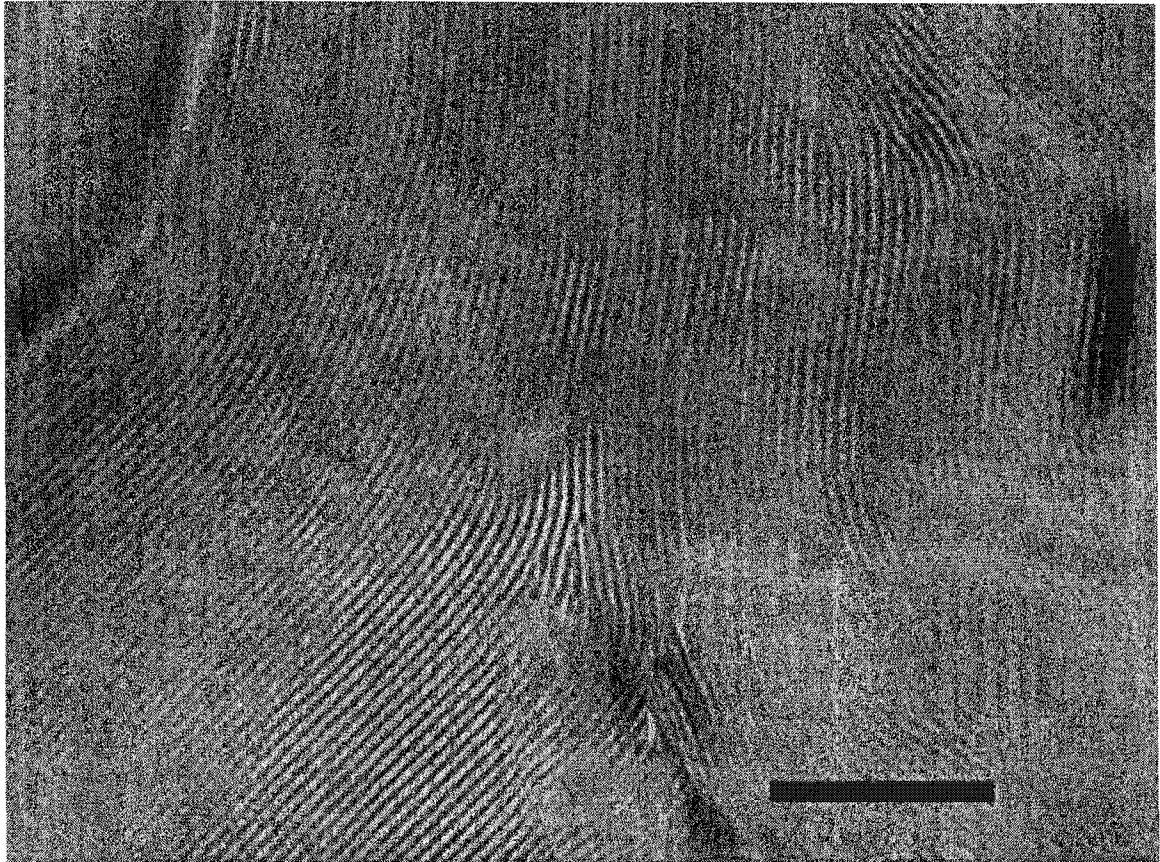


Figure 3.7 Photomicrograph between crossed polarizers of a completely anisotropic sample before the addition of blue dextran showing characteristic fingerprint texture and only a few disclinations (scale bar 100  $\mu\text{m}$ ).

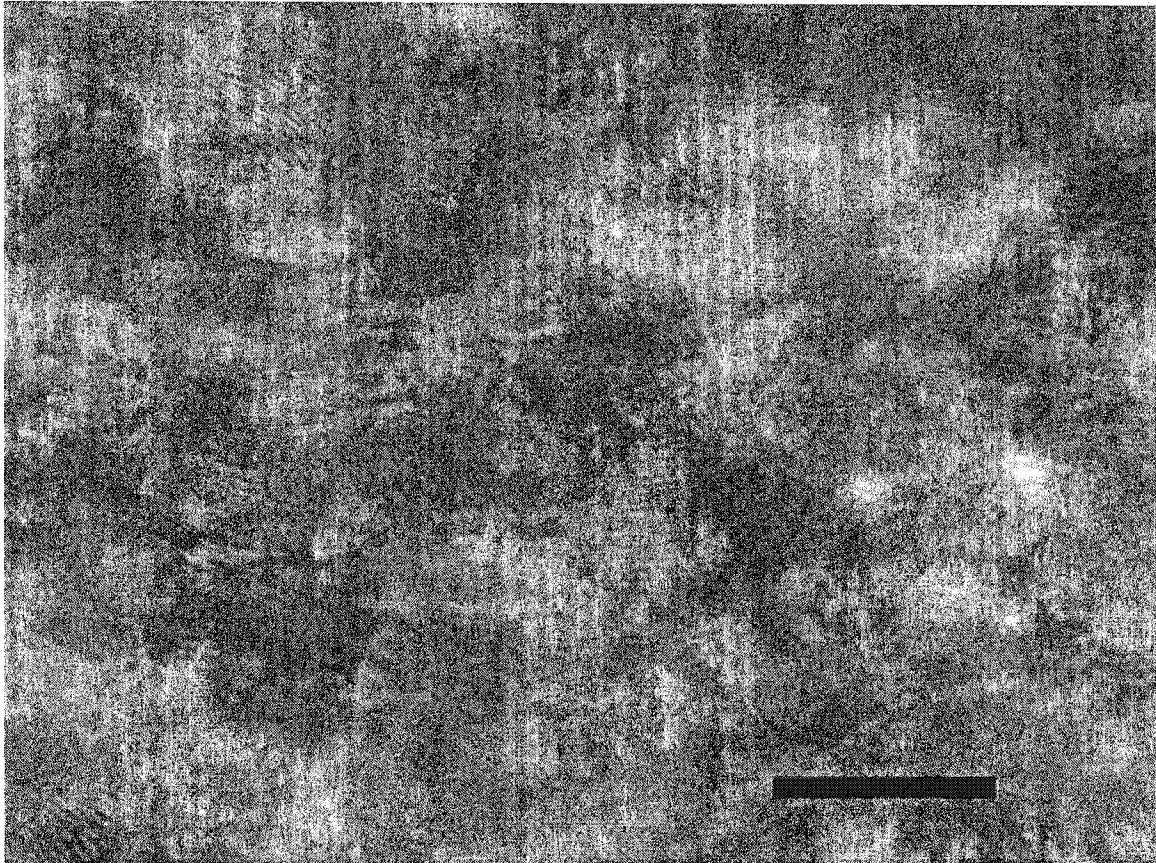


Figure 3.8 Photomicrograph between crossed polarizers of a lower dextran-poor phase showing distorted fingerprint texture and numerous disclinations (scale bar 100  $\mu\text{m}$ ).

3.8). The fingerprint texture indicates that the structure is initially uniform, and free from distortions and defects over macroscopic distances, in the absence of dextran molecules. Because of their size and shape, dextran coils can't readily fit into the chiral nematic structure assumed by the suspension of rods. They are however compatible with dilute isotropic suspension of rods, and apparently even with the more concentrated isotropic suspensions of rods in the two-phase region. However, the exclusion from the anisotropic phase is not complete. The question is, how do the coils fit into the ordered phase at relatively high coil and rod concentrations? Comparison of Figures 3.7 and 3.8 suggest that the dextran-rich phases are also defect-rich. The creation of distortions and defects in a liquid crystalline phase costs energy, thus destabilizing the ordered phase with respect to the isotropic phase, and contributing to the appearance of the isotropic phase. Furthermore, by definition, defects are regions where the liquid crystalline director is undefined<sup>24</sup>. The dimensions of such regions must be at least of the order of the length of the rods, and it seems possible that the dextran coils can "hide" in these defects. Thus we postulate that in addition to the effects of size and shape, the defect texture of liquid crystalline phases may contribute to the partitioning of coils between the ordered and disordered phases in situations where the rod-coil interactions are athermal and concentrations are high.

### 3.4 CONCLUSIONS

The partitioning of dextran between isotropic and anisotropic phases of cellulose suspensions is influenced by, and has an influence on, the relative rod concentrations in each phase. In purely isotropic suspensions, the two components coexist since the entropy of mixing dominates the interaction at low cellulose concentrations. In biphasic samples, the blue dextran is preferentially partitioned into the isotropic phase, the phase with the lower cellulose rod concentration. The addition of blue dextran to these samples causes a widening of the biphasic region due to a mutual exclusion between the cellulose rods and the dextran coils. In completely anisotropic samples, the addition of dextran induces a phase separation into a coil-rich, rod-poor isotropic phase and a coil-poor, rod-

rich anisotropic phase. The presence of dextran in the anisotropic phase results in a distorted liquid crystalline texture.

### 3.5 REFERENCES

- (1) Revol, J.-F.; Godbout, L.; Dong, X.-M.; Gray, D. G.; Chanzy, H.; Maret, G. *Liquid Crystals* **1994**, *16*, 127-134.
- (2) Onsager, L. *Annals New York Academy of Sciences* **1949**, *51*, 627-659.
- (3) Dong, X. M.; Kimura, T.; Revol, J.-F.; Gray, D. G. *Langmuir* **1996**, *12*, 2076-2082.
- (4) Krässig, H. A. *Cellulose: Structure, Accessibility, and Reactivity*; Gordon and Breach Science Publishers: Yverdon, 1993.
- (5) Ioan, C. E.; Aberle, T.; Burchard, W. *Macromolecules* **2000**, *33*, 5730-5739.
- (6) Adams, M.; Fraden, S. *Biophysical Journal* **1998**, *74*, 669-677.
- (7) Bianchi, E.; Ciferri, A.; Tealdi, A. *Macromolecules* **1982**, *15*, 1268-1272.
- (8) Inomata, K.; Ohara, N.; Shimizu, H.; Nose, T. *Polymer* **1998**, *39*, 3379-3386.
- (9) Ramzi, M.; Borgström, J.; Piculell, L. *Macromolecules* **1999**, *32*, 2250-2255.
- (10) Takayanagi, M.; Ogata, T.; Morikawa, M.; Kai, T. *Journal of Macromolecular Science - Physics* **1980**, *B17*, 591-615.
- (11) Hwang, W.-F.; Wiff, D. R.; Benner, C. L.; Helminiak, T. E. *Journal of Macromolecular Science - Physics* **1983**, *B22*, 231-257.
- (12) Adams, M.; Dogic, Z.; Keller, S. L.; Fraden, S. *Nature* **1998**, *393*, 349-352.
- (13) Koenderink, G. H.; Vliegenthart, G. A.; Kluijtmans, S. G. J. M.; van Blaaderen, A.; Philipse, A. P.; Lekkerkerker, H. N. W. *Langmuir* **1999**, *15*, 4693-4696.
- (14) Flory, P. J. *Macromolecules* **1978**, *11*, 1138-1141.
- (15) Flory, P. J. In *Liquid Crystal Polymers I*; Gordon, M., Ed.; Springer-Verlag: Berlin, 1984; Vol. 59.
- (16) Vliegenthart, G. A.; Lekkerkerker, H. N. W. *Journal of Chemical Physics* **1999**, *111*, 4153-4157.
- (17) Dong, X. M.; Gray, D. G. *Langmuir* **1997**, *13*, 2404-2409.
- (18) Nordmeier, E. *Journal of Physical Chemistry* **1993**, *97*, 5770-5785.
- (19) Sigma-Aldrich Product No. D5751 Blue Dextran, Product Information, 1997.
- (20) Mao, Y.; Cates, M. E.; Lekkerkerker, H. N. W. *Journal of Chemical Physics* **1997**, *106*, 3721-3729.
- (21) Sperry, P. R. *Journal of Colloid and Interface Science* **1984**, *99*, 97-108.
- (22) Hamad, E. Z.; Ijaz, W.; Ali, S. A.; Hastaoglu, M. A. *Biotechnology Progress* **1996**, *12*, 173-177.

- (23) Sear, R. P. *Journal de Physique II* 1997, 7, 877-886.
- (24) Collings, P. J.; Hird, M. *Introduction to Liquid Crystals*; Taylor & Francis Ltd.: London, 1998.

## **Chapter 4**

### **Induced Circular Dichroism of Chiral Nematic Cellulose Films**

## 4.1 INTRODUCTION

Nematic liquid crystals are known to form spontaneously from solutions of rigid, rod-like molecules. This behaviour, which was first explained theoretically by Onsager<sup>1</sup>, has been observed for a range of colloidal particles including tobacco mosaic virus<sup>2</sup>, poly(tetrafluoroethylene)<sup>3</sup>, and boehmite<sup>4</sup>. When the particles involved are optically active, chiral nematic liquid crystals may be formed. Colloidal suspensions of cellulose and chitin, optically active biopolymers, have both been shown to display liquid crystalline behaviour<sup>5</sup>. Colloidal suspensions of cellulose crystallites form chiral nematic liquid crystals upon reaching a critical concentration<sup>6</sup>. The rod-like cellulose crystallites line up parallel to each other in pseudo-layers, with the orientation of the rods in each layer rotated slightly with respect to the layer below, forming a helicoidal superstructure. The axis of the helicoidal superstructure runs perpendicular to the long axis of the individual cellulose rods. Due to this unique structure, colloidal suspensions of cellulose crystallites have novel optical properties.

Handedness and pitch are the two major features that characterize the helicoidal superstructure formed by chiral nematic liquid crystals. The orientation of pseudo-layers in a right-handed chiral nematic changes in a clockwise direction on moving away from the observer along the chiral nematic axis; the layers rotate anticlockwise in a left-handed chiral nematic. The pitch of a helicoid is the distance required for the pseudo-layers to complete one full rotation. The chiral nematic pitch,  $P$ , is related to the wavelength of maximum reflection,  $\lambda$ , by

$$\lambda = n P \tag{IV.1}$$

where  $n$  is the average refractive index<sup>7</sup>. When the incident light is not normal to the surface of the liquid crystal, an angular dependence arises and wavelength becomes

$$\lambda = n P \sin \varphi \tag{IV.2}$$

where  $\varphi$  is the angle of incidence. Since the reflected wavelength changes with angle of incidence, chiral nematic liquid crystals exhibit iridescent colours. In addition to reflecting a particular wavelength of light, the light reflected by chiral nematic liquid crystals is also selectively polarized: left-handed liquid crystals reflect left-handed circularly polarized light (CPL) and right-handed liquid crystals reflect right-handed

CPL<sup>8</sup>. Circular dichroism can be used to measure the difference in apparent absorption of right- and left-handed circularly polarized light for chiral nematic liquid crystals. The reflection of CPL appears as apparent absorption of the incident light.

Optical properties of chiral nematic solutions and films of cellulose derivatives have been investigated. Circular dichroism was observed for mesophases of cellulose derivatives such as (ethoxypropyl)cellulose<sup>9</sup>, (hydroxypropyl)cellulose<sup>10</sup>, (acetyl)(ethyl)cellulose<sup>11,12</sup>, and cellulose acetate and triacetate<sup>13</sup>. The handedness of the chiral nematic mesophase could be determined from CD measurements. Most of the cellulose derivatives were found to form right-handed chiral nematics<sup>9,10,12</sup>, while cellulose triacetate formed a left-handed chiral nematic<sup>13</sup>. In some cases the handedness was found to depend on the degree of substitution of the cellulose derivative<sup>11</sup>.

The handedness of mesophases of cellulose itself can be determined in a similar manner. Since cellulose has no chromophores that absorb in regions easily accessible to most spectropolarimeters, mesophases of cellulose crystallites must first be doped with an achiral dye that forms a close association with the cellulose backbone, such as Congo red or Trypan blue<sup>14</sup>. The structure of the cellulose mesophase can then be inferred from the induced circular dichroism (ICD) of the dye, which has been placed in a chiral environment.

Circular dichroism is defined as the difference in absorption of left- and right-handed circularly polarized light

$$CD = A_L - A_R \quad (IV.3)$$

where  $A_L$  is the absorption of left-handed CPL and  $A_R$ , the absorption of right-handed CPL<sup>15</sup>. Thus, if a chiral nematic sample predominantly reflects left-handed CPL, the light transmitted through the sample will be reduced by the amount of reflected light, resulting in the apparent absorption of left CPL, but not of right CPL. The CD signal will therefore be positive and will indicate a left-handed helical structure. Conversely, right-handed helices will give rise to negative CD signals<sup>16</sup>. Thus, for chiral nematic samples that reflect visible light, the sign of the apparent CD signal resulting from the reflection of circularly polarized light gives the handedness of the chiral nematic helicoidal structure. Determining the handedness of the chiral nematic structure from induced CD measurements is slightly more involved.

To determine the handedness of the chiral nematic structures from ICD measurements, the ratio of  $\lambda_0$ , the wavelength of the chiral nematic reflection band, to  $\lambda_{ab}$ , the wavelength of dye absorption, must be known. Saeva *et al.* have shown that for  $\lambda_0/\lambda_{ab} > 1$  a positive ICD spectrum indicates a right-handed arrangement and a negative ICD spectrum, a left-handed arrangement<sup>17</sup>. The opposite is true for  $\lambda_0/\lambda_{ab} < 1$ . (Note that Saeva *et al.* defined a left-handed helix as one that selectively *transmits* left-handed CPL, whereas following the definition in this paper a left-handed helix selectively *reflects* left-handed CPL; the above terms have already been reversed to correspond with this paper). Experimental measurements on cholesteric mesophases of known handedness, such as N-(p-methoxybenzylidene)-p-butylaniline in cholesteryl chloride and cholesteryl nonanoate<sup>18</sup> and pyrene and anthracene in cholesteryl chloride-cholesteryl nonanoate<sup>17</sup> lead to this interpretation of the sign of the ICD signals. This relation between the sign of the ICD signal and the position of the chiral nematic reflection band is also supported by theoretical calculations<sup>19</sup>.

Previously, the ICD of colloidal suspensions of cellulose crystallites was measured<sup>14</sup>; in the present study, we focus on the ICD of solid cellulose films. Under appropriate conditions, the chiral nematic order of the colloidal suspensions can be preserved in solid films. If the solid films have a helicoidal structure an ICD peak should be observed on addition of a suitable dye. Modifying the preparation conditions changes both the pitch of the films and the degree of order in the films. Further ICD measurements indicate the effect of these changes on the superstructure of the films.

## 4.2 EXPERIMENTAL

### 4.2.1 Sample Preparation

A colloidal suspension of cellulose crystallites was prepared by hydrolyzing a high-cellulose-content dissolving grade softwood pulp (Temalfa, Tembec Inc.) following the procedure described in Chapter 2. The final aqueous suspension was 2.5% concentration by weight with a pH of 2.9. Stock solutions of sodium chloride (0.01 M, J. T. Baker) and Trypan blue (0.001 M, Aldrich) were prepared in volumetric flasks using purified water.

Solid cellulose films were made by the slow evaporation of the colloidal suspension under ambient conditions. 5-mL aliquots of the suspension were pipetted into 50-mm petri dishes (Canada Wide Scientific), forming solid films  $45 \pm 5 \mu\text{m}$  thick. The doped films were prepared by adding the appropriate volume (20  $\mu\text{L}$  - 500  $\mu\text{L}$ ) of 0.001 *M* Trypan blue to the colloidal suspension and mixing until a homogeneous solution was obtained. The water was allowed to evaporate, leaving approximately  $8 \times 10^{-4}$  g of dye per gram of cellulose film.

The original salt-free cellulose suspension forms films that reflect in the infrared region. To produce films that reflect in the visible and ultraviolet regions an appropriate amount of the stock NaCl solution was added prior to evaporation in order to decrease the pitch of the films<sup>20</sup>.

Magnetically aligned films were prepared by drying the cellulose suspension in a magnetic field generated by a NMR spectrometer (Chemagnetics M100 or CMX 300). The two different spectrometers generated magnetic fields of 2.1 T and 7.1 T, respectively. The petri dish was placed on a Teflon adapter that was secured on top of the probe such that the sample sat perpendicular to the direction of the magnetic field. Due to the negative diamagnetic susceptibility of cellulose, this alignment should promote the formation of planar texture, as the cellulose crystallites tend to orient with their long axes perpendicular to the magnetic field<sup>21,22</sup>.

#### 4.2.2 Instrument Measurements

UV-visible absorption spectra were measured using a Perkin Elmer Lambda 14 UV/VIS Spectrometer. The absorption spectra of dyed films were obtained by subtracting the spectrum of an equivalent film with no dye added.

Left- and right-handed circular polarizers were constructed by aligning a linear polarizer with a 1/4 wave retarder (Edmund Scientific) in the proper orientation. The individual absorbance spectra for incident left-handed circularly polarized light (CPL) and right-handed CPL were then measured by placing the appropriate circular polarizer in front of the incident beam to block either right- or left-handed CPL.

Circular dichroism (CD) spectra were measured using a Jasco 710 Spectropolarimeter. Samples were scanned at 100 nm/min with a step resolution of 0.2

nm and a 1 nm bandwidth. Baseline corrections were made by subtracting the spectrum of an equivalent film containing no dye. The spectropolarimeter measures the differences in absorption, or apparent absorption, of left- and right-handed CPL and this difference is expressed in terms of ellipticity in mdeg. For the magnetically aligned samples, spectra shown are an average of spectra taken at 30° intervals as the sample was rotated through 180°.

Photomicrographs were taken using a Nikon Microphot-FXA optical microscope equipped with a camera, with crossed-polarizers and a 530-nm red plate in place.

### 4.3 RESULTS AND DISCUSSION

The pitch of the chiral nematic liquid crystal can be controlled by varying the salt content of the cellulose suspension. Adding salt increases the ionic strength and this has been found to result in a decrease in chiral nematic pitch leading to a tighter helix<sup>20</sup>. In this way, solid films were made with their maximum apparent absorbance in the infrared, visible, and ultraviolet regions of the electromagnetic spectrum. These three types of films were subsequently doped with Trypan blue in order to measure induced circular dichroism.

#### 4.3.1 Films with reflection band in the infrared region

When an aqueous solution of Trypan blue is measured in the spectropolarimeter no CD signal is obtained, indicating that Trypan blue is a CD inactive dye. The CD spectrum of an undoped cellulose film also results in a flat CD signal. However, when the dye molecules are combined with the cellulose crystallites in a solid film a negative CD peak is obtained (Figure 4.1). The induced circular dichroism (ICD) peak occurs at the maximum absorbance wavelength of Trypan blue, suggesting that the dye molecules are now in a chiral environment. It is assumed that the dye molecules have aligned their long axes parallel to the long axes of the cellulose crystallites, also forming a supermolecular helical array. This chiral arrangement of chromophores leads to the ICD signal.

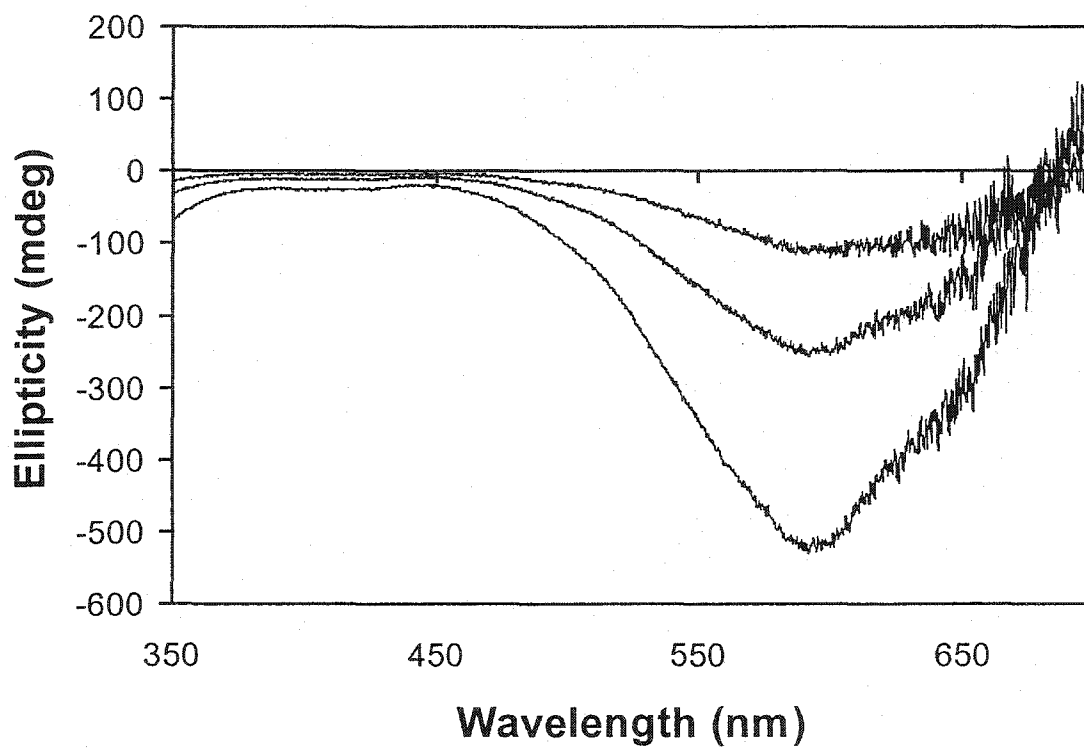


Figure 4.1 ICD spectra of cellulose films with reflection band in the IR region. The films were doped with Trypan blue ( $1.9 \times 10^{-5}$ ,  $4.8 \times 10^{-5}$ ,  $9.6 \times 10^{-5}$  g).

The detection of an ICD peak confirms that the chiral nematic order of the cellulose suspension has been preserved in the solid film. The reflection band of the chiral nematic is at a larger wavelength than the dye absorption band,  $\lambda_0/\lambda_{ab} > 1$ , so the observed negative ICD peak indicates a left-handed chiral nematic<sup>17</sup>. Previous studies on cellulose triacetate also showed CD peaks indicating a left-handed structure<sup>13</sup>.

As the concentration of Trypan blue in the films is increased, the measured ellipticity also increases, as was previously observed for anisotropic suspensions of cellulose crystallites doped with Congo red<sup>14</sup>. The relationship between dye concentration and measured ellipticity was found to be linear at low concentrations, levelling off near the upper limit of the spectropolarimeter.

If the observed ICD peak is in fact due to the chiral nematic structure, changes to the structure should cause changes in the measured ellipticity. As the chiral nematic pitch of an anisotropic suspension decreases, the measured ellipticity of the dye decreases<sup>14</sup>. In the present research, two structural changes were investigated: decreasing the pitch of the chiral nematic films and increasing the order in the films through magnetic alignment.

#### 4.3.2 Films with reflection band in the visible region

Sodium chloride was added to the cellulose suspension in order to produce shorter pitch chiral nematic films that reflected light in the visible region. The ICD measurements of these films, which were doped with 100  $\mu\text{L}$  of 0.001 M Trypan blue, went off the scale of the spectropolarimeter. However, this is not necessarily due to a larger ICD signal. There are two distinct optical effects occurring in these doped cellulose films: the reflection of CPL due to chiral nematic structure and the absorption of CPL due to the presence of dye molecules in a chiral environment. The sign and wavelength of the apparent CD peak, caused by the reflection of CPL, are related to the handedness and pitch of the cellulose film. The sign of the induced CD peak is also related to the handedness of the film, but the wavelength is determined by the maximum absorption wavelength of the dye. Due to the imperfect orientation of the chiral nematic phase in a solid film, the samples have wide reflection band peaks. Thus, the reflection band of the films in the visible region overlaps with the absorption peak of the dye. Since

the circular reflectivity due to the structure of the film is a much larger effect than that caused by the dye, measurements in the visible region by the highly sensitive spectropolarimeter went off scale. Complete reflection of one hand of circularly polarized light corresponds to 50% absorption of the peak wavelength. Absorption of 50% of the incident light corresponds to 0.3 absorption units, yet the spectropolarimeter measures to a maximum of 2000 mdeg or 0.06 absorption units.

The reflection of circularly polarized light from these films with reflection bands in the visible range can, however, be measured in an ordinary UV-visible spectrometer if one hand of CPL is blocked by a circular polarizer. This method is much less sensitive than spectropolarimetry. Results obtained in this way showed that the apparent absorbance of left-handed CPL was greater than the apparent absorbance of right-handed CPL, resulting in a positive apparent CD signal. Thus, although quantitative spectropolarimeter measurements were not possible due to the intense and broad chiral nematic reflection bands, UV-visible measurements showed that films with reflection bands in the visible range exhibit a left-handed chiral nematic structure. This more straightforward measurement of CD supports the interpretation of the ICD results, which also suggest a left-handed helical structure.

#### **4.3.3 Films with reflection band in the ultraviolet region**

Since the measurement of CD by the UV-visible spectrometer is not quantitative, we cannot compare the intensity of the peak with the pitch of the sample. When more salt was added to the cellulose suspension the chiral nematic pitch decreases and films reflecting in the UV region are formed. It was hoped that the circular reflectivity of these films should not interfere with the maximum absorption of Trypan blue.

UV films were made by adding 1, 1.5, and 2 mL of 0.01 M NaCl to 5 mL of the cellulose suspension. When these films were measured in the spectropolarimeter, the CD signal still was off scale. Checking the apparent absorbance of these films in the UV-visible spectrometer, it was found that although their maximum apparent absorbance was in the UV region, the tail of the reflection band still reflected light in the visible region, causing the CD peak to go off scale. New films were made with an even higher salt concentration (1 mL of 0.1 M NaCl). The UV-visible spectrum showed that the films had

only a minor apparent absorption in the visible region with their maximum apparent absorbance greater than 200 nm.

However, when these films, with reflection bands in the far ultraviolet, were measured in the spectropolarimeter, no ICD peak was obtained. The absence of ICD peak in the spectrum suggests that the chiral nematic order was not preserved in these high-salt-content films. The films were subsequently examined in a microscope between crossed polars. No birefringence was observed, indicating that the large amount of salt added had caused a precipitation of the colloidal particles on drying and an isotropic film had been formed. The fact that no ICD signal is observed for dye molecules in an isotropic film supports the belief that the ICD peak is caused by the dye molecules aligning in a helical array rather than just a chiral interaction between the dye molecules and chiral centres on the cellulose chains. For a similar system of rod-like cellulose particles, derived from cotton linters, it was also found that increasing salt concentration resulted in a disruption of the ordered arrangement<sup>23</sup>. Other researchers also found that the helicoidal structure was essential for the observation of an ICD signal; when the chiral nematic structure was unwound into a nematic structure using an electric field the ICD signal disappeared<sup>17</sup>.

When too much salt is added to the cellulose suspension, the resulting films lose their chiral nematic texture. As indicated by the ICD peaks, films with reflection bands in the IR and the visible regions maintained their chiral nematic structure. The textures of these films were examined under the microscope and were found to have a "grainy" texture with many small domains of aligned particles oriented randomly throughout the film (Figure 4.2). Although the texture of these films was not as ordered as an anisotropic liquid sample, it was still ordered enough to produce an ICD peak. When the film becomes isotropic and loses its liquid crystalline texture, the ICD signal disappears completely. Conversely, if the chiral nematic order of the film could be increased, the intensity of the ICD signal should increase accordingly.

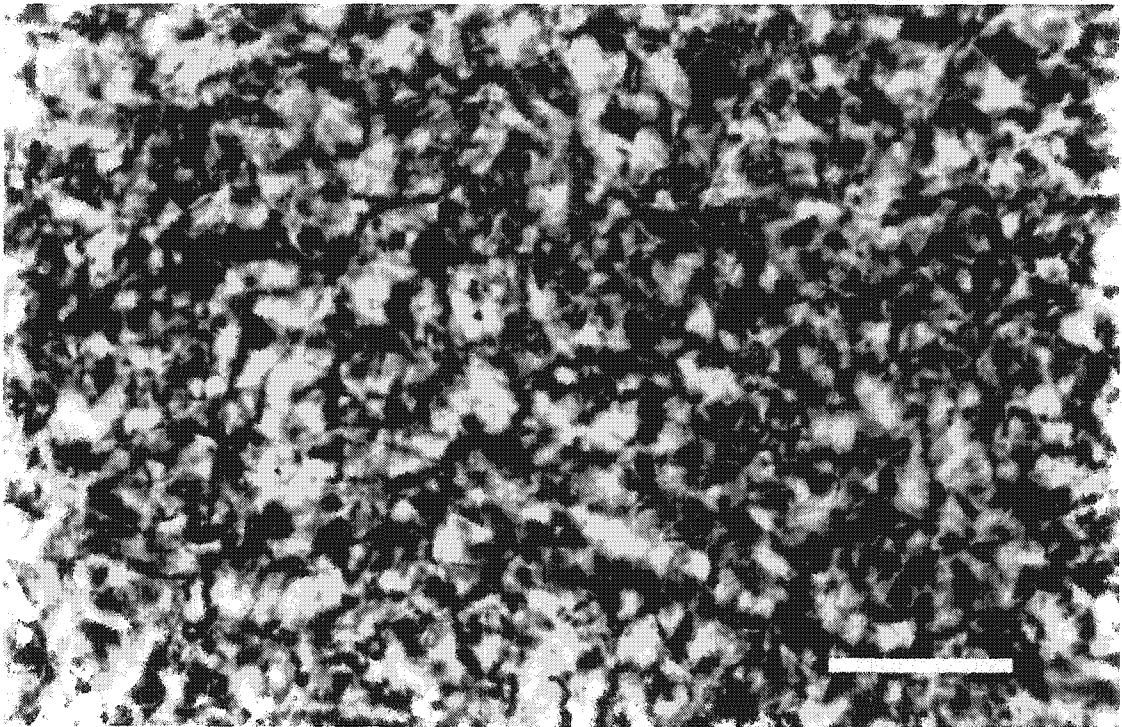


Figure 4.2 Photomicrograph between crossed polars of the grainy polydomain texture of a cellulose film that reflects light in the IR region (scale bar 1mm).

#### 4.3.4 Magnetic Alignment

Cellulose has been found to have a negative magnetic susceptibility<sup>21</sup>. Thus, aligning the particles in a magnetic field during the drying of the film should increase the order in the film. Two different electromagnets with field strengths of 2.1 T and 7.1 T were used to align the salt-free films. Photomicrographs of films prepared in each magnet are shown in Figure 4.3. The texture of the film aligned in the smaller magnet shows larger ordered domains than that of a film prepared in the absence of a magnet (Figure 4.2). The film aligned in the larger magnet shows a more ordered, oriented texture. However, the texture is far from planar, presumably due to the shrinkage stresses on the film during the drying process.

When measured in the spectropolarimeter, there was a significant difference in the ICD peak intensity of films aligned in a magnet and those not magnetically aligned (Figure 4.4). There was a smaller difference observed between the films aligned in the 2.1 T magnet and those aligned in the 7.1 T magnet. These ICD results confirm the increase in order suggested by the photomicrographs. Since dye concentration also has an effect on the intensity of the ICD peak, it was important to ensure that the dye concentrations in the dried films were uniform. Measurements with the UV-visible spectrometer showed that the total absorbance at 580 nm was very similar for all three films. Therefore the increase in ICD peak intensity can indeed be attributed to the increase in order due to magnetic alignment of the cellulose particles.

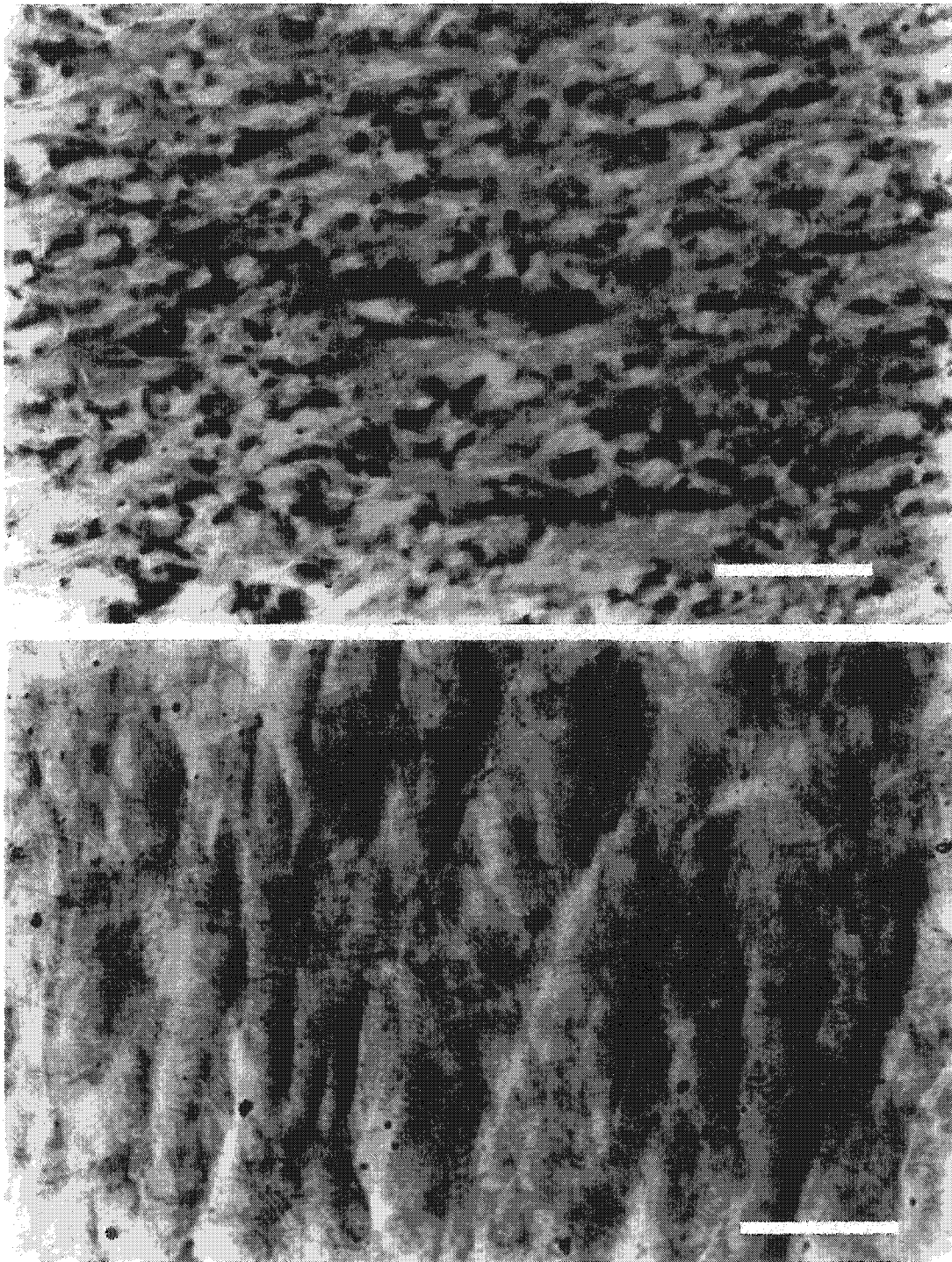


Figure 4.3 Photomicrographs between crossed polars of cellulose films (reflection band in IR region) aligned in a 2.1 T magnetic field (upper) and a 7.1 T magnetic field (lower). The magnetic field was oriented normal to the plane of the images (scale bar 1mm).

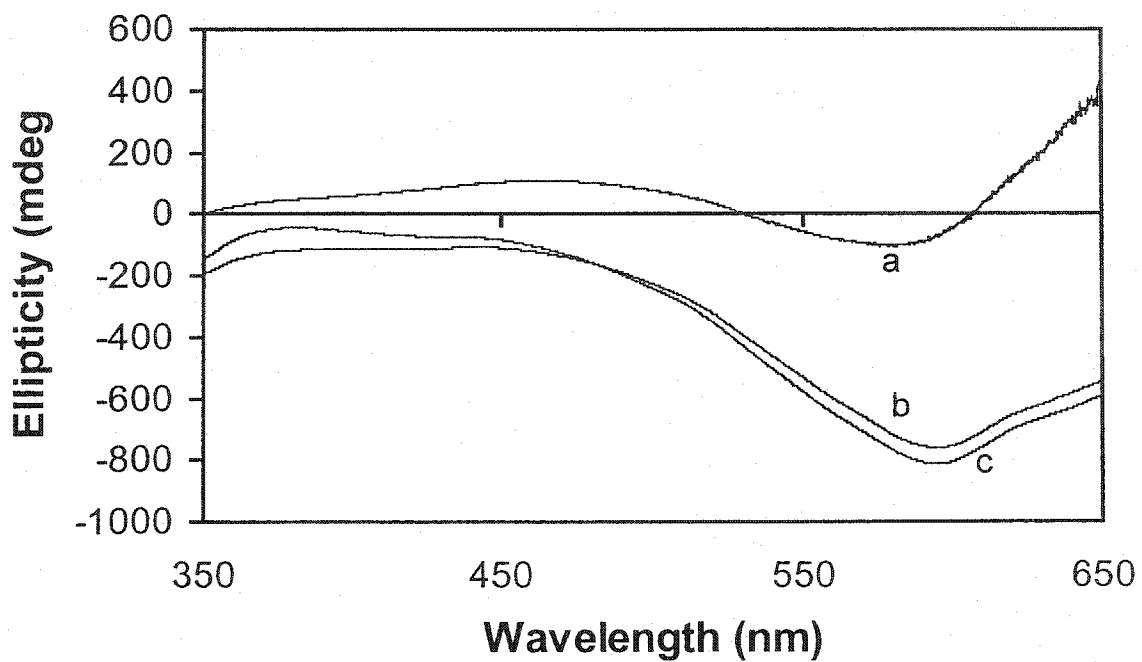


Figure 4.4 ICD spectra of cellulose films (reflection band in IR region) doped with Trypan blue ( $9.6 \times 10^{-5}$  g) and dried (a) with no aligning field; (b) in a 2.1 T magnetic field; (c) in a 7.1 T magnetic field. The magnetic field was applied normal to the plane of the film.

## 4.4 CONCLUSIONS

Both the handedness and the degree of order of a chiral nematic cellulose film can be inferred from measurements of ICD. Measurements on films reflecting light in the IR region show a negative ICD peak, indicating a left-handed chiral nematic structure. The observation of an ICD peak confirms that the liquid crystalline texture of the cellulose suspension has been preserved in a solid film. Films cast from suspensions with high electrolyte concentrations, however, showed no ICD signal, indicating the formation of an isotropic film. Films prepared in the presence of a magnetic field showed an increase in intensity of the ICD signal, suggesting an increase in the degree of order in the film. Thus, ICD has been shown to be a useful tool for characterizing chiral nematic cellulose films.

## 4.5 REFERENCES

- (1) Onsager, L. *Annals New York Academy of Sciences* **1949**, *51*, 627-659.
- (2) Fraden, S.; Maret, G.; Caspar, D. L. D.; Meyer, R. B. *Physical Review Letters* **1989**, *63*, 2068-2071.
- (3) Folda, T.; Hoffman, H.; Chanzy, H.; Smith, P. *Nature* **1988**, *333*, 55-56.
- (4) Buining, P. A.; Lekkerkerker, H. N. W. *Journal of Physical Chemistry* **1993**, *97*, 11510-11516.
- (5) Marchessault, R. H.; Morehead, F. F.; Walter, N. M. *Nature* **1959**, *184*, 632-633.
- (6) Revol, J.-F.; Bradford, H.; Giasson, J.; Marchessault, R. H.; Gray, D. G. *International Journal of Biological Macromolecules* **1992**, *14*, 170-172.
- (7) de Vries, H. *Acta Crystallographica* **1951**, *4*, 219-226.
- (8) Gottarelli, G.; Spada, G. P. In *Circular Dichroism Principles and Applications*; Nakanishi, K., Berova, N., Woody, R. W., Eds.; VCH Publishers: New York, 1994.
- (9) Ritcey, A. M.; Gray, D. G. *Macromolecules* **1988**, *21*, 1251-1255.
- (10) Ritcey, A. M.; Charlet, G.; Gray, D. G. *Canadian Journal of Chemistry* **1988**, *66*, 2229-2233.
- (11) Guo, J.-X.; Gray, D. G. *Macromolecules* **1989**, *22*, 2082-2086.
- (12) Guo, J.-X.; Gray, D. G. *Macromolecules* **1989**, *22*, 2086-2090.

- (13) Ritcey, A. M.; Holme, K. R.; Gray, D. G. *Macromolecules* **1988**, *21*, 2914-2917.
- (14) Dong, X.-M.; Gray, D. G. *Langmuir* **1997**, *13*, 3029-3034.
- (15) Rodger, A.; Norden, B. *Circular Dichroism and Linear Dichroism*; Oxford University Press: Oxford, 1997.
- (16) Hatano, M. In *Induced Circular Dichroism in Biopolymer-Dye Systems*; Okamura, S., Ed.; Springer-Verlag: Berlin, 1986; Vol. 77.
- (17) Saeva, F. D.; Sharpe, P. E.; Olin, G. R. *Journal of the American Chemical Society* **1973**, *95*, 7656-7659.
- (18) Saeva, F. D.; Wysocki, J. J. *Journal of the American Chemical Society* **1971**, *93*, 5928-5929.
- (19) Holzwarth, G.; Holzwarth, N. A. W. *Journal of the Optical Society of America* **1973**, *63*, 324-331.
- (20) Dong, X. M.; Kimura, T.; Revol, J.-F.; Gray, D. G. *Langmuir* **1996**, *12*, 2076-2082.
- (21) Sugiyama, J.; Chanzy, H.; Maret, G. *Macromolecules* **1992**, *25*, 4232-4234.
- (22) Revol, J.-F.; Godbout, L.; Dong, X.-M.; Gray, D. G.; Chanzy, H.; Maret, G. *Liquid Crystals* **1994**, *16*, 127-134.
- (23) Furuta, T.; Yamahara, E.; Konishi, T.; Ise, N. *Macromolecules* **1996**, *29*, 8994-8995.

## **Chapter 5**

### **Characterization of Model Cellulose I Surfaces Created from Nanocrystal Suspensions**

## 5.1 INTRODUCTION

Nanocrystals of cellulose may be prepared by hydrolysing dissolving pulp or cotton filter paper with sulfuric acid<sup>1</sup>. Due to the rod-like shape of the nanocrystals, suspensions and films of the cellulose particles possess liquid crystalline properties<sup>2,3</sup>. The nano-scale dimensions of the particles also impart the potential to create films with smooth surfaces. Smooth cellulose surfaces would be useful to investigate force interactions and adsorption phenomena. Fundamental studies on model cellulose surfaces could lead to a greater understanding of cellulose interactions during the manufacturing of, for example, specialty cellulose products, cotton-based textiles, and pulp and paper.

Most naturally occurring cellulose is cellulose I<sup>4</sup>, but the surface is typically not flat and so a model surface is required to study interactions between cellulose surfaces. Model surfaces have previously been prepared in a variety of ways. Early research used cellulose films regenerated from viscose and cellulose acetate<sup>5</sup>. More recent studies used microcrystalline cellulose dissolved in trifluoroacetic acid and spin-coated onto mica<sup>6</sup>. Subsequent researchers coated trimethylsilyl cellulose on hydrophobized mica using the Langmuir-Blodgett technique<sup>7</sup>. These methods are different, yet the resulting cellulose films are all amorphous surfaces of regenerated cellulose. A different approach is needed in order to produce model surfaces of the naturally occurring cellulose I.

Our cellulose nanocrystals originate from wood pulp or cotton cellulose. The acid hydrolysis preferentially targets the amorphous regions, leaving highly crystalline cellulose I. Freestanding films of the cellulose nanocrystals will be characterized by XPS and X-ray analysis. The model surface must be smooth so that interactions are due to the chemical nature of the surface and are not caused by surface irregularities. This chapter will describe the process of creating smooth cellulose surfaces from our cellulose suspensions. Several preparation techniques are examined in order to determine the best method for achieving a smooth, stable, and reproducible surface. The surfaces of our model cellulose I films will be characterized by atomic force microscopy.

## 5.2 EXPERIMENTAL

### 5.2.1 Sample Preparation

Suspensions of cellulose nanocrystals were prepared as described in Chapter 2. Model cellulose surfaces were prepared either on a freshly cleaved mica surface (Cedarlane Laboratories Ltd.) or in a polystyrene petri dish (Canadawide Scientific Ltd.). A dilute suspension (2.0% w/w) of cellulose nanocrystals was filtered through a 0.45- $\mu\text{m}$  membrane and a few drops were placed on a square of mica ( $\sim 1 \text{ cm}^2$ ) and allowed to dry under ambient conditions to form a smooth thin film. Freestanding films were formed by allowing 5-mL aliquots of the cellulose suspension to evaporate in petri dishes. Subsequent analysis was done on the bottom side of the films. Oriented cellulose surfaces were created by three different methods. The first technique was to spin-coat a dilute suspension of cellulose onto a mica surface, using a Thelco Model 14 spin-coater (Precision Scientific Co.) at 2700 rpm for 60 seconds. For the second method, a concentrated drop of suspension was sheared along a long strip of mica. For the third technique, a dilute suspension of cellulose was placed in a petri dish and allowed to concentrate. When the suspension became viscous, the excess was poured out by tilting the petri dish in one direction. The remaining suspension was then allowed to dry in a tilted position.

### 5.2.2 X-ray Photoelectron Spectroscopy

X-ray photoelectron spectroscopy (XPS) was performed to determine the surface composition of solid cellulose films originating from both dissolving pulp (Aliceta HD, Western Pulp Partnership, Port Alice, British Columbia) and cotton fibres (Whatman No. 1 filter paper). The analysis was carried out at the Helsinki University of Technology Center for Chemical Analysis. The films were secured between layers of filter paper during transport in order to minimize possible contamination. The XPS measurements were performed with an AXIS 165 electron spectrometer (Kratos Analytical) using a monochromated Al  $K\alpha$  X-ray source (12.5 kV, 8 mA). A small piece was cut from the middle of each cellulose film and secured to the sample holder with metal clips. The low-resolution survey scans were taken with a 1 eV step and 80 eV analyser pass energy;

high-resolution spectra were taken with a 0.1 eV step and 20 eV analyser pass energy. The analysis area was less than 1 mm<sup>2</sup> and measurements were taken at three different locations on each film, resulting in standard deviations of less than 1% for the surface concentrations of oxygen and carbon and 0.1% for sulfur. The standard deviation of the oxygen to carbon ratio is 0.02.

### 5.2.3 X-Ray Analysis

Solid cellulose films, coated with a finely ground powder of NaF for calibration purposes, were used for X-ray analysis. Powder diagrams of the cellulose films were recorded with a flat film camera using a Philips X-ray generator with Ni-filtered Cu K $\alpha_1$  radiation (40 kV, 20 mA). The films were exposed for 6 hours under vacuum conditions. Analysis was performed by placing the powder diagram on a light box and measuring the ring spacings at five different locations, resulting in standard deviations of 0.005 nm for the d-spacings and 0.05 degrees for the 2 $\theta$  angles. Results shown are for the film derived from Whatman filter paper, but the film derived from wood pulp showed the same pattern.

### 5.2.4 Atomic Force Microscopy

The model cellulose surfaces were attached to AFM specimen discs and examined by atomic force microscopy as described in Chapter 2. Images were analyzed using the roughness analysis tool provided with the AFM software (Digital Instruments, Version 4.32r1). Values for both root-mean-square roughness,  $R_q$ , and maximum z-range,  $R_{max}$ , were obtained from the average of five different scans on three different samples, resulting in standard deviations of 0.2 nm for  $R_q$  and 2 nm for  $R_{max}$  for the cellulose films. For mica, the standard deviations are 0.01 nm for  $R_q$  and 0.4 nm for  $R_{max}$ . The section analysis tool was used to show the contour profiles of the model surfaces.

## 5.3 RESULTS AND DISCUSSION

Our model cellulose surfaces were first characterized by XPS in order to determine the purity of the cellulose. Next the samples were analyzed by X-ray diffraction to distinguish between native cellulose I and regenerated cellulose. In order to be useful for future studies on force interactions the cellulose surfaces must be smooth. We used AFM to assess the smoothness of our model cellulose.

### 5.3.1 X-ray Photoelectron Spectroscopy of Cellulose Films

Survey scan XPS results for the cellulose films, derived from both Whatman filter paper and wood pulp, show that only carbon, oxygen, and sulfur are present on the surface. (Note that hydrogen is not detected with this technique). A summary of the elemental surface concentrations for the two films is given in Table 5.1. While both films contain the same trace amount of sulfur (0.3%), they vary in relative amounts of oxygen and carbon, with the Whatman film having the higher oxygen concentration. The trace amounts of sulfur are due to sulfate ester groups resulting from hydrolysis with sulfuric acid during preparation of the cellulose nanocrystals.

The high-resolution carbon spectra further highlight the differences between the Whatman and wood pulp films. The carbon signal can be resolved into four component peaks, which reflect the local environments of the carbon atoms. The peak for a carbon atom bonded only to other carbon atoms and hydrogen atoms has a binding energy of 285 eV. When carbon bonds to oxygen, the local environment changes. As the number of carbon-oxygen bonds increases, the binding energy increases. The four component peaks are therefore categorized by the number of C-O bonds: C1 has no oxygen bonds, C2 has one oxygen bond, C3 has two oxygen bonds, and C4 has three oxygen bonds<sup>8</sup>. In our samples, there is a slight tail on the C3 peak that may be interpreted as a minor C4 peak, but we have included this as part of the C3 peak.

The high-resolution carbon spectra show the relative amounts of each carbon type in the films cast from the Whatman and wood pulp suspensions (Figure 5.1). The most apparent difference between the two films is the larger C1 peak for the film derived from

Table 5.1 Elemental surface concentrations for cellulose films derived from wood pulp and Whatman suspensions.

	Surface Concentration (Atomic %)		
	O	C	S
Wood pulp	39.4	60.3	0.3
Whatman	42.6	57.1	0.3

the wood pulp suspension, accounting for 23.1% of the carbon as compared to only 12.5% in the film derived from the Whatman suspension. The relative proportions of each carbon type are summarized in Table 5.2, which shows that both films deviate from the theoretical values expected for pure cellulose. Pure cellulose does not contain any hydrocarbons, yet both films have C1 peaks. Hydrocarbons tend to be the most common surface contaminant, and it is quite common to see C1 peaks in cellulose samples<sup>9</sup>. Although the films were handled carefully, it is possible that some surface contamination occurred. The high surface area of the cellulose nanocrystals makes it difficult to completely avoid contamination of the original suspension and also during film formation and storage. The Whatman film has a much lower percentage of C1 than the wood pulp film and its ratio of oxygen to carbon (0.75) is closer to the theoretical value for cellulose (0.83) so a valence band spectrum was run on this sample (Figure 5.2). The valence band spectrum for the Whatman film is in good agreement with a reference valence band spectrum for cellulose<sup>10</sup>, indicating that our cellulose films are composed of fairly pure cellulose.

### 5.3.2 X-ray Diffraction Analysis of Cellulose Films

Cellulose films were next examined by X-ray diffraction analysis. Since native and regenerated cellulose differ in stability and reactivity, it is important to identify the exact nature of the cellulose sample. X-ray diffraction is the most common technique for distinguishing the polymorphs of cellulose. While cellulose is known to consist of both crystalline and amorphous regions, our cellulose nanocrystals are highly crystalline and can therefore be characterized by X-ray analysis.

Although the structure of cellulose has been studied by X-ray diffraction for many years, there has been much controversy regarding the interpretation of results to determine the exact nature of the unit cell. The intense controversy may be partly explained by the realization, through the use of solid-state carbon-13 NMR, that native cellulose I is actually a composite of two distinct crystalline forms<sup>11</sup>. Native cellulose is composed of cellulose I<sub>α</sub> (triclinic) and cellulose I<sub>β</sub> (monoclinic) in various proportions depending on the origin of the cellulose sample<sup>12</sup>. Algal and bacterial celluloses have a

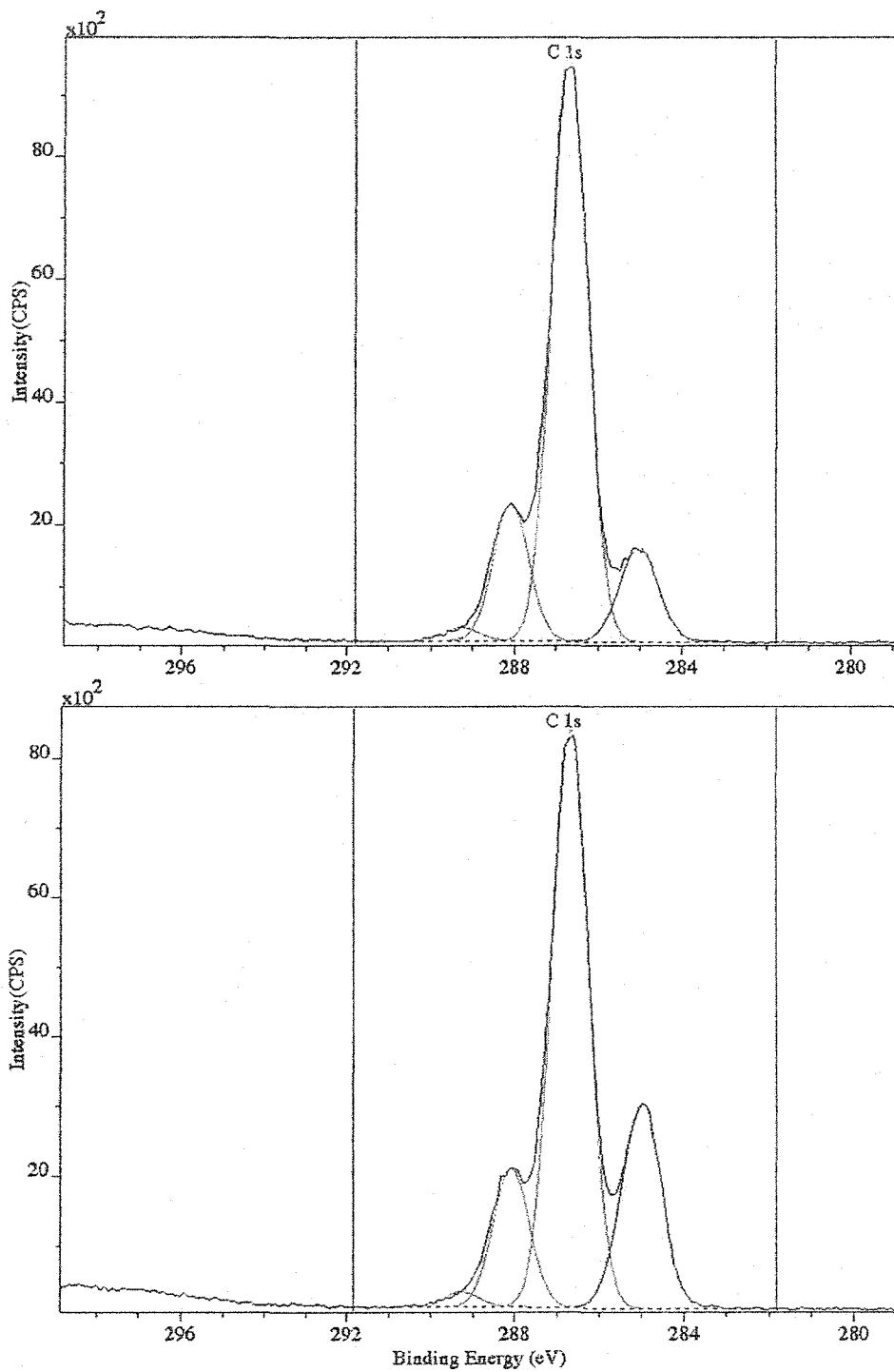


Figure 5.1 High-resolution carbon spectra for cellulose films derived from Whatman (upper) and wood pulp (lower) suspensions. The right-most peak at 285 eV is the C1 peak, the middle peak is the C2 peak, and the left-hand peak is the C3 peak. The area under the tail of C3 peak has been added to the C3 peak.

Table 5.2 Surface concentrations of carbon for cellulose films derived from wood pulp and Whatman suspensions compared to theoretical values.

	Surface Concentration (Atomic %)			O/C Ratio
	C1	C2	C3	
Wood pulp	23.1	60.8	16.1	0.66
Whatman	12.5	69.6	18.1	0.75
Cellulose (Theoretical)	-	83.3	16.7	0.83

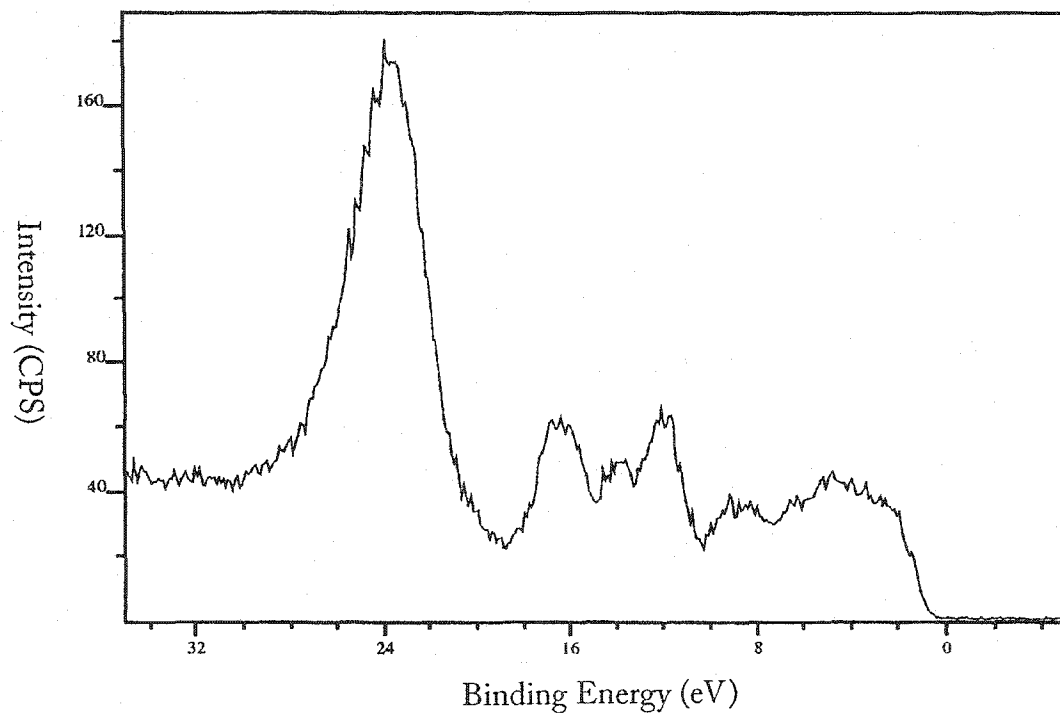


Figure 5.2 The valence band spectrum for a cellulose film derived from the Whatman suspension shows the pattern expected for a cellulose sample.

higher proportion of cellulose  $I_{\alpha}$ , whereas higher plants, such as the wood and cotton samples used in our study, contain more cellulose  $I_{\beta}$ <sup>13</sup>. Although the ratio of cellulose  $I_{\alpha}$  to cellulose  $I_{\beta}$  has been determined using X-ray diffraction<sup>14</sup>, this is not the goal of our present study. We are interested in distinguishing between cellulose I and cellulose II and therefore we will focus on the cellulose  $I_{\beta}$  form since it is dominant in higher plants.

In crystalline regions of cellulose  $I_{\beta}$ , the chains are arranged in a monoclinic unit cell where the three sides have different lengths ( $a \neq b \neq c$ ) and two of the corner angles are  $90^{\circ}$ , while the third is not ( $\alpha = \gamma = 90^{\circ} \neq \beta$ ). There are several families of planes that cut through the unit cell at different angles. Each crystal structure has a characteristic X-ray pattern that indicates the distance between planes, known as interplanar spacing, or d-spacing. From the d-spacing the dimensions of the unit cell can be calculated. Since there are many possible planes through a unit cell, they are identified systematically using Miller Indices, a set of three integers (hkl) indicating the number of times a family of planes intersects the a, b, and c-axes of the unit cell. For cellulose, the three most common planes, 002,  $10\bar{1}$ , and 101, are depicted in Figure 5.3 for both cellulose I and cellulose II. (Note that these planes have been defined with 'b' as the fibre axis). When X-rays strike these planes, constructive interference occurs when the path length difference between two planes is an integral number of wavelengths, following the Bragg equation

$$n\lambda = 2d \sin \theta \quad (V.1)$$

The characteristic interplanar spacings ( $d$ ) for a crystalline sample can be obtained from a powder diffraction diagram.

The powder diffraction diagram obtained from cellulose film derived from Whatman filter paper is shown in Figure 5.4. (The diffraction diagram obtained for a film derived from wood pulp showed the same pattern.) In order to show that the film consists of cellulose I, the  $2\theta$  angles and d-spacings were obtained from the powder diagram and compared with literature values. As shown in Table 5.3, the experimentally determined d-spacings for our cellulose sample (0.39 nm, 0.53 nm, and 0.60 nm) are in good agreement with literature values for cellulose I (0.39 nm, 0.54 nm, and 0.61 nm)<sup>15</sup>.

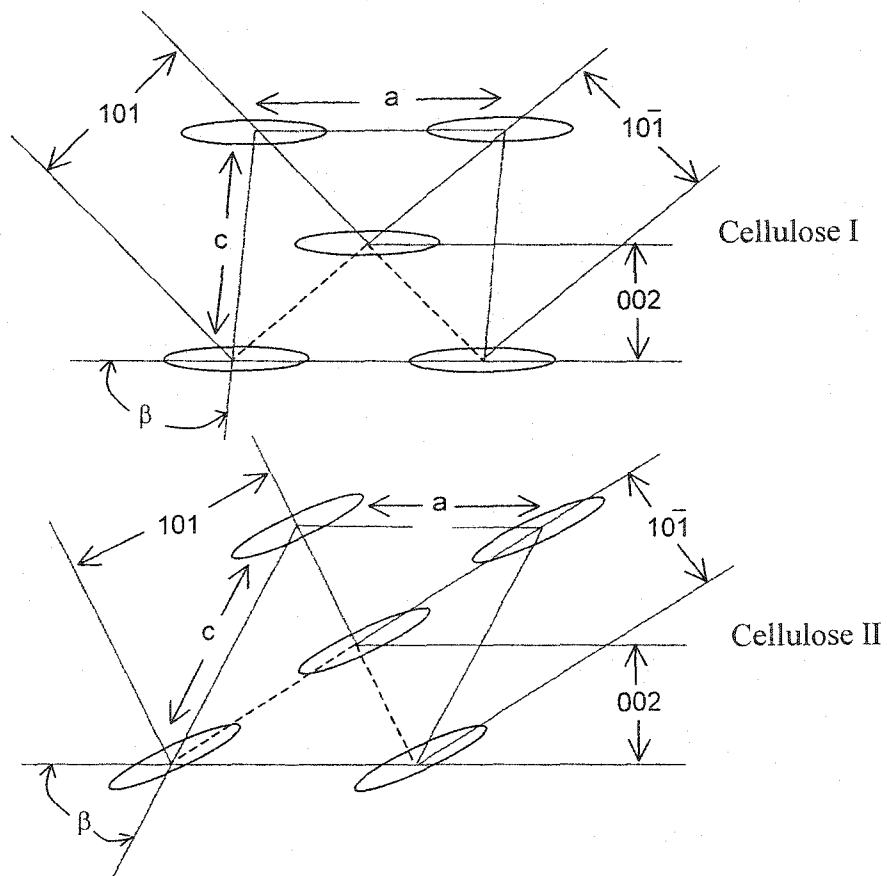


Figure 5.3 Schematic diagram showing the 002,  $10\bar{1}$ , and  $101$  planes for both cellulose I and cellulose II.

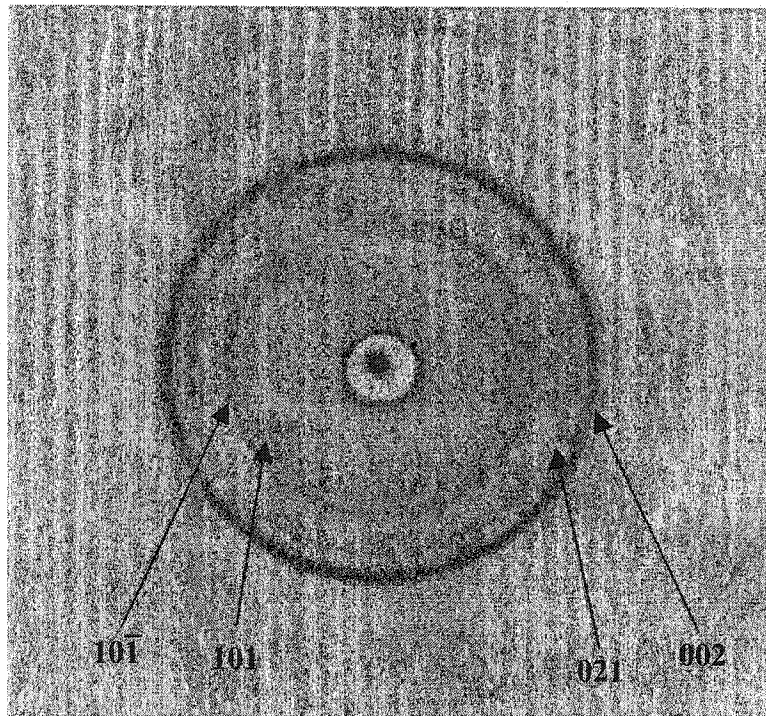


Figure 5.4 An X-ray powder diffraction diagram for a cellulose film derived from the Whatman suspension, showing the major diffraction rings  $101$ ,  $10\bar{1}$ ,  $021$ , and  $002$ .

Table 5.3 X-ray band intensity and d-spacing of our model cellulose film compared to literature values.

Lattice Plane	Band Intensity	Experimental d-Spacing (nm)	Literature d-Spacing <sup>(a)</sup> (nm)
002	Strong	0.39	0.39
10 $\bar{1}$	Medium	0.53	0.54
101	Medium	0.60	0.61

<sup>(a)</sup> From Preston, 1974

The  $2\theta$  angles obtained from our powder diagram were compared with values from samples of untreated (cellulose I) and mercerized (cellulose II) cotton. As seen in Table 5.4, our experimental value match most closely with the cellulose I untreated cotton sample. The different cotton samples show that there are distinct differences between the crystallographic structure of cellulose I and cellulose II<sup>17</sup>. There are large differences between our sample and the cellulose II found in mercerized cotton, indicating that our sample is composed of cellulose I.

### 5.3.3 Creating Smooth Cellulose I Surfaces

Now that we have determined that our cellulose films are relatively pure cellulose I, it is important to characterize the surface of the films. To obtain the smoothest surface possible several film casting techniques were explored. Since freshly cleaved mica provides a molecularly smooth surface, it would be ideal to cast films on a base of mica and then peel off the cellulose to expose the bottom side that was formed against the smooth mica surface. Initially, it was impossible to remove the cellulose from the mica without destroying the film. Subsequent attempts were carried out with a more concentrated cellulose suspension in order to produce thicker films. The thicker films tended to curl up around the edges, facilitating removal from the mica base. Some films even popped off the mica surface at the end of the drying stage. Roughness values obtained from atomic force microscopy indicated that these films were very smooth; however, the AFM images closely resembled those of pure mica surfaces. Close examination revealed that a very thin layer of mica was attached to the bottom of the cellulose film. This thin layer could be removed with tape; however, if the mica coverage was not uniform the cellulose could be contaminated with adhesive. Samples prepared from the Whatman suspension using this method gave an average root-mean-square roughness of 2.5 nm and a maximum z-range, which represents the distance between the lowest trough and the highest peak over the 1000-nm scanned area, of 48 nm (Table 5.5). Since the roughness values were less than optimal, no samples using the wood pulp suspension were made using this technique.

The next technique also used a mica surface, but this time the film was left on the mica and the smoothness of the top side of the cellulose was measured. It was hoped that

Table 5.4  $2\theta$  angles for samples of cotton in both cellulose I and cellulose II forms compared to our model cellulose film.

Lattice Plane	Cotton, Untreated <sup>(b)</sup> I	Cotton, Mercerized <sup>(b)</sup> I	Cotton, Mercerized <sup>(b)</sup> II	Model Cellulose Film I
002	22.7	22.7	21.8	22.9
021	20.5	20.2	-	20.7
10 $\bar{1}$	16.8	16.8	20.0	16.7
101	14.7	14.8	12.3	14.7

<sup>(b)</sup> From Krässig, 1993

Table 5.5 Roughness values determined from AFM images for cellulose films prepared by a variety of methods compared to mica.

Sample	Root-mean-square Roughness (nm)	Maximum z-range (nm)
Whatman peeled off of mica	2.5	48
Whatman on mica	2.3	20
Wood pulp on mica	1.5	13
Whatman cast on polystyrene	1.2	10
Wood pulp cast on polystyrene	1.0	9
Mica	0.28	3.0

flat cellulose layers would form against the mica base and that this smooth arrangement would continue throughout the thin film up to the top surface. Cellulose films formed in this way were smoother than the films cast from the Whatman suspension and peeled off the mica. The Whatman suspension yielded films with a root-mean-square roughness of 2.3 nm and a maximum z-range of 20 nm, while the film from the wood pulp suspension gave values of 1.5 nm and 13 nm, respectively.

After experimenting with charged surfaces and dipping techniques, it seemed that casting films was the best method, due to the low volatility of the aqueous suspensions. We needed a smooth, flat surface that would not delaminate. As well, it was important that cellulose would not stick to the surface. After testing a variety of materials, we discovered that the best choice was a standard polystyrene petri dish. The bottom sides of the films cast in petri dishes gave average root-mean-square roughness values and maximum z-ranges of 1.2 nm and 10 nm, respectively, for films cast from the Whatman suspension; and 1.0 nm and 9 nm, respectively, for films cast from the wood pulp suspension (Table 5.5). For means of comparison, the root-mean-square roughness measured for mica was 0.28 nm and the maximum z-range was 3.0 nm. Surface images of films cast from the Whatman and wood pulp suspensions are shown in Figure 5.5. Beside each figure is the contour profile of the line through the middle of each image.

Measurements of cellulose surface forces have been carried out on regenerated cellulose films with surface roughness estimated to be 2 – 5 nm<sup>6</sup>. Thus, our films of native cellulose with surface roughness around 1 nm should be suitable as a model surface to study force interactions.

#### 5.3.4 Creating Oriented Cellulose I Surfaces

Due to the anisotropic nature of cellulose, it would be interesting to study the interactions not only between cellulose surfaces, but also between oriented cellulose surfaces. We have used a variety of techniques to control the alignment of our cellulose nanocrystals in order to create oriented surfaces. By spin coating the nanocrystal suspension onto a glass or mica surface, a radial arrangement of nanocrystals is obtained. When viewed between crossed polarizers, the spin coated samples display a Maltese cross (Figure 5.6), indicating that orientation of the nanocrystals comes to a point in the

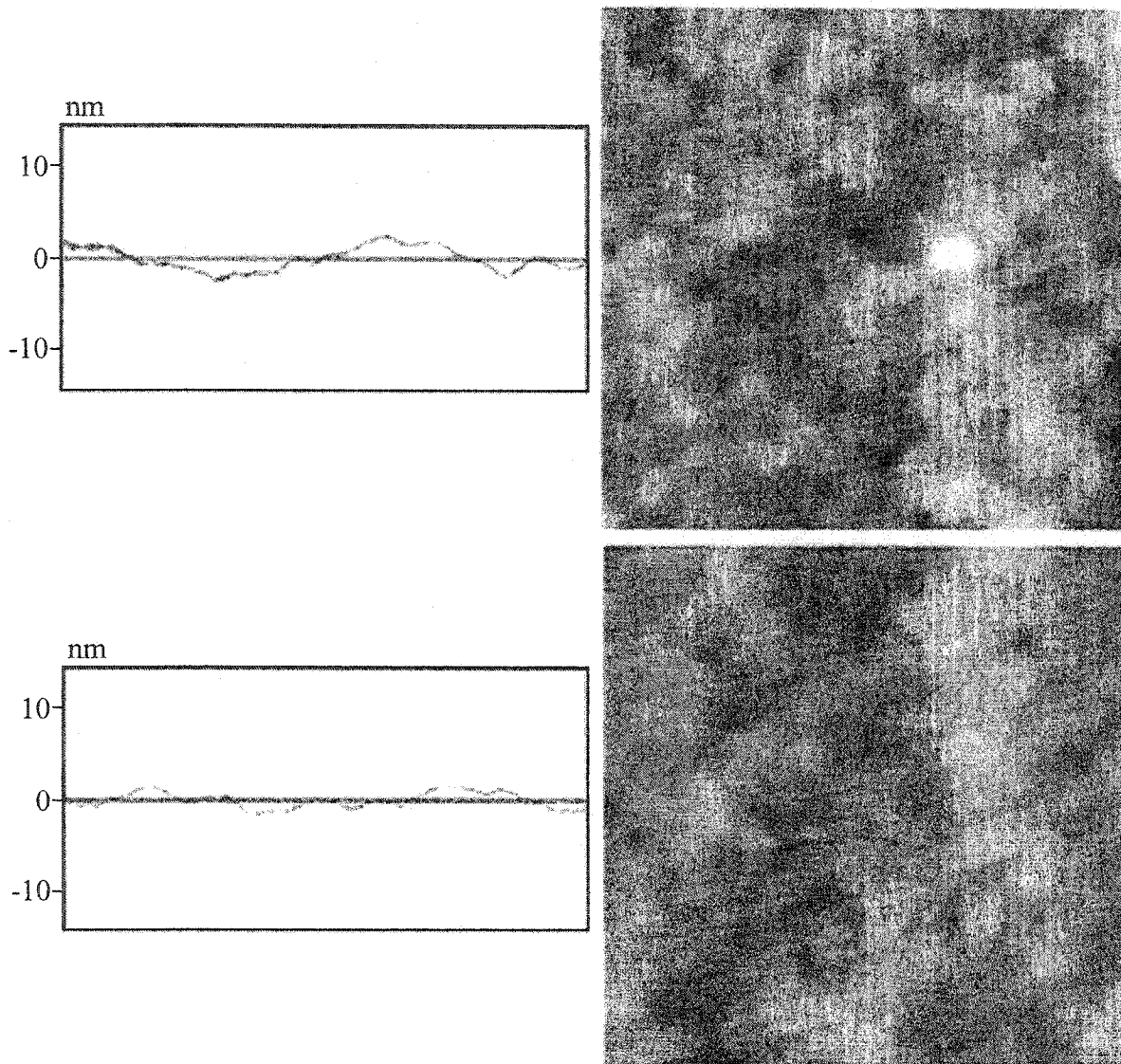


Figure 5.5 AFM images of a film cast from the Whatman suspension (upper) and a film cast from the wood pulp suspension (lower). A contour profile from a line across the middle of the image is shown next to each sample. Images are 1  $\mu\text{m}$  by 1  $\mu\text{m}$ , shown in height mode.

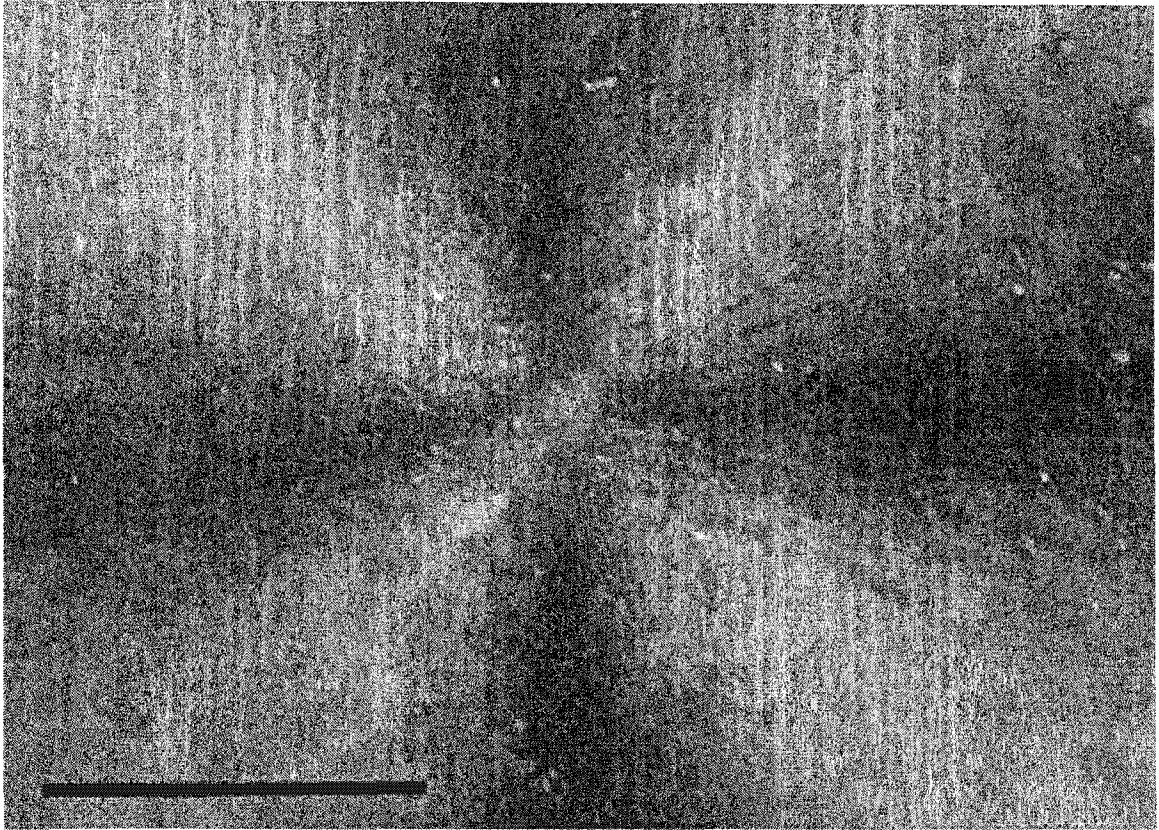


Figure 5.6 A digital image between crossed polarizers of a cellulose suspension spin-coated onto a glass surface, showing the radial orientation of the cellulose nanocrystals. The polarizers are oriented vertically and horizontally and the scale bar is 5 mm.

centre and radiates outwards from there. At any position away from the centre, the nanocrystals are oriented along the same direction, lying roughly parallel to neighbouring rods. Oriented samples were also obtained by shearing a concentrated drop of suspension along a mica or glass surface. When viewed in a polarizing microscope, it was evident that the nanocrystals had been aligned in the direction of shear. Samples prepared by spin-coating and by shearing were analyzed by AFM to measure their surface roughness. The root-mean-square roughness and maximum z-range for the spin-coated samples were 2.6 nm and 23 nm, respectively, while those for the sheared samples were 2.4 nm and 21 nm, respectively. Since the roughness of these oriented samples was higher than the roughness of films cast on polystyrene, a third technique to orient the nanocrystals was investigated. Aliquots of cellulose suspension were placed in petri dishes and allowed to concentrate. When the suspension became viscous, the petri dish was tilted in one direction to pour off excess suspension and then allowed to dry at a slight angle. When viewed in a polarizing microscope it was seen that the nanocrystals in these films were preferentially aligned in one direction.

### **5.3.5 Assessing the Stability of Cellulose Films**

We have now produced smooth cellulose I surfaces that can be oriented if desired. These model surfaces could be useful for studies of cellulose interactions. It is conceivable that such investigations would involve the examination of surface forces under aqueous conditions with a range in pH and ionic strength. It is therefore important to assess the stability of the films.

When water is added to the films they swell slightly but remain intact. However, slight agitation causes the films to disperse. In order to stabilize the films they were heat treated in an oven overnight at 105 °C. Following this treatment, the films were stable upon the addition of water even after agitation. (It has also been found that after a milder treatment, heating the films in a vacuum oven at 35 °C for 24 hours, the films did not redisperse in water<sup>18</sup>). Thus, after stabilizing the films by heating they are suitable for examination in an aqueous environment.

## 5.4 CONCLUSIONS

For many applications it would be beneficial to study the force interactions between cellulose surfaces. Force interactions have been previously conducted on various cellulose samples, but they all involved amorphous, regenerated cellulose. However, most naturally occurring cellulose is cellulose I. We have prepared a model cellulose I surface from our nanocrystal suspensions. XPS results showed that the films were relatively pure cellulose and X-ray analysis indicated that the films were composed solely of cellulose I. By casting the films in polystyrene petri dishes, relatively smooth surfaces, with root-mean-square roughness on the order of 1 nm, could be formed. These films may also be oriented and stabilized against aqueous solutions in order to be used in future studies on the surface interactions of cellulose I.

## 5.5 REFERENCES

- (1) Revol, J.-F.; Bradford, H.; Giasson, J.; Marchessault, R. H.; Gray, D. G. *International Journal of Biological Macromolecules* **1992**, *14*, 170-172.
- (2) Revol, J.-F.; Godbout, L.; Dong, X.-M.; Gray, D. G.; Chanzy, H.; Maret, G. *Liquid Crystals* **1994**, *16*, 127-134.
- (3) Revol, J.-F.; Godbout, L.; Gray, D. G. *Journal of Pulp and Paper Science* **1998**, *24*, 146-149.
- (4) Marchessault, R. H.; Sundararajan, P. R. In *The Polysaccharides*; Aspinall, G. O., Ed.; Academic Press: New York, 1983; Vol. 2.
- (5) Luner, P.; Sandell, M. *Journal of Polymer Science: Part C* **1969**, *28*, 115-142.
- (6) Neuman, R. D.; Berg, J. M.; Claesson, P. M. *Nordic Pulp and Paper Research Journal* **1993**, *8*, 96-104.
- (7) Holmberg, M.; Berg, J.; Stemme, S.; Ödberg, L.; Rasmusson, J.; Claesson, P. *Journal of Colloid and Interface Science* **1997**, *186*, 369-381.
- (8) Dorris, G. M.; Gray, D. G. *Cellulose Chemistry and Technology* **1978**, *12*, 9-23.
- (9) Johansson, L.-S.; Campbell, J. M.; Koljonen, K.; Stenius, P. *Applied Surface Science* **1999**, *144-145*, 92-95.
- (10) Beamson, G.; Briggs, D. *High Resolution XPS of Organic Polymers: The Scienta ESCA300 Database*; John Wiley & Sons: New York, 1992.

- (11) Atalla, R. H.; VanderHart, D. L. *Science (Washington, D. C., 1883-)* **1984**, *223*, 283-285.
- (12) Sugiyama, J.; Vuong, R.; Chanzy, H. *Macromolecules* **1991**, *24*, 4168-4175.
- (13) Horii, F.; Hirai, A.; Kitamaru, R. *Macromolecules* **1987**, *20*, 2117-2120.
- (14) Wada, M.; Okano, T.; Sugiyama, J. *Journal of Wood Science* **2001**, *47*, 124-128.
- (15) Preston, R. D. *The Physical Biology of Plant Cell Walls*; Chapman and Hall: London, 1974.
- (16) Meyer, K. H.; Misch, L. *Helvetica Chimica Acta* **1937**, *20*, 232-244.
- (17) Krässig, H. A. *Cellulose: Structure, Accessibility, and Reactivity*; Gordon and Breach Science Publishers: Yverdon, 1993.
- (18) Dong, X. M.; Gray, D. G. *Langmuir* **1997**, *13*, 2404-2409.

## **Chapter 6**

### **General Conclusions**

## 6.1 CONCLUSIONS

Examination of the cellulose nanocrystals at various concentrations has enhanced the understanding of cellulose suspensions and films. The behaviour of the colloidal cellulose rods is distinctive at each concentration range. The investigations in each chapter combine to provide a greater overall understanding of this unique cellulose system.

Since the phase behaviour of the liquid crystalline suspensions of cellulose nanocrystals is highly dependent on the aspect ratio of the rods, the first research goal was to develop an efficient technique to characterize the particle size. Analysis by atomic force microscopy showed that the average particle size for the nanocrystals derived from Whatman filter paper was 110 nm by 10 nm. For the particles derived from wood pulp the average dimensions were 70 nm by 6 nm. Both the cotton and pulp samples were polydisperse, but the pulp sample had a narrower distribution of particle lengths.

Having determined average particle dimensions it was then possible to investigate the phase behaviour of the cellulose suspensions and compare experimental results with theoretical predictions. At low concentrations the cellulose suspensions are isotropic. Upon reaching a critical concentration the cellulose suspensions become anisotropic, with the rods forming a chiral nematic liquid crystal. At intermediate concentrations the suspensions are biphasic with an upper isotropic phase and a lower anisotropic phase. Experiments with blue dextran clearly showed that the coiled dextran particles were preferentially partitioned into the isotropic phase of the cellulose suspensions. The trends observed experimentally matched those that were suggested by theory. Relatively good agreement between experimental and calculated partition coefficients was found, keeping in mind that the cellulose rods are polydisperse and that the theory used is rigorous only to an order of magnitude. These are the first experiments showing the effect of mixing a polymer with the cellulose suspensions.

Like most biopolymers, cellulose is a chiral material. The chiral nematic order observed in these solid films is due to the inherent chirality of cellulose. This system of colloidal cellulose rods is unique in that it has liquid crystalline properties not only in

solution, but also the ordered arrangement can be conserved in solid films. Experiments with induced circular dichroism confirmed that the liquid crystalline order had been preserved in solid films. The negative ICD peak indicated that the rods were arranged in a left-handed helicoidal superstructure. By developing a technique to quantify the order in the chiral nematic films it is then possible to try to enhance the order. The chiral nematic order of the films was successfully increased by allowing the films to dry in the presence of a magnetic field.

Since the cellulose suspensions could be used to cast solid films, a method was developed to create smooth films. Atomic force microscopy was used to characterize these smooth films, which could be an ideal substrate for future investigations on the nature of cellulose. X-ray photoelectron spectroscopy showed that the films were relatively pure cellulose; X-ray diffraction analysis showed that the films consisted solely of cellulose I.

The research in this thesis has added to our knowledge of the liquid crystalline properties of cellulose nanocrystals, and has also presented a method to make a model cellulose I surface that will facilitate investigations of the fundamental nature of cellulose itself.

## **6.2 ORIGINAL CONTRIBUTIONS TO KNOWLEDGE**

- (1) A technique using atomic force microscopy was devised to characterize the length and width, as well as the polydispersity, of the cellulose nanocrystals.
- (2) An addition to the knowledge base on cellulose crystallite dimensions originating from different sources was made. It was shown that for the same preparation conditions cellulose nanocrystals originating from cotton are significantly longer than those derived from pulp samples.
- (3) The influence of coiled particles on the phase behaviour of suspensions of rod-like particles was examined for the first time with cellulose suspensions. It was

determined that dextran is preferentially partitioned into the isotropic phase of a cellulose suspension.

- (4) The cellulose-dextran system was introduced as a suitable experimental system to test and compare theoretical predictions on the interactions of coiled and rod-like particles.
- (5) A technique using induced circular dichroism was developed in order to measure the relative degree of order in chiral nematic cellulose films. It was demonstrated that the chiral nematic order in solid cellulose films could be enhanced by casting the films in the presence of a magnetic field.
- (6) A method to make a smooth model cellulose I surface from the suspensions was devised. This model surface may be useful for future investigations of cellulose interactions. The model surface was characterized using x-ray photoelectron spectroscopy, x-ray diffraction analysis, and atomic force microscopy.

### 6.3 SUGGESTIONS FOR FUTURE RESEARCH

Each chapter in this thesis explored a unique aspect of the cellulose suspensions and films, increasing the overall breadth of knowledge. It was important to first gain a broad understanding of this cellulose system in order to guide future research. There would be no point in having a well-characterized system of cellulose rods if there was no potential to do anything with it. Conversely, it would be difficult to fully understand the phase behaviour a rod-coil system without knowing the particle dimensions. With each chapter a new journey has begun. Each of these topics could be further explored in order to increase the depth of knowledge. As well, knowing more about the properties of these cellulose nanocrystals some potential applications could be investigated.

- (1) Characterizing particle size. Atomic force microscopy has been shown to be an effective tool for characterizing length, width, and polydispersity of cellulose nanocrystals. However, this technique would be somewhat tedious if a large number

of samples needed to be analyzed. Future research could assess the potential of using a flow-through method of particle determination. For example, Polymer Laboratories has recently developed a 'Particle Size Distribution Analyser,' which separates different particle sizes using packed column hydrodynamic chromatography prior to analysis. While this technique would provide both a mean particle size and a particle size distribution, sometimes only the mean particle size may be required. If this is the case, future research could assess the potential of using other techniques to determine the mean particle size.

- (2) Reducing polydispersity. If the suspensions of cellulose nanocrystals were more monodisperse, the experimental phase behaviour would match more closely with that predicted by theory, the size of the biphasic region would decrease, and perhaps a more ordered smectic phase would be observed. In addition, the order in the chiral nematic phase itself may be enhanced, leading to a greater partitioning of coiled-particles. There are two main approaches to obtaining a more monodisperse sample: fractionation and careful selection of starting material. Fractionation techniques such as sucrose density gradient centrifugation or flow-through centrifugation may be investigated. However, the first technique is likely quite tedious and would be difficult to obtain large quantities of a monodisperse sample and the second technique requires highly specialized equipment. The alternative approach would be to select a source of cellulose that nature has created with a monodisperse crystallite size. The fact that nanocrystals derived from pulp cellulose were found to be more monodisperse than those from cotton cellulose makes this approach seem reasonable. However, the actual selection of a desirable cellulose starting material may be a hit and miss process. Perhaps a good place to start would be with a pre-fractionated pulp source such as the primary wall of juvenile softwood.
- (3) Expanding partitioning studies. Using blue dextran particles was an appropriate choice to initially examine the phase behaviour of rod-coil systems. Further investigations may be carried out changing variables such as particle size, pH, temperature, and ionic strength; however, these would be done strictly for academic purposes. It may be more interesting to experiment with particles that are of

biological interest since the cellulose suspensions are in an aqueous environment and can be pH-adjusted as necessary. In addition, the interfacial tension between the isotropic and the anisotropic phases is very small and would therefore be unlikely to damage delicate biological molecules. Thus, partitioning with the biphasic cellulose suspensions may be an alternative for delicate molecules that would be damaged during centrifugal separations.

- (4) Optimizing chiral nematic order. Now that a technique using induced circular dichroism has been developed to assess the order in the chiral nematic films, different methods to increase the alignment in cellulose films can be examined. If it were possible to vary the field strength, it would be interesting to quantify the relationship between magnetic field strength and chiral nematic order. Is there a minimum threshold field required to obtain an initial response? Is there a maximum field beyond which no improvement is seen? This ICD technique could also be used to determine if there is an increase in the order of cellulose suspensions that have been fractionated to obtain a more monodisperse sample.
- (5) Measuring cellulose interactions. The next logical step after developing a model cellulose I surface is to measure cellulose-cellulose interactions. This could potentially be done using surface force apparatus or by using atomic force microscopy and obtaining force-distance curves. The model cellulose films could first be measured alone, varying the pH and the ionic strength if the measurements were carried out in an AFM fluid cell. Subsequently, the model films could be coated with various polymers that are typically used as additives in the pulp and paper industry.
- (6) Creating 'micro fines'. Since it has been shown that smooth cellulose films can be created from the cellulose nanocrystals, it seems feasible that the smoothness of paper products could be enhanced with the nanocrystals. Cellulose nanocrystals could be added to paper products either during the papermaking process or subsequently as a coating step. Ideally, these nanocrystals would behave like 'micro fines,' decreasing the porosity and enhancing the smoothness of paper samples.

(7) Drawing nanocrystal fibres. Cellulose has high tensile strength and therefore is desirable for producing fibres. Since the cellulose nanocrystals have a rigid, rod-like shape they can be easily aligned and potentially drawn out into fibres. Concentrated suspensions of cellulose nanocrystals were extruded through a narrow syringe into a non-solvent, forming worm-like threads of cellulose. Unfortunately these threads were too brittle to be of any use. Thus, a composite material is necessary. Future research could experiment with adding different polymers, such as (hydroxypropyl)cellulose, to suspensions of nanocrystals in order to increase the viscosity and tackiness of the solution in order to obtain more durable fibres. Once a desirable additive has been determined, it may also be added during the formation of solid films to make them more resilient.

## APPENDIX

### Theories on the Phase Behaviour of Rod-like Particles and Rod-Coil Systems

#### Onsager's Theory

Onsager<sup>1</sup> showed that ordered phases did not need attractive interparticle forces to form; excluded volume, based on particle shape, was sufficient to explain entropy driven phase separations. Since many colloids depend on electrostatic repulsion, he also considered the effect of charge on the phase separations. For a spherical colloid of radius  $a$  modeled as a 'hard' core, there exists a larger imaginary sphere of radius  $2a$  around it from which the centres of other spheres are excluded. Thus, the excluded volume is eight times the actual volume of the spherical particle. Onsager calculated the excluded volume for the more complicated case of cylindrical particles, where the excluded volume depends on the angle between the two interacting particles. The excluded volume,  $\beta_1$ , for a pair of cylinders as a function of orientation angle,  $\gamma$ , particle length,  $L$ , and particle diameter,  $D$ , is given by

$$-\beta_1(\gamma) = \frac{\pi}{4} D_1 D_2 (D_1 + D_2) \sin \gamma + \frac{\pi}{4} (L_1 D_1^2 + L_2 D_2^2) + \frac{\pi}{4} (L_1 D_2^2 + L_2 D_1^2) |\cos \gamma| \\ + (L_1 + L_2) D_1 D_2 E(\sin \gamma) + L_1 L_2 (D_1 + D_2) \sin \gamma \quad (\text{A.1})$$

$$\text{where } E(\sin \gamma) = \int_0^{\pi/2} (1 - \sin^2 \gamma \sin^2 \varphi)^{1/2} d\varphi \quad (\text{A.2})$$

For two cylinders of equal length and diameter oriented parallel to each other ( $\gamma = 0$ ) the above expression simplifies to

$$8 \left( \frac{\pi}{4} \right) L D^2 \quad (\text{A.3})$$

showing that the excluded volume is eight times the volume of the cylinder. The general equation has been solved for other special cases. For example for  $L_1 \gg D_1 + D_2 \ll L_2$ , i.e. for rods with a high aspect ratio, the excluded volume is

$$L_1 L_2 (D_1 + D_2) \sin \gamma \quad (\text{A.4})$$

The angular dependence of this equation shows that the excluded volume is a maximum for the perpendicular orientation and decreases as the particles become more aligned. For highly anisotropic particles the ratio of excluded volume to particle volume,  $v_p$ , is roughly equal to the ratio of particle length to diameter

$$\frac{-\beta_1}{2v_p} \approx \frac{L}{D} \quad (\text{A.5})$$

For charged rods, starting from the Poisson-Boltzmann differential equation for electric potential, Onsager determined the potential of the average force,  $\omega$ , between two cylinders to be

$$\frac{\omega}{kT} = \frac{Ae^{-\kappa x}}{\sin \gamma} \quad (\text{A.6})$$

where  $A$  is a constant depending on electrical charge,  $\kappa^{-1}$  is the Debye screening length,  $x$  is the distance and  $\gamma$  is the angle between rod-like cylinders. Thus, the average force between charged cylindrical particles is a maximum in the parallel orientation and decreases as the particles approach the perpendicular arrangement. Based solely on the electrostatic repulsion the particles are most stable in a perpendicular configuration. To calculate the equilibrium state of the colloidal suspension, the potential of average force between particles is found by solving the following integral equation

$$B_p(N_p, V, T) = \frac{\int e^{-\omega/kT} d\tau}{N_p!} \quad (\text{A.7})$$

where  $\omega$  is the potential of average force,  $d\tau$  is a volume element, and  $N_p$  is the number of particles in the system. The free energy,  $F$ , and subsequently the osmotic pressure,  $\Pi$ , and chemical potential,  $\mu$ , can be expressed in terms of  $B_p$  as follows

$$F(\text{solution}) - F(\text{solvent}) = N_p \mu_p^\circ(T, \text{solvent}) - kT \log B_p(N_p, V, T) \quad (\text{A.8})$$

$$\Pi = kT \left( \frac{\partial \log B_p}{\partial V} \right) \quad (\text{A.9})$$

$$\mu_p = \mu_p^\circ - kT \left( \frac{\partial \log B_p}{\partial N_p} \right) \quad (\text{A.10})$$

F(solution) refers to volumes that contain colloid particles and F(solvent) is just for the suspending fluid. In order for isotropic and anisotropic phases to coexist, their respective osmotic pressures and chemical potentials must be equal.

If the forces are assumed to be pairwise additive

$$\omega = \sum_{i < j} \omega_{ij} \quad (\text{A.11})$$

the above integral equation can be evaluated with the use of irreducible cluster integrals, according to the methods of Mayer and Mayer. The first cluster integral,  $\beta_1$ , involves the interaction of two particles, while the second cluster integral,  $\beta_2$ , involves three particle interactions. Once these terms have been evaluated they are used in an expanded equation for  $B_p$  as first and second order correction terms.

$$\beta_1 = \frac{1}{V} \int f_{12} d\tau_1 d\tau_2 \quad (\text{A.12})$$

$$\beta_2 = \frac{1}{2V} \int f_{12} f_{23} f_{31} d\tau_1 d\tau_2 d\tau_3 \quad (\text{A.13})$$

$$\log B_p = N_p \left\{ 1 + \log(V/N_p) + \frac{1}{2} \beta_1 (N_p/V) + \frac{1}{3} \beta_2 (N_p/V)^2 + \dots \right\} \quad (\text{A.14})$$

The first cluster integral is equal to the excluded volume discussed above. The calculations for the second cluster integral are much more complex, involving interactions of three particles, so Onsager just approximated the order of magnitude of  $\beta_2$  and his theory is only applicable to dilute suspensions, in which two-particle interactions are the most common.

Knowing the value of  $\beta_1$ , the osmotic pressure of rod-like colloidal particles can be calculated. The free energy of the system, which depends on the distribution of particle orientations, can also be computed. From this Onsager predicted that an isotropic suspension would form an ordered anisotropic phase once the ratio of excluded volume to particle volume exceeded a critical value. The volume fraction of rods in each phase is given by

$$\varphi_i = 3.3D/L \quad (\text{A.15})$$

$$\varphi_a = 4.5D/L \quad (\text{A.16})$$

for long hard rods of aspect ratio  $L/D$ .

## SLO Theory

Stroobants, Lekkerkerker, and Odijk<sup>2</sup> (SLO) showed that the electrostatic interactions between charged rods could be characterized by two factors: one accounting for the increased effective diameter and another incorporating a twisting effect. Both factors are influenced by the thickness of the electrical double layer, which in turn depends on the ionic strength of the medium.

For rod-like particles the electrostatic repulsion depends on the orientation of the rods. Thus, electric forces will differ in the isotropic and anisotropic phases. The electrostatic interaction favours perpendicular orientation, yet this interaction leads to an increased effective diameter, amplifying the excluded volume effect<sup>1</sup>. The excluded volume effect favours the parallel arrangement of rods. A twisting factor,  $h$ , was derived, which depends on both the effective particle diameter,  $D_{eff}$ , and the Debye screening length,  $\kappa^{-1}$

$$h = \frac{\kappa^{-1}}{D_{eff}} \quad (\text{A.17})$$

A thicker double layer will increase the particles' tendency to twist away from each other. On the other hand,  $h$  decreases as the effective particle diameter increases. As effective particle diameter increases, the excluded volume increases and the particles then prefer a parallel alignment in order to minimize the increase in excluded volume.

The volume fractions given by SLO theory are<sup>3</sup>

$$\varphi_i = 3.290[(1 - 0.675h)b]^{-1} \quad (\text{A.18})$$

$$\varphi_a = 4.191[(1 - 0.730h)b]^{-1} \quad (\text{A.19})$$

where  $h$  is defined as above and  $b$  is the second virial coefficient of the system

$$b = \frac{\pi}{4} L^2 D_{eff} \quad (\text{A.20})$$

## Sear's Theory

Adding particles of different shapes, such as colloidal spheres or random-coil polymers, will influence the phase behaviour of a rod-like system. Much of the theoretical work on rod-sphere systems focuses on systems where the diameter of the spheres is much greater than the length of the rods<sup>4</sup>. Experimental work carried out with

narrow rods and large colloidal spheres has shown that very low concentrations of rods can cause a depletion-induced phase separation<sup>5</sup>. One theory, by Sear<sup>6</sup> examines the phase behaviour of rod-coil systems where the length of the rods is comparable to the radius of gyration of the coils. Compared to previous theories on phase behaviour of two-particle systems, Sear's approach matches most closely the experimental parameters of our cellulose-dextran system.

Sear considers the excluded volume interactions of more than one type of particle; one particle has a relatively large diameter, such as DNA molecules or cellulose nanocrystals, and acts like a rigid-rod. The other particle is a flexible polymer with a very small diameter. The theory is valid for relatively dilute concentrations of the two polymers, and for polymers with no attractive interactions. The diameter of the rigid polymer,  $D$ , is less than the radius of gyration,  $R_g$ , of the flexible polymer; while the length of the rigid polymer,  $L$ , can be greater than, less than, or comparable to  $R_g$ .

The free energy,  $A$ , of a mixture of rigid-rods and flexible polymers up to the second order in density for an isotropic fluid phase is

$$\frac{A}{VT} = c_r(\ln c_r v_r - 1) + c_c(\ln c_c v_c - 1) + B_r c_r^2 + B_c c_c^2 + B_{rc} c_r c_c \quad (\text{A.21})$$

where  $V$  is the volume,  $T$  is the temperature,  $c_r$  and  $c_c$  are the number densities of the rigid and flexible polymers,  $v_r$  and  $v_c$  are thermal volumes, and  $B_r$ ,  $B_c$ , and  $B_{rc}$  are virial coefficients. From the above expression for the free energy the chemical potential of the rods and coils may be derived. The chemical potential of the rods is

$$\frac{\mu_r}{T} = \ln c_r v_r + 2B_r c_r + B_{rc} c_c \quad (\text{A.22})$$

and the chemical potential of the coils is essentially the same

$$\frac{\mu_c}{T} = \ln c_c v_c + 2B_c c_c + B_{rc} c_r \quad (\text{A.23})$$

The second virial coefficient for rod-coil interactions can be obtained by integrating over the potential of mean force,  $u(r)$ , between the rod and the coil

$$B_{rc} \approx \int dr \left( 1 - \exp \left[ \frac{-u(r)}{T} \right] \right) \quad (\text{A.24})$$

For  $L \gg R_g$  this gives

$$B_{rc} \approx LD^{1/2}R_g^{3/2} \quad (\text{A.25})$$

For  $L \ll R_g$  the second virial coefficient is also given by A.25. For  $L \sim R_g$ , the theory should take into account the relative positions of the rods and coils, but since it is only rigorous to an order of magnitude, the above expression for  $B_{rc}$  is used for all ratios of  $L$  to  $R_g$ .

For the second virial coefficient for the interaction between a pair of rods,  $B_r$ , the expression derived by Onsager is used

$$B_r \approx L^2 D \quad (\text{A.26})$$

The second virial coefficient for the interaction between coils is given by

$$B_c \approx R_g^3 \quad (\text{A.27})$$

In order to study the phase behaviour of an isotropic-nematic system it is also necessary to derive the free energy of the mixture in the ordered phase

$$\frac{A}{VT} = c_r (\ln c_r v_r \alpha - 2) + c_c (\ln c_c v_c - 1) + B_r \frac{4}{(\pi\alpha)^{1/2}} c_r^2 + B_c c_c^2 + B_{rc} c_r c_c \quad (\text{A.28})$$

where  $\alpha$  is a parameter related to the nematic ordering. The equilibrium value of  $\alpha$  is given by

$$\alpha = \frac{(2c_r B_r)^2}{\pi} \quad (\text{A.29})$$

Substituting equation A.29 into equation A.28 gives

$$\frac{A}{VT} = c_r \ln \left( \frac{4B_r^2 c_r^3 v_r}{\pi} \right) + c_c (\ln c_c v_c - 1) + B_c c_c^2 + B_{rc} c_r c_c \quad (\text{A.30})$$

From this expression, the chemical potential of the rods in the nematic phase can be calculated

$$\frac{\mu_r}{T} = \ln \left( \frac{4B_r^2 c_r^3 v_r}{\pi} \right) + B_{rc} c_c \quad (\text{A.31})$$

The chemical potential of the coils is given by the same expression in the nematic phase as it is in the isotropic phase (A.23).

In order to examine the partitioning of polymer coils between the phases of rigid rods, the limit that the density of the coils is much less than the density of the rods is

considered. Within this limit, the interactions between coils can be neglected and the expression for the chemical potential of the coils simplifies to

$$\beta\mu_c = \ln c_c v_c + B_{rc} c_r \quad (\text{A.32})$$

where  $\beta$  has been used instead of  $1/T$ . Then, the density of coils in the isotropic phase is

$$c_c^i = \exp(\beta\mu_c - B_{rc} c_r^i) \quad (\text{A.33})$$

where  $c_r^i$  is the density of rods in the isotropic phase. The analogous equation relates the density of the coils in the nematic phase

$$c_c^n = \exp(\beta\mu_c - B_{rc} c_r^n) \quad (\text{A.34})$$

Since at equilibrium the chemical potential must be the same in both phases, the ratio of coils in the isotropic phase to coils in the nematic phase, or the partition coefficient,  $K$ , is given by the following equation

$$K = \frac{c_c^i}{c_c^n} = \exp(B_{rc} (c_r^n - c_r^i)) \quad (\text{A.35})$$

Equation A.35 is analogous to Equation III.3 in Chapter 3 and can be used to compare theoretical predictions with experimental results based on measured rod densities.

Estimating that the rod densities at coexistence differ by an order of about  $1/B_{cr}$  and using equations A.25 and A.26, the above expression can be simplified to

$$K \approx \frac{c_c^i}{c_c^n} \approx \exp\left(\frac{B_{rc}}{B_r}\right) \approx \exp\left(\frac{R_g^{3/2}}{LD^{2/3}}\right) \quad (\text{A.36})$$

Thus, the partition coefficient can be determined based solely on the geometries of the particles involved.

## REFERENCES

- (1) Onsager, L. *Annals New York Academy of Sciences* **1949**, *51*, 627-659.
- (2) Stroobants, A.; Lekkerkerker, H. N. W.; Odijk, T. *Macromolecules* **1986**, *19*, 2232-2238.
- (3) Odijk, T. *Macromolecules* **1986**, *19*, 2313-29.
- (4) Vliegthart, G. A.; Lekkerkerker, H. N. W. *Journal of Chemical Physics* **1999**, *111*, 4153-4157.
- (5) Koenderink, G. H.; Vliegthart, G. A.; Kluijtmans, S. G. J. M.; van Blaaderen, A.; Philipse, A. P.; Lekkerkerker, H. N. W. *Langmuir* **1999**, *15*, 4693-4696.
- (6) Sear, R. P. *Journal de Physique II* **1997**, *7*, 877-886.